BRIDGING DEPRESSION AND MITOCHONDRIA: FUNCTIONAL INSIGHTS FROM CELLULAR MODELS IN CASE STUDY PATIENTS

DISSERTATION

ZUR ERLANGUNG DES DOKTORGRADES

DER NATURWISSENSCHAFTEN (DR. RER. NAT.)

DER FAKULTÄT FÜR BIOLOGIE UND VORKLINISCHE MEDIZIN

DER UNIVERSITÄT REGENSBURG

vorgelegt von

Iseline Cardon

aus

Alès, France

im Jahr

2023

Das Promotionsgesuch wurde eingereicht am:
23. Oktober 2023

Die Arbeit wurde angeleitet von:
Prof. Dr. rer. nat. Christian Wetzel

Unterschrift:

Table of contents

Abstract

Despite extensive research and a constantly rising prevalence, the biological mechanisms underlying major depressive disorder (MDD) remain partially elusive. Evidence of a link between mitochondria and depression is accumulating, underscored by both mitochondria's involvement in many mechanisms identified in depression, and a high prevalence of MDD in individuals with mitochondrial disorders. Specifically, mitochondrial functions and energy metabolism are increasingly considered to be involved in MDD's pathogenesis, either by contributing to an individual's susceptibility or as a result of the pathology.

In this study, we expanded on prior research on a human cellular model of MDD and focused on cellular and mitochondrial (dys)function in two atypical patients, aiming to gain a more comprehensive understanding of ways in which mitochondria can influence cellular function and potentially contribute to the development of depression. The case study patients are an antidepressant non-responding MDD patient ("Non-R"), and a patient suffering from a mitochondriopathy with unknown cause ("Mito").

Using skin biopsies of these two patients and non-depressed controls, we obtained dermal fibroblasts, and generated induced pluripotent stem cells, neural progenitors, neurons, and astrocytes. We observed that cellular and mitochondrial functions and neuronal electrophysiology in the Mito patient resembled findings in the MDD patients cohort. This included decreased respiration, mitochondrial membrane potential and depolarised resting membrane potential, associated with smaller sodium currents. In contrast, the Non-R patient's cells were affected in an opposite manner in many of the measured parameters, including increased respiratory rates and mitochondrial calcium, and hyperpolarized resting membrane potential. Notably, smaller cell sizes were consistently observed across all patient-derived cells compared to healthy controls.

The Non-R patient's data offered a new perspective on MDD, suggesting a detrimental imbalance in mitochondrial and cellular processes, rather than simply reduced functions. Meanwhile, the Mito patient's data revealed the extensive effects of mitochondrial dysfunctions on cellular functions, potentially highlighting new MDD-associated impairments.

Together, findings in these case study patients bring a new dimension to our understanding of MDD.

Zusammenfassung

Trotz kontinuierlich steigender Prävalenz und umfangreicher Forschungsbemühungen, bleiben die biologischen Mechanismen, die der Major Depression zugrunde liegen, bis heute teilweise ungeklärt. Die Beteiligung der Mitochondrien an zahlreichen Mechanismen, die mit Depressionen assoziiert werden, liefert zunehmend Evidenz für einen Zusammenhang zwischen Mitochondrien und Depressionen. Darüber hinaus zeigt sich eine Komorbidität zwischen mitochondrialen Störungen und MDD. Es wird zunehmend angenommen, dass Störungen der mitochondrialen Funktionen, insbesondere des zellulären Energiestoffwechsels, Teil der Pathogenese der MDD darstellen, indem sie zur Vulnerabilität beitragen oder als Folge der Pathologie auftreten.

Im Rahmen dieser Studie wurden frühere Untersuchungen an einem humanen Zellmodell der MDD erweitert. Dabei wurden zelluläre sowie mitochondriale (Dys-)Funktion bei zwei atypischen Patienten eingehend analysiert, um ein umfassenderes Verständnis für die Wechselwirkungen mitochondrialer Funktion und zellulärer Homöostase zu erlangen und deren potenzielle Rolle bei der Entstehung einer Depression zu beleuchten. Diese beiden Fallstudien umfassen einen Patienten, der nicht auf Antidepressiva anspricht ("Non-R"), sowie einen Patienten, der an einer Mitochondriopathie unbekannter Ursache ("Mito") leidet.

Mittels Hautbiopsien von beiden Patienten und nicht-depressiven Kontrollpersonen konnten dermale Fibroblasten isoliert und induzierte pluripotente Stammzellen, neurale Vorläuferzellen, Neuronen und Astrozyten generiert werden.

In diesem Zusammenhang wurde festgestellt, dass die zellulären und mitochondrialen Funktionen sowie die neuronalen elektrophysiologischen Eigenschaften des Mito-Patienten Ähnlichkeiten zu den Ergebnissen der MDD-Patientenkohorte aufwiesen. Dies schloss eine verminderte mitochondriale Atmung, ein reduziertes mitochondriales Membranpotenzial und ein depolarisiertes Ruhemembranpotenzial ein, begleitet von verringerten Natriumströmen. Im Gegensatz dazu zeigten die Zellen des Non-R-Patienten in vielen der erhobenen Parameter entgegengesetzte Veränderungen, darunter eine gesteigerte Atmung, erhöhte mitochondriale Calzium-Level und ein hyperpolarisiertem Ruhemembranpotenzial. Interessanterweise wurde bei allen Patientenzellen eine konsistente Verringerung der Zellgröße im Vergleich zu gesunden Kontrollpersonen beobachtet. Die Eigenschaften des Non-R-Patienten eröffnen eine neue Perspektive für das Verständnis der MDD, indem sie auf eine verminderte Mitochondrienfunktion und ein Ungleichgewicht in mitochondrialen und zellulären Prozessen hinweisen. Die Ergebnisse des Mito-Patienten verdeutlichen die weitreichenden Auswirkungen mitochondrialer Dysfunktionen auf zelluläre Funktionen und zeigen möglicherweise bisher unbekannte Zusammenhänge mit der MDD auf.

Zusammengenommen erweitern die Erkenntnisse aus dieser Fallstudie unser Verständnis der zugrundeliegenden zellulären Pathomechanismen der Majoren Depression erheblich.

1 Introduction

1.1 Major depressive disorder (MDD)

1.1.1 Epidemiology and impact

Depression is an increasingly widespread condition affecting greatly the patients' quality of life. It is the most prevalent mental disorder in adults, affecting 280 million people worldwide in 2019, including 193 million people suffering from a major depressive disorder (MDD). This number has surged by 26% as a result of the COVID-19 pandemic, reaching a staggering 246 million people. In addition to this very high prevalence, depression has a huge negative impact on patients' lives and it is the second leading cause of global years lived with disability (World Health Organization, 2020). Although it is complex to estimate the mortality due to mental disorders, it was shown that people with mental health conditions have significantly higher mortality rates than the general population (World Health Organization, 2018). One study performed in 2010 estimated that 2.2 million excess deaths were attributable to MDD (Charlson et al., 2014). Moreover, suicide ranks as the fourth primary cause of death among 15–29-year-olds, contributing to approximately 8% of all deaths in this age group.

1.1.2 Symptoms and diagnosis

MDD presents multifaceted clinical manifestations that are not restricted to the commonly expected detrimental impact on mood. It also involves a high degree of heterogeneity.

The clinical picture consists of symptoms and signs associated with mood, cognition, anxiety, decision-making, interest, anhedonia, volition and motivation, psychomotor changes, energy, appetite, weight, speech, suicidal behaviour, circadian effects, melancholia, depersonalisation and derealisation (Kendler, 2016).

According to the *Diagnostic and Statistical Manual of Mental Disorders V* (DSM V), the three main symptoms are depressed mood, anhedonia, and a lack of drive, that must last for more than two weeks, and be associated with impaired social and occupational functions.

In addition, at least five of these nine specific symptoms must be present nearly every day: depressed or irritable mood most of the day; reduced interest or pleasure in most activities, most of each day; major alterations in weight or in appetite; altered sleep, insomnia or hypersomnia; alterations in activity, psychomotor agitation or retardation; fatigue or loss of energy; feelings of guilt/worthlessness; problems with concentration or indecisiveness; and suicidal behaviour or ideation (American Psychiatric Association, 2022).

However, as highlighted by the psychiatrist Kenneth Kendler, it is important to note that the depressive syndrome is not entirely constituted by the DSM V criteria, and that this list of symptoms does not capture adequately the range of human experience of the mood state of

depression and the range of self-derogatory/pessimistic depressive cognitions (Kendler, 2016).

The diagnosis of MDD is based on interviews by a trained practitioner. They provide an assessment of the person's clinical symptoms, but also of the thought content, specifically whether themes of hopelessness or pessimism, self-harm or suicide are present, and positive thoughts or plans are absent. In addition, rating scales, such as the Hamilton Depression Rating Scale (HAM-D) provide an indication of the severity and allow to categorise depression into mild, moderate or severe forms, based on the gravity of symptoms (Hamilton, 1980). Severity is also assessed depending on the impact of symptoms on several areas of life, such as social and occupational functioning.

1.1.3 Aetiology of MDD

The development of MDD is often attributed to the combination of psychosocial aspects, such as stress or traumatic experiences, biological factors such as genetic predisposition or epigenetics, and physical factors such as inflammation or cardiovascular disease. However, despite decades of research, the precise neurobiological underpinnings of depression remain elusive. A number of hypotheses were put forward over the years regarding the aetiology of MDD.

The earliest hypothesis was formulated in the 1960's, after observing that an antihypertensive drug, reserpine, depleted monoamine neurotransmitters (dopamine, serotonin, norepinephrine) and caused depression. Additionally, imipramine and iproniazid had the unforeseen effects of improving mood and increasing monoamines in the synaptic cleft (Ban, 2001). Based on these observations, the psychiatrist Alec Coppen was the first to attribute depression to a serotonin deficiency and over the years, the theory was supported by considerable evidence (Coppen, 1967; Jauhar et al., 2023). However, the foundations of this theory have recently been called into question by a systematic review, which has sparked many discussions in the field (Jauhar et al., 2023; Moncrieff et al., 2022).

Given that treatments restoring monoamines levels within hours only alleviate symptoms after several weeks, some argue that MDD is mainly a result of reduced neuroplasticity resulting from impaired BDNF signalling (Casarotto et al., 2021; Liu et al., 2017). In line with this theory, Casarotto *et al.* showed that common antidepressants (ADs) likely exert their clinical effects through their binding to the neurotrophins receptor TRKB (Casarotto et al., 2021). Numerous studies link depression and inflammation. Patients with inflammatory diseases show greater rates of MDD (Beurel et al., 2020), and conversely, patients with MDD show elevated peripheral inflammatory factors (Maes et al., 1992; Sluzewska, 1999). Inflammation can be caused by stress (Maydych, 2019), and stress can result in disturbed feedback mechanism of the hypothalamus-pituitary-adrenal axis (HPA), which is strongly

associated with MDD (Vreeburg et al., 2009). Deciphering which of these manifestations are the causes of MDD and which are the consequences is a complex challenge. Furthermore, impaired mitochondrial function is increasingly considered to be involved in the etiology of depression (Gardner & Boles, 2011; Klinedinst & Regenold, 2015; Kuffner et al., 2020; Manji et al., 2012; Moretti et al., 2003).

1.1.4 Therapy options for MDD

1.1.4.1 Antidepressants

The first line of treatment classically offered to patients suffering from MDD is pharmacotherapy with ADs. Typical ADs such as tricyclic ADs, serotonin selective reuptake inhibitors, and monoamine oxidase inhibitors, increase the synaptic concentrations of monoamines by inhibiting their reuptake or metabolism. Alternatively, fast-acting antidepressants like ketamine inhibit NMDA-type glutamate receptors. However, as previously mentioned, some argue that their clinical effect is actually due to their binding to the TRKB receptor (Casarotto et al., 2021).

1.1.4.2 Non-pharmacological interventions

In addition, depression can also be tackled using non-pharmacological interventions. Frequently used psychological interventions can have a positive impact on mental functioning, social relationships, level of discomfort and engagement in everyday activities (Kolovos et al., 2016). However, the best way to combat depression effectively is to fight it on several fronts. A meta-analysis compared the differential efficacy of psychotherapy alone, or in combination with pharmacotherapy and found a clinically meaningful advantage of combined therapy in more severely depressed patients (Thase, 1997). Consistently, studies showed that cognitive behavioural therapy combined to AD treatment produced significantly improved short-term (Bowers, 1990) and long-term (I. W. Miller et al., 1989) outcomes compared with pharmacotherapy alone. For more severe MDD, another effective intervention is electroconvulsive therapy (ECT), offering relief to at least half of treatment-resistant MDD patients (Karlinsky & Shulman, 1984).

1.1.5 Treatment resistant depression

Despite numerous therapeutic options, treatment-resistant depression (TRD) remains a serious issue. There is no consensual definition of TRD yet, but commonly, a patient is categorised as treatment-resistant after the failure of at least two appropriately prescribed ADs (Berlim & Turecki, 2007; El-Hage et al., 2013). Due to this lack of consensus, estimating the proportion of TRD patients is complex. Remission rate after primary AD treatment is estimated to range between 30 and 45% (Fava & Rush, 2006). Keller *et al.* reported that 10

to 20% of MDD patients remained significantly symptomatic for at least 2 years even after sequential treatments. In 2006, the “Sequenced Treatment Alternatives to Relieve Depression” (STAR*D) trial was the largest study to examine TRD. It involved four different treatment levels, including pharmaco- and psychotherapy. TRD patients progressed to the next level if they did not achieve remission. The results showed that remission rates fell drastically after two treatment steps, and ranged between 7 and 14% in Level 4, indicating that many participants failed to attain remission even after trying four different treatment strategies (Sinyor et al., 2009).

The mechanisms underlying AD response remain elusive, but some biomarkers can help predict the response to pharmacotherapy (reviewed in El-Hage et al., 2013). These markers include for example polymorphism in drug transporters genes, such as ABCB1, genetic differences in drug-metabolizing hepatic enzymes, alteration in the serotonergic system, polymorphism on the BDNF gene and defect in the HPA axis regulation (El-Hage et al., 2013). Environmental and psychosocial factors also play a critical role. Smoking impacts AD concentration (Suzuki et al., 2011). Older age correlates with poorer remission whereas marital status was found to be protective (Barnhart et al., 2018). Failure to remit can also be favoured by poor compliance to treatment in relation to low income, health insurance status, and ethnicity (El-Hage et al., 2013). Finally, the patient’s expectations of the treatment outcome has a powerful impact and increasing them has the potential to optimise clinical response (Rutherford et al., 2010).

1.2 The mitochondrion

As atmospheric levels of oxygen increased in early Earth development, selective pressure favoured eukaryotic cells that acquired aerobic respiration through endosymbiosis of aerobic prokaryotic microorganisms, the protomitochondrion. This endosymbiont eventually evolved into mitochondria and has become a crucial part of cellular function (Gray, 1989; Lyons et al., 2014).

But mitochondria’s reach extends far beyond the cell membrane. They can influence metabolic processes in nearby cells, but also in distant organs, by releasing signals in the systemic circulation (Picard & Shirihai, 2022). They ensure species survival through sexual reproduction by synthesising steroid hormones (W. L. Miller, 2013). They can even be transferred to another cell for rescue (Cheng et al., 2020; Spees et al., 2006).

Mitochondria are multifaceted organelles involved in a wide range of processes including energy production, calcium storage (Ichas et al., 1994), apoptotic cell death (Green & Reed, 1998), thermogenesis and iron, lipid and neurotransmitter metabolism (Hertz, 2013; Jones & Jones, 1969; Nedergaard et al., 2001). They are highly dynamic and remodel their network by frequent fusion and fission. Since endosymbiosis, mitochondria have delegated the

production of some of their proteins to the cytoplasmic machinery, from nuclear encoded genes, but they also have remained semi-autonomous, in that they possess their own small genome and the necessary machinery to manufacture some of their own proteins (van der Bliek et al., 2017).

1.2.1 Structure, morphology, and dynamics

Testimony to their bacterial origin, mitochondria possess a double membrane.

The outer mitochondrial membrane (OMM) contains porins, through which molecules can diffuse, enzymes involved in diverse pathways, and trafficking proteins such as the voltage-dependent anion channel (VDAC). The OMM can associate with the endoplasmic reticulum membrane to create a collaboration for calcium signalling. Under the OMM lies the intermembrane space (IMS) (Figure 1A and B). If the OMM is disrupted, leaking of IMS proteins in the cytosol will cause apoptotic cell death (Chipuk et al., 2006).

The inner mitochondrial membrane (IMM) encloses the mitochondrial matrix. It comprises the inner boundary membrane, parallel to the OMM, and invaginations called cristae, which extend into the matrix (Kühlbrandt, 2015). In contrast with the OMM, the IMM is impermeable to ions and molecules, and as a result, an electrochemical membrane potential of about 150-180 mV builds up across the IMM (Kühlbrandt, 2015). The cristae membrane contains the protein complexes of mitochondrial respiration: the electron transport chain and the ATP-synthase (Davies & Daum, 2013) (Figure 1A and B).

The mitochondrial matrix is composed of densely concentrated enzymes and proteins and is the site of many biosynthetic reactions. It also contains mitochondrial DNA (mtDNA) and the machinery for its replication, transcription, and translation into proteins (Anderson et al., 1981) (Figure 1B).

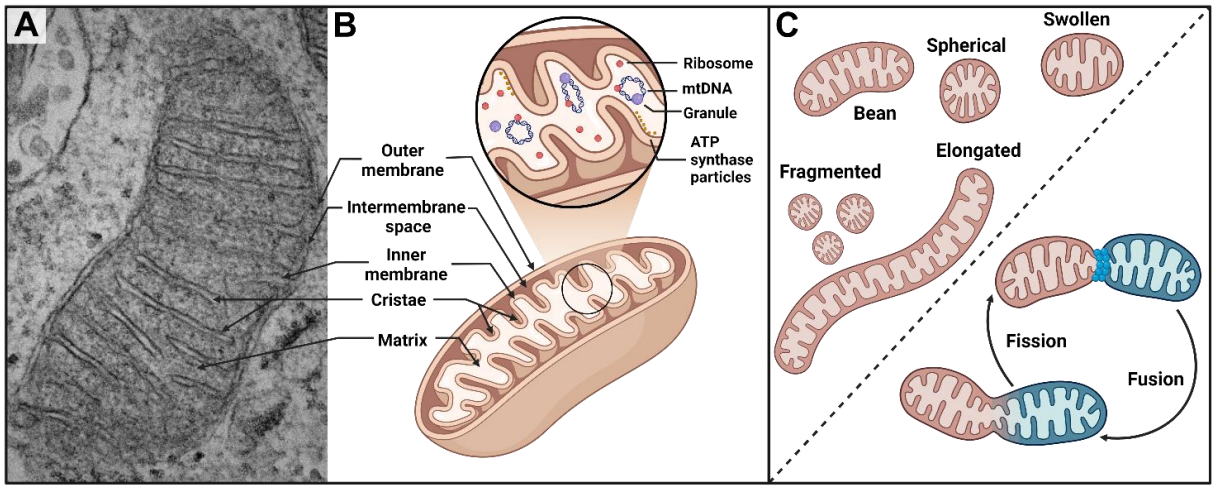

Figure 1: Mitochondrial structure and morphology. (A) Electron microscopy image illustrating a mitochondrion in cultured astrocytes. **(B)** Schematic illustration of mitochondrial structure. Mitochondria have a double-membrane structure with an outer and inner membrane. The OMM contains various porins and enzymes that regulate the exchange between mitochondria and cytosol. The IMM is impermeable to most molecules and ions and is extensively folded into structures called cristae, which increase the surface area to contain a large number

of proteins required for respiratory chain and other critical reactions for the mitochondria's varied functions. The IMS is the narrow space between the two differentially permeable membranes, which allows the creation of ions gradients. The mitochondrial matrix contains a highly concentrated mixture of enzymes, ribosomes, granules, RNA, and several copies of the mitochondrial DNA. **(C)** Mitochondrial shape varies extensively to adapt to function or in response to stress. Mitochondrial morphology is maintained by a balance between fusion and fission. Created with BioRender.com.

Mitochondria exist in a variety of different shapes, by far exceeding the textbook bean-shape. Mitochondrial shape dynamically adapts to function (Figure 1C). Tubular mitochondria form an interconnected network in metabolically active cells, whereas they are small and fragmented in quiescent cells (Westermann, 2012). Shape also varies in response to cellular perturbations. Mitochondria in apoptotic cells are highly fragmented but they are swollen and elongated during autophagy (Evans & Holzbaur, 2020). Ahmad *et al.* showed that mitochondria change their shape from tubular to donut or blob forms with increasing reactive oxygen species (ROS) (Ahmad et al., 2013). Horn *et al.* observed that mitochondria respond to plasma membrane injury by becoming fragmented and localising to the wound site (Horn et al., 2020).

Mitochondria maintain their shape, distribution and size through balanced fusion and fission (Figure 1C), while damaged or old mitochondria are eliminated through mitophagy. This quality control is crucial, especially in energy-demanding cells like neurons (Evans & Holzbaur, 2020). Interestingly, Scaini *et al.* reported impaired quality control machinery in MDD patients (Scaini et al., 2021).

1.2.2 Role in cellular metabolism

Mitochondria have a manifold role in cellular metabolism. They are known as bioenergetics powerhouses but they are also biosynthetic centres, managers of redox reactions, and waste processing centres. They are involved in iron metabolism and haem synthesis (Jones & Jones, 1969; Shah et al., 2012) and control glutamate metabolism (Frigerio et al., 2008).

However, mitochondria's most critical role is to transform organic molecules into cellular energy in the form of ATP. They do so mainly by oxidising major products of glucose produced in the cytosol, pyruvate and NADH, using the tricarboxylic acid (TCA) cycle and oxidative phosphorylation (OXPHOS). On the other hand, fatty acid oxidation (FAO) converts fatty acids to acetyl-Coenzyme A, which enters the TCA and eventually feeds into OXPHOS to produce ATP (Alberts, 2015).

1.2.2.1 Oxidative phosphorylation

OXPHOS, also called mitochondrial respiration, uses breathed oxygen to generate energy. Glycolysis, TCA cycle and FAO pathways produce the reducing equivalents NADH and $FADH_2$. Electrons from reducing equivalents are shuttled through the complexes of the electron transport chain (ETC), located in the IMM (Figure 2). The ETC passes the electrons

from donors to acceptors and uses the energy released to transport protons across the membrane. After these successive redox reactions, oxygen, the final electron acceptor, is reduced to water, in a reaction releasing half of the total energy (Alberts, 2015) (Figure 2).

The ATP synthase generates the remaining energy. The exact mechanism was proposed by Peter D. Mitchell with his “chemiosmotic hypothesis” that won him a Nobel Prize in 1978. Mitchell showed that the protons transferred into the IMS during electron transport accumulate, and create an electrochemical gradient, where “electro” stands for the difference in electrical potential created by the positively charged protons, and “chemical” for the pH gradient constituted by the protons. This gradient, also called the proton-motive force, drives the rotation of parts of the ATP-synthase. This motion provides energy to phosphorylate ADP into ATP (Figure 2) (Mitchell, 1961). Adenine nucleotide translocases (ANTs) then transport ATP to the cytosol.

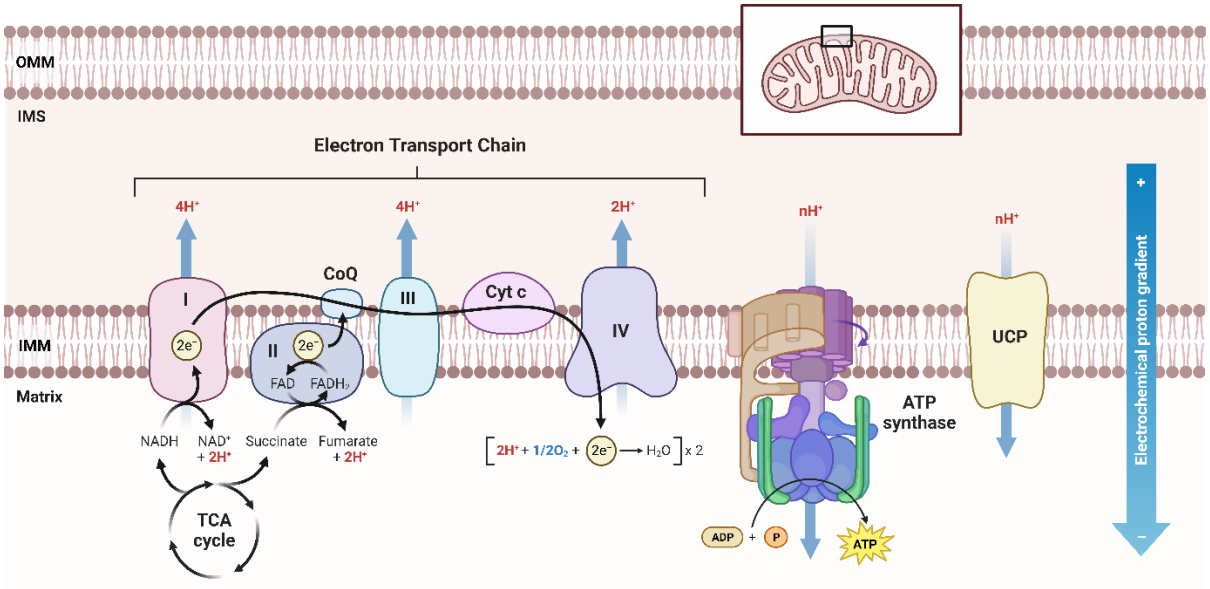

Figure 2: Mitochondrial oxidative phosphorylation. The reduced cofactors NADH and $FADH_2$ generated from prior metabolic processes including tricarboxylic acid cycle (TCA) donate electrons (e^-) to complex I and complex II, respectively. The electrons are then passed along the electron transport chain through a series of redox reactions until the final acceptor oxygen (O_2), which is reduced to water (H_2O). Electron transfer fuels proton (H^+) pumping from the matrix to the IMS, creating an electrochemical gradient. The flow of protons back to the matrix through the ATP synthase drives the phosphorylation of ADP into ATP. Created with BioRender.com

1.2.2.2 Mitochondrial membrane potential

As mentioned above, one component of the electrochemical gradient is the electrical potential created at the IMM. It is referred to as mitochondrial membrane potential (MMP). MMP varies across cell types and physiological activity but is typically around -150 mV in a normally functioning cell (Gerencser et al., 2012; Kamo et al., 1979).

Different factors influence MMP. The functioning of the ETC generates it, and the ATP synthase uses it to phosphorylate ADP to ATP. Less commonly, when mitochondrial respiration is not operating normally, ATP synthase activity can be reversed, leading to hydrolysis of ATP and increased MMP (Walker, 2013; Zorova et al., 2018). Proton leak

through the IMM can dissipate MMP. Unregulated proton leak can occur passively through anion carriers or through the membrane, depending on its composition and integrity. Proton leak can be regulated and mediated by the ANT and uncoupling proteins (UCP) (Figure 2) (Jastroch et al., 2010). Conversely, reverse operation of the ANT, importing ATP into mitochondria, can support MMP (Chinopoulos, 2011). Finally, increased calcium (Ca^{2+}) levels in the matrix speeds up TCA cycle activity and thereby OXPHOS activity which increases the MMP (Duchen, 2000).

In addition to its crucial role in ATP production, MMP is a driving force for transporting charged compounds into mitochondria, a critical process for viability. For example, MMP is the primary driver of Ca^{2+} import (Gunter & Pfeiffer, 1990), which allows mitochondria to be major players in Ca^{2+} homeostasis.

1.2.2.3 Calcium homeostasis

Ca^{2+} is an essential ion that plays a crucial role in various cellular processes including cell differentiation and proliferation, gene transcription, oxidative metabolism regulation and neuronal transmission (Berridge et al., 2000). As a second messenger involved in many signalling pathways, it translates external stimuli into cell response.

Hence, the finely tuned Ca^{2+} cytosolic concentration is crucial, orchestrated by a dynamic interplay between the endoplasmic reticulum (ER) and mitochondria. They fulfil an important Ca^{2+} buffering function, with mitochondria accommodating a wide range of Ca^{2+} concentrations (50 to 500 nM) (Romero-Garcia & Prado-Garcia, 2019).

To be imported into mitochondria, Ca^{2+} has to cross its double membrane. The OMM is highly permeable to Ca^{2+} due to the presence of VDCA1. In contrast, crossing the IMM is an electrogenic process occurring at the mitochondrial Ca^{2+} uniporter (MCU) complex, and driven by the negative MMP (Kamer & Mootha, 2015).

The relationship between mitochondria and Ca^{2+} goes both ways. Mitochondria play a vital role in modulating Ca^{2+} dynamics, but they also rely on Ca^{2+} for many of their functions. Several enzymes of the TCA cycle are directly activated by Ca^{2+}, which triggers oxidative metabolism and ATP production. When it is accumulating, mitochondrial Ca^{2+} also leads to the collapse of MMP and initiates programmed cell death through the opening of the mitochondrial permeability transition pore (mPTP), leading to the release of pro-apoptotic factors in the cytosol (Haworth & Hunter, 1979).

Therefore, it is clear that Ca^{2+} concentration in the matrix must be tightly regulated through influx and efflux mechanisms. Carafoli *et al.* were the first to propose that a sodium (Na^+)/Ca^{2+} exchanger was responsible for Ca^{2+} extrusion from the mitochondria in 1974 (Carafoli et al., 1974), but its molecular identity remained unknown until Palty *et al.* described the lithium-dependent Na^+/Ca^{2+} exchanger, NCLX, more than 30 years later (Palty et al.,

2010). Transient opening of the mPTP and a H^+/ Ca^{2+} exchanger also play a role in Ca^{2+} efflux (Takeuchi et al., 2015).

1.2.2.4 Reactive oxygen species production and regulation

Mitochondria being the site of cellular respiration, they are also logically the main sources of reactive oxygen species (ROS). The reduction of O_2 produces superoxide (O_{2-}), which is the precursor for most other ROS. O_{2-} production occurs predominantly at complex I of the ETC, where NADH from the TCA cycle passes an electron to the cofactor flavin mononucleotide (FMN) (Murphy, 2009). The reaction of O_2 with reduced FMN then yields O_{2-}. In physiological conditions, NADH/NAD^+ ratio, and therefore the rate of O_{2-} production, can be influenced by low ATP demand and consequent low respiration rate and by reverse electron transport (RET). RET occurs when a fraction of electrons from reduced ubiquinol is driven back towards complex I by a high proton-motive force, where it reduces NAD^+ to NADH (Murphy, 2009). Additionally but to a lesser extent, complex III generates O_{2-} into the IMS and the matrix (Murphy, 2009; Zhang et al., 1998).

In order to balance ROS production, cells evolved an antioxidant system composed of enzymes and antioxidant molecules. Superoxide dismutase enzymes dismutate O_{2-} into the more stable hydrogen peroxide (H_2O_2). H_2O_2 is further dismutated into H_2O and O_2 by various antioxidant enzymes including catalase, glutathione peroxidase (GPx), and peroxiredoxins (Sies & Jones, 2020). GPx turns H_2O_2 into $2H_2O$ by oxidising glutathione (GSH to GSSG) (Kaplowitz et al., 1985). In addition to the antioxidant system, cytochrome C in the ETC is able to scavenge O_{2-} (Pasdois et al., 2011) and high mitochondrial ROS activate uncoupling proteins (UCP), thereby dissipating the proton gradient, decreasing respiratory rates and the resulting ROS production (Brand et al., 2004).

If an excessive ROS production overwhelms the cells antioxidant system, oxidative stress will cause unspecific protein oxidation, damage biomolecules, and initiate detrimental signalling. For instance, lipid peroxidation generates 8-isoprostane which can activate the MAPK/ERK pathway and thereby influence the expression of inflammatory molecules (Scholz et al., 2003). Oxidative nuclear DNA damage favours mutagenesis and cancer development, while mtDNA damage results in mitochondrial dysfunction (Ide et al., 2001; Jackson & Bartek, 2009).

In contrast, low levels of ROS are essential for physiological redox signalling. H_2O_2-mediated specific and reversible oxidation alters protein activity, localisation and interactions which can influence various processes including cell proliferation, differentiation, and migration (Sies & Jones, 2020). O_{2-} has the potential to regulate mitochondrial energetics by uncoupling ETC activity and ATP synthesis through its interaction with UCP1 (Echtay et al., 2002).

1.3 Mitochondrial diseases

Mitochondrial diseases (MDs) are a group of genetic disorders caused by mutations in nuclear or mitochondrial DNA. Affected genes encode structural mitochondrial proteins or proteins involved in mitochondrial function. Mutations primarily result in OXPHOS defects. MDs are the most common inherited metabolic disorders and it is likely that their prevalence is underestimated, due to obstacles in the epidemiological study of MDs (Schaefer et al., 2019). Indeed, the bi-genomic nature of MDs results in high clinical heterogeneity. In the most recent review on the topic, authors estimated the prevalence of childhood-onset MDs to range between 5 and 15 cases per 10,000 (Schaefer et al., 2019).

Organs most affected by MDs are those, which predominantly rely on mitochondrial energy production such as the eyes, ears, heart, and peripheral and central nervous systems. Accordingly, symptoms include hearing and visual loss, cardiomyopathy, neuropathy, neurological problems like seizures, developmental delays and stroke-like episodes (Rahman, 2020). However, MDs can also affect the gastrointestinal tract, kidneys, and endocrine organs, among others. Another factor adding to MDs complexity is the fact that many patients present a mixture of mutated and wild-type mtDNA, known as heteroplasmy. The proportion of mutant mtDNA often determines clinical severity (Wallace & Chalkia, 2013). The unspecificity and high variability of symptoms complicates diagnosis as only a high level of clinical suspicion will lead to the specific genetic testing and invasive muscle biopsy, which are necessary to confirm the diagnosis (Schaefer et al., 2019).

Treatment options for MDs are limited. Dietary supplements to support mitochondrial function are commonly used for the symptomatic management, but evidence of their efficacy is lacking. Further interventions mainly deal with organ-specific complications (Gorman et al., 2016).

1.4 The bioenergetics hypothesis of MDD

Since the formulation of the monoamine theory of depression in the 1960's, a lot of knowledge has been gained and new theories have arisen. As a result, many biological factors are suspected to underlie the pathophysiology of depression, including stress hormones and inflammatory cytokines, glucocorticoid neurotoxicity, decreased neurotrophic factors and decreased neurogenesis, altered GABAergic and glutamatergic neurotransmission, and circadian rhythms alterations. Mitochondria assume a central role in many of these proposed biological processes and a lot of evidence support a link between mitochondrial dysfunction, associated with bioenergetics impairments, and the development of MDD.

1.4.1 Mitochondrial and bioenergetics abnormalities in depressed patients

1.4.1.1 Genetic proof of a link between MDD and mitochondrial dysfunction

There is a recognised genetic element to MDD, as demonstrated by a 35-40% heritability in twin studies (Kendler et al., 2006). A number of genetic studies point toward mitochondrial abnormalities in people with depression, strengthening the hypothesis of a role of energy metabolism in the pathogenesis of depression. Mitochondria are maternally inherited (Pyle et al., 2015) and certain families are burdened by a maternal inheritance of depression. Bergemann and Boles inspected the pedigrees of 672 individuals with early-onset MDD and found that matrilineal relatives were more likely to suffer from depression than nonmatrilineal relatives, suggesting that a predisposing genetic factor was passed on via the mitochondrial genome (Bergemann and Boles, 2010). Furthermore, different types of mtDNA defects were reported in depressed patients, including decreased gene expression (M.-Y. Kim et al., 2011), heteroplasmy (Cai et al., 2015), copy number variations, and deletions (Gardner et al., 2003).

1.4.1.2 MDD and mitochondrial functions in the brain: neuroimaging studies

Neuroimaging in depressed patients also revealed some abnormalities in brain energy metabolism. Several studies reported decreased ATP in the brain of MDD patients, and one reported increased AMP in the frontal lobe (reviewed in Klinedinst & Regenold, 2015). Interestingly, Iosifescu *et al.* demonstrated that ATP decrease could be reversed by a successful antidepressant therapy (Iosifescu et al., 2008). They prescribed a thyroid hormone augmentation to MDD patients who failed to respond to selective serotonin reuptake inhibitor (SSRI) antidepressant drugs. They observed a significant increase of ATP and phosphocreatine, which buffers ATP, in patients who responded to the T3 augmentation (Iosifescu et al., 2008).

1.4.1.3 Insight from post-mortem studies

In addition to genetic studies carried out on blood samples, studies were conducted on post-mortem brain tissue from depressed patients and revealed that the impairments observed at the peripheral level were also present and even possibly worse in the brain (Gardner & Boles, 2011; Manji et al., 2012). Indeed, in a case report on a severely depressed patient, researchers observed mitochondrial abnormalities in all tissues studied, but remarkably more mtDNA deletions in the brain than in skeletal muscles (Suomalainen et al., 1992). These findings suggest that the accumulation of mtDNA deletions in the brain could play a role in the pathophysiology of depression in some cases.

1.4.1.4 MDD and mitochondria interplay in patients' cells

Several studies have measured mitochondrial function directly in MDD patients' cells. Gardner *et al.* found decreased ATP production and respiratory enzymes activity in muscle cells (Gardner et al., 2003). Hroudová *et al.* found a reduced mitochondrial respiration in platelets (Hroudová et al., 2013). In peripheral blood mononuclear cells obtained from 22 MDD patients, Karabatsiakis *et al.* observed a decrease in several respiratory parameters, including ATP turnover-related respiration and coupling efficiency. Interestingly, they also showed that respiration was negatively correlated with the severity of depressive symptoms (Karabatsiakis et al., 2014). Garbett *et al.* measured stress-induced changes in mRNA of MDD patients fibroblasts and revealed impairments in pathways involved in the control of metabolism and energy production (Garbett et al., 2015). Based on a cohort of MDD patients, Kuffner *et al.* found decreased respiration and ATP in fibroblasts (Kuffner et al., 2020). Triebelhorn *et al.* observed similar respiration impairments in neural progenitors as well as MDD-associated electrophysiological changes in neurons (Triebelhorn et al., 2022).

1.4.2 Mitochondrial disorders and MDD

Moreover, among the plethora of evidence associating mitochondrial dysfunction with MDD, many connections exist between mitochondrial diseases and psychiatric conditions, and particularly MDD.

Indeed, people living with MDs have a higher risk to develop a major mental illness. In a study of 24 individuals with MD, Mancuso *et al.* recorded that 63% met the criteria for psychiatric illness, and among them, 58% had MDD, as compared to 20-30% in the general population in this country (Mancuso et al., 2013). Fattal *et al.* conducted a similar study with the largest sample to date, including 36 patients with mitochondrial cytopathies. They reported a 70% lifetime prevalence of psychiatric illness. Here as well, MDD was the most common diagnosis with 54% of patients, followed by bipolar disorder in 17% of patients and panic disorder in 11% of patients (Fattal et al., 2007).

One might expect that the challenge of a chronic disorder such as a MD could be difficult to bear for the patients, leading to depressive symptoms. To address this, Inczedy-Farkas *et al.* assessed psychiatric symptoms in 19 adults with mitochondrial mutations and 10 patients with a non-mitochondrial chronic disorder. They found significantly higher scores on depression scales in the MD group, although the level of disability was similar in both disorders (Inczedy-Farkas et al., 2012). In fact, psychiatric symptoms often precede the diagnosis of a MD, by an average of 7.5 years. In a study on 35 paediatric patients, Koene *et al.* reported that 14% of those eventually diagnosed with a MD initially presented depressive symptoms (Koene et al., 2009). Similarly, in families with the Mitochondrial Encephalopathy, Lactic Acidosis, and Stroke-like episodes (MELAS) mutation, 42% of the symptomatic

carriers, but also 22% of the asymptomatic carriers had depressive traits, as compared with 7% in the control group. This might suggest that psychiatric symptoms were an early clinical presentation of the mutation (DiMauro and Schon, 2008).

All in all, the evidence that characterised mitochondrial dysfunction provoke symptoms that can meet the full criteria for major depression, be it before or after the MD diagnosis, suggests that mitochondrial impairments themselves can underlie the full syndrome of MDD. This suggests that mitochondrial dysfunction alone can underlie the development of the full syndrome of MDD, or at least plays a central role in the pathophysiology of MDD.

1.5 Context and aim of the thesis

Our research aims at investigating the bioenergetics hypothesis of MDD, postulating a critical role of mitochondrial dysfunction in the pathophysiology of MDD. To tackle this question, our approach was to examine mitochondrial and cellular functions in patients-derived cell lines. The present thesis builds on data previously obtained in cells from a cohort of MDD patients and non-depressed controls (Kuffner et al., 2020; Triebelhorn et al., 2022). In this thesis, I used the MDD cohort data as a reference to investigate in depth specific aspects of the pathophysiology of MDD by conducting two case studies.

1.5.1 Basis of the thesis: previous research in the lab

1.5.1.1 MDD is associated with impaired mitochondrial function in skin fibroblasts, Kuffner *et al.*

To investigate the biological underpinnings of depression, a human cellular model of MDD was established. At the end of their stay in the psychiatric clinic, 16 MDD patients underwent skin biopsies in order to collect dermal fibroblasts

. 16 non-depressed volunteers donated their cells to form the control group. Kuffner *et al.* investigated mitochondrial and cellular function in fibroblasts from the MDD cohort by measuring OXPHOS activity, MMP, cytosolic Ca^{2+}, ATP content, and mtDNA copy number. MDD cells had lower mitochondrial respiration rates and ATP concentration. MMP was increased, but cytosolic Ca^{2+} was unchanged. There were no differences in mtDNA copy number between MDD patients and non-depressed controls, suggesting a mitochondrial dysfunction in patients fibroblasts rather than a decreased mitochondrial content (Kuffner et al., 2020).

1.5.1.2 Induced neural progenitor cells and iPS-neurons from MDD patients show altered bioenergetics and electrophysiological properties, Triebelhorn *et al.*

Fibroblasts from the MDD and controls cohort were reprogrammed to induced pluripotent stem cells (iPSCs) and differentiated into neural progenitor cells (NPCs) and neurons. Triebelhorn *et al.* investigated molecular mechanisms related to mitochondrial function in NPCs from 8 MDD patients and 8 non-depressed controls. In MDD patients' NPCs, MMP and ATP content were unchanged, while cytosolic Ca^{2+} was increased and respiration and cell size were decreased. Additionally, Triebelhorn *et al.* inspected electrophysiological properties of neurons and found decreased capacitance, resting membrane potential and spontaneous activity, and increased sodium current densities (Triebelhorn et al., 2022).

Taken together, these two studies demonstrate that mitochondrial function is impaired in MDD patients, in line with the bioenergetics hypothesis of MDD, and offer insight into the impact of the pathology on several cellular and mitochondrial processes.

1.5.2 Going further: case studies

Building on these two previous studies, the present thesis focuses on two specific patients in the form of case studies, to gain new insight on the pathophysiology of MDD.

1.5.2.1 Concept, scope, and advantages of a case study

Case studies are often opposed to population or cohort studies and qualitative research to quantitative research. However, as phrased by James Mahoney and Gary Goertz, they could rather be compared to two cultures having their own traditions and specificities, but being complementary (Mahoney & Goertz, 2006).

Case studies are detailed and intensive studies that seek to explain particular cases and understand causal mechanisms and processes. They allow an in-depth understanding of the factors under study. In biomedical research, they generally consist in investigating deeply atypical patients with interesting characteristics. Usually, case studies focus on deviant or outlier cases that do not fit the general theory. This brings the potential to help understand mechanisms that had not been explored before. This is comprised in the concept of "equifinality", wherein different paths can lead to the same outcome (Mahoney & Goertz, 2006). This, in turn, allows to develop new theories or to enrich the original theory. For instance, studying an atypical MDD patient could uncover a new factor in the disease's aetiology.

Importantly, case studies are not meant to be representative of an entire population. It is not their scope nor their goal, even though, in some instances, results can be generalised to a specific group, for example, patients with a very similar clinical presentation. More specifically, quantitative research (cohort studies) have a broad scope and a homogeneous

population to maximize generalisation, whereas qualitative research (case studies) adopt a narrow scope to avoid causal heterogeneity (Mahoney & Goertz, 2006). In other words, quantitative research measures a lot of cases roughly, with a limited number of parameters, whereas qualitative research aims to measure a few cases very precisely in order to understand the interplay between different parameters. When combining both methods, the strengths of one can offset the weaknesses of another.
This thesis is built on this idea and combines the present case studies to the previous cohort studies to go further in the understanding of the interplay between mitochondrial (dys)function and MDD.

1.5.2.2 Presentation of the case study patients

1.5.2.2.1 Antidepressant non-responder patient (Non-R)

The first case study patient was defined as anti-depressant non-responder, based on the most commonly accepted definition of TRD, according to which a depression case is considered resistant when at least two treatment regimens failed to induce remission (Berlim & Turecki, 2007). Upon the patient's admission at the clinic, trained psychiatrists diagnosed him with very severe MDD after extensive interview and using the Hamilton Depression Rating Scale (HAM-D, score 34). The patient was first treated with the serotonin-norepinephrine reuptake inhibitor (SNRI) duloxetine. When this treatment brought no improvement, psychiatrists prescribed venlafaxine, another SNRI. The patient did not respond to venlafaxine either, so the treatment was augmented with lithium. Indeed, lithium has been shown to be efficient in case of TRD (Alevizos et al., 2012). However, the patient did not remit, and eventually left the clinic after 12 weeks, still presenting severe depression (HAM-D score 22). This is when the patient accepted to participate in our study and the biopsy was conducted. The patient also had a light hypertension, which was medicated with Enalapril. He was a heavy smoker, as is often the case for people suffering from MDD. This patient is referred to as "Non-R".

1.5.2.2.2 Mitochondriopathy patient (Mito)

The second case study patient was diagnosed with a mild mitochondriopathy with unknown causes. The patient presented several neurological symptoms and pains and was directed to the centre for rare diseases in Regensburg (Zentrum für Seltene Erkrankungen). The symptoms included recurrent pain of the musculoskeletal system (affecting tendons, joints, toes, fingers, and back) over the last 11 years, neurological deficits (such as paraesthesia of the arms, and numbness in the legs), abdominal pain, weakness, general fatigue, hypersomnia, and myopia. Clinical findings allowed to rule out inflammatory bowel disease

but showed a slight narrowing of the coeliac trunk, which could explain the abdominal pain. Blood tests ruled out immune-related diseases, thyroid disorders, ankylosing spondylitis, rheumatoid arthritis, osteoporosis, celiac disease, borreliosis, carcinoma, and neuroblastoma. However, some markers related to lactate chemistry and mitochondrial functions were altered. Blood levels of some lactate dehydrogenase (LDH) isoenzymes were abnormal (increased LDH4, decreased LDH2). The levels of citrate, cis-aconitate and isocitrate, which are involved in the TCA cycle, were decreased. The level of pyruvate kinase isoenzyme M2, which catalyses the last step of glycolysis, was found to be increased. Additionally, there was a vitamin D3 and coenzyme Q10 deficiency. Coenzyme Q10 is an electron carrier in the ETC and a deficiency causes respiratory chain defects and ROS production (Quinzii & Hirano, 2010). Vitamin D3 regulates mitochondrial respiration and oxidative stress, while hypovitaminosis D is known to reduce mitochondrial activity (Matta Reddy et al., 2022). Exome sequencing and mitochondrial genome sequencing revealed no anomaly. A genetic mitochondrial disease was therefore excluded. However, based on the patient's symptoms and on blood test results, the differential diagnosis of a mild mitochondriopathy was established. Interestingly, the patient, referred to as "Mito", also had a very low levels of 5-Hydroxyindoleacetic acid (5-HIAA) in their urine. 5-HIAA is a serotonin metabolite, and its low presence indicates inadequate serotonin production, which has been linked to depression. Notably, low levels of 5-HIAA have been found in the cerebrospinal fluid of depressed patients (Cheetham et al., 1991).

1.5.3 Aim of the case studies

1.5.3.1 Antidepressant non-responder patient (Non-R)

In contrast with patients from the MDD cohort who all achieved a certain degree of remission (average remission 58±7%), the Non-R patient still suffered from severe MDD at the time of the biopsy. Studying this patient was therefore an opportunity to investigate how cellular and mitochondrial functions differed between remitted, treatment-responding MDD patients and a severely depressed, treatment-resistant MDD patient. Additionally, initial respiratory measurements in this patient's cells showed very different results to the MDD cohort, which highlighted the potential to enrich the mitochondrial theory of MDD.

1.5.3.2 Mitochondriopathy patient (Mito)

Previous studies revealed mitochondrial dysfunctions in MDD patients. The present patient was diagnosed with a mitochondriopathy, but does not suffer from MDD. Studying this patient provided an opportunity to observe the interplay between different cellular and mitochondrial parameters and compare them within the context of a mitochondrial disorder and MDD. Another aim was to understand how specific cellular processes and

characteristics, such as electrophysiological properties, were influenced by mitochondrial (dys)function, rather than being a consequence of MDD. This case study seemed therefore relevant to our understanding of different aspects of MDD pathophysiology related to mitochondria.

2 Material and Methods

2.1 Material

2.1.1 Laboratory consumables and equipment

Table 1: Laboratory consumables

Consumable	Manufacturer
60µ-Dish (Ø 35 mm, high)	Ibidi GmbH; Gräfelfing; Germany
Cell culture plates	Corning Incorporated; Tewksbury, Massachusetts
CellTrics 50 µm cell strainer	Sysmex; Hamburg, Germany
Coverslips, glass (Ø 25 mm; Ø 12 mm)	VWR by Avantor; Radnor, Pennsylvania
Cryo vials 1.5 mL/2 mL	Sarstedt; Nümbrecht, Germany
Falcon tubes (15 mL, 50 mL)	Greiner Bio One; Kremsmünster, Austria
Falcon® 5mL Round Bottom Polystyrene Test Tube, with Cell Strainer Snap Cap	Omnilab; Bremen, Germany
Microplates 96-well	Greiner Bio One; Kremsmünster, Austria
Pipette filter tips	Greiner Bio One; Kremsmünster, Austria
Pipette tips	Eppendorf; Hamburg, Germany
Seahorse XFp-Flux-Pack	Agilent Technologies; Santa Clara, California

Table 2: Laboratory equipment

Equipment	Manufacturer
5415R centrifuge	Eppendorf; Hamburg, Germany
Chamber for coverslips (Ø 25 mm)	Warner Instruments; Hamden, Conneticut
FACS Celesta™	BD Biosciences; Franklin Lakes, New Jersey
Heracell 150 Incubator	Thermo Fisher Scientific; Carlsbad, California
Laminar Flow Hood	Thermo Fisher Scientific; Carlsbad, California
Megafuge 1.0 centrifuge	Heraeus; Hanau, Germany
Mikro 220R centrifuge	Hettich; Tuttlingen, Germany
Pipet controller accu-jet® pro	Brand; Wertheim & Grossostheim, Germany
Pipettes	Eppendorf; Hamburg, Germany
Seahorse XFp Flux Analyser	Agilent Technologies; Santa Clara, California
VarioSkan plate reader	Thermo Fisher Scientific; Carlsbad, California

2.1.2 Chemicals, reagents, and kits

Table 3: Chemicals and reagents

Chemical and reagent	Manufacturer
Accutase	Gibco by Life Technologies; Carlsbad, California
Advanced DMEM/F12	Gibco by Life Technologies; Carlsbad, California
Antimycin A	Biomol GmbH; Hamburg, Germany
Ascorbic acid (Vitamin C)	Carl Roth; Karlsruhe, Germany
Astrocyte Medium (ScienCell)	Provitro AG; Berlin, Germany
B-27 Plus Supplement	Thermo Fisher Scientific; Carlsbad, California
CryoStor CS10	STEMCELL Technologies; Vancouver, Canada
Culture One Supplement	Thermo Fisher Scientific; Carlsbad, California
Cytosine arabinoside (Ara-C)	Biomol GmbH; Hamburg, Germany
Dibutyryl-cAMP (dcAMP)	STEMCELL Technologies; Vancouver, Canada
DMEM/F12	Gibco by Life Technologies; Carlsbad, California
DMSO	Sigma-Aldrich; St. Louis, Missouri
DPBS	Gibco by Life Technologies; Carlsbad, California
FCCP	Biomol GmbH; Hamburg, Germany
FBS	Sigma-Aldrich; St. Louis, Missouri
Fluorescent Mounting Medium	Dako; Carpinteria, California
Fura-2/AM	Hölzel Biotec; Köln, Germany
Geltrex LDEC	Thermo Fisher Scientific; Carlsbad, California
Glucose	Carl Roth; Karlsruhe, Germany
GlutaMax (100x)	Gibco by Life Technologies; Carlsbad, California
H2DCFDA	Invitrogen by Life Technologies; Carlsbad, California
HBSS	Sigma-Aldrich; St. Louis, Missouri
Hoechst	Thermo Fisher Scientific; Carlsbad, California
Isopropyl alcohol	Carl Roth; Karlsruhe, Germany
ImmersolTM 518 F Immersion Oil	Carl Zeiss; Jena, Germany
JC-1	Invitrogen by Life Technologies; Carlsbad, California
Laminin	Sigma-Aldrich; St. Louis, Missouri
L-Glutamine	Sigma-Aldrich; St. Louis, Missouri
Matrigel	Corning Incorporated; Tewksbury, Massachusetts
MitoSOX Red	Invitrogen by Life Technologies; Carlsbad, California
MitoTracker Green	Invitrogen by Life Technologies; Carlsbad, California

N2-Supplement	Thermo Fisher Scientific; Carlsbad, California
Neurobasal Medium	Gibco by Life Technologies; Carlsbad, California
Neurobasal Medium Plus	Gibco by Life Technologies; Carlsbad, California
Non-essential amino acids	Gibco by Life Technologies; Carlsbad, California
Normal goat serum	Thermo Fisher Scientific; Carlsbad, California
Oligomycin	Biomol GmbH; Hamburg, Germany
Opti-MEM	Gibco by Life Technologies; Carlsbad, California
Paraformaldehyde	Carl Roth; Karlsruhe, Germany
Penicillin-Streptomycin Solution	Sigma-Aldrich; St. Louis, Missouri
Pluronic 10% F127	Thermo Fisher Scientific; Carlsbad, California
Poly-L-ornithine solution	Sigma-Aldrich; St. Louis, Missouri
PSC Neural Induction Supplement (50x)	Gibco by Life Technologies; Carlsbad, California
Pyruvate	Sigma-Aldrich; St. Louis, Missouri
rH-BDNF	PreproTech; Rocky Hill, USA
rH-GDNF	PreproTech; Rocky Hill, USA
Rhod-2/AM	Hölzel Biotech; Köln, Germany
Rotenone	Biomol GmbH; Hamburg, Germany
Seahorse XF DMEM assay medium, pH 7.4	Agilent Technologies; Santa Clara, California
Sodium pyruvate	Gibco by Life Technologies; Carlsbad, California
STEMdiff Nural Progenitor Freezing Medium	STEMCELL Technologies; Vancouver, Canada
Triton X-100	Sigma-Aldrich; St. Louis, Missouri
Trypan Blue	Sigma-Aldrich; St. Louis, Missouri

Table 4: Kits

Kit	Manufacturer
CellTiter-Glo® Cell Viability Assay	Promega; Madison, Wisconsin
Pierce™ BCA Protein Assay	Thermo Fisher Scientific; Carlsbad, California
8-isoprostane ELISA Kit	Cayman Chemical; Ann Harbor, Michigan

2.1.3 Culture media and buffer composition

Table 5: Buffer and media

Buffer/Media	Composition
Astrocyte Medium	Astrocyte Medium (ScienCell) 2% FBS 1% Astrocyte growth supplement
Neural Induction Medium (NIM)	Neurobasal Medium 2% Neural Induction Supplement 0.5% Penicillin/Streptomycin
Neural Expansion Medium (NEM)	48.75% Neurobasal Medium 48.75% Advanced DMEM/F12 2% Neural Induction Supplement 0.5% Penicillin/Streptomycin
Neuronal Medium	Neurobasal Medium 1% B27 Plus 0.5% GlutaMax 0.5% non-essential amino acids 0.5% CultureOne 200 nM Ascorbic acid 20 ng/mL BDNF 20 ng/mL GDNF 1 mM dibutyryl-cAMP 100 µg Laminin 50 U/mL Penicillin 50 µg/mL Streptomycin
Seahorse Assay Medium (pH 7.4)	1 mM Pyruvate 2 mM L-Gultamine 10 mM Glucose Seahorse XF DMEM assay medium
Antibody Buffer (pH 7.4)	0.1% Triton X-100 2% goat serum 1x PBS
Blocking Buffer (pH 7.4)	0.5% Triton X-100 10% goat serum 1x PBS
Ringer's Solution (pH 7.4)	140 mM NaCl 5 mM KCl 2 mM $CaCl_2$ 1 mM $MgCl_2$ 10 mM HEPES 5 mM Glucose
Intracellular patch-clamp solution	140 mM KCl 1 mM $MgCl_2$ 0.1 mM $CaCl_2$ 5 mM EGTA 10 mM HEPES

2.2 Methods

2.2.1 Cell culture methods

2.2.1.1 Skin biopsy and primary human fibroblasts cultivation

Skin biopsies were conducted by the Department of Dermatology, University Hospital of Regensburg, Germany. The study was approved by University of Regensburg's ethics committee (ref: 13-101-0271), and all participants provided written informed consent.

Biopsy samples of healthy skin were sectioned into smaller pieces, and distributed into a 6-well plate (Sarstedt). They were allowed to attach for 5-7 min and covered with primary fibroblast medium (PrimFibM) (Table 5). The primary fibroblasts were then cultured for a period of 2–3 weeks under standard conditions (37 °C and 5% CO_2) until they reached confluency. Cells were split, amplified and stored in a robotic storage system (SmartFreezer®, Angelantoni) in the Central Biobank Regensburg at the vapour phase of liquid nitrogen. For splitting, detachment was initiated with 1 mM ethylenediaminetetraacetic acid (EDTA), a chelator of divalent ions (Ca^{2+}, Mg^{2+}) (Invitrogen), in phosphate-buffered saline (PBS, Gibco). Subsequently, the cells were enzymatically detached with Trypsin (Sigma-Aldrich). The reaction was stopped with DMEM/F12. For storage, 1 million cells were frozen in PrimFibM, supplemented with 10% dimethyl sulfoxide (DMSO). For further growth or for experimental purposes, cells were seeded into T75 flasks or 6-well plates, respectively. Cryopreserved fibroblasts were thawed in a 37°C water bath and transferred into pre-warmed DMEM/F12. After centrifugation, the pellet was resuspended in PrimFibM and seeded into a T75 flask.

2.2.1.2 Human induced pluripotent stem cells

Fibroblasts were reprogrammed to induced pluripotent stem cells (iPSCs) using non-integrating episomal plasmid vectors encoding pluripotency-associated genes, also called "Yamanaka factors": KLF4, SOX2, L-MYC, LIN28, OCT3/4, and p53DD (pCXB-EBNS, pCE-hsk, pCE-hUL, pCE-hOCT3/4, and pCE-mp53DD (Addgene plasmid #41857, #41814, #41855, #41813, and #41856, gifted by Shinya Yamanaka)). $5x10^5$ fibroblasts were electroporated with 600 ng of each factor using the Amaxa Nucleofector (Lonza) and cultured in TeSR-E7 medium for 3-4 weeks on Matrigel-coated dishes (Corning, 8.7 µg/cm^2) until colonies appeared. iPSC colonies were manually picked, and cultured on Matrigel with mTeSR Plus medium supplemented with 50 µg/mL Gentamycin. Pluripotency was confirmed by the PluriTest® method, a patented bioinformatics assay for the quality assessment of iPSCs, which was adjusted for next-generation sequencing (Schulze et al., 2016). The medium was changed daily and areas of spontaneous differentiation, characterised by irregular colony morphology, were mechanically removed by aspiration.

For passaging, iPSCs were incubated with 1 U/mL dispase at 37°C until the edges of the colonies started to detach. The dispase was washed off with DMEM/F12 and mTeSR was added. The colonies were broken into small clusters using a 5 mL glass pipette, carefully lifted, and transferred to a fresh Matrigel-coated plate, in a 37°C, 5% CO_2 incubator. iPSCs were passaged at 70-80% confluency with a split ratio of 1:3. iPSCs were cryopreserved in CryoStore CS10 freezing medium in liquid nitrogen. Cryopreserved iPSCs were thawed in a 37°C water bath, transferred into pre-warmed DMEM/F12, and spun down. Fresh mTeSR was added on top of the pelleted colonies and they were resuspended by gentle shaking, before being seeded onto a Matrigel-coated plate.

2.2.1.3 Neural progenitor cells

iPSCs to neural progenitor cells (NPCs) differentiation was carried out following a monolayer culture method developed by Yan *et al.* (Yan et al., 2013). iPSCs were detached into small colonies and plated onto Matrigel-coated plates. On the next day, mTeSR was exchanged for Neural Induction Medium (Table 5). On day 7, the differentiating cells were detached and dissociated using Accutase (Life Technologies), then passed through a 50 µm strainer. After centrifugation, cells were resuspended in Neural Expansion Medium (NEM) (Table 5). Cells were then maintained and expanded on Geltrex-coated dishes (0.5mg/mL) at a density of $1x10^5$ cells per cm^2. Cells were passaged, strained, and treated overnight with 5 µM ROCK inhibitor to favour attachment until passage 5, at which point a pure culture of NPCs was obtained. NPCs were cryopreserved in STEMdiff Neural Progenitor Freezing Medium in liquid nitrogen. NPCs were thawed in a 37°C water bath, transferred into pre-warmed DMEM/F12, and centrifuged. Pellets were resuspended in fresh NEM and plated onto Geltrex-coated plates.

2.2.1.4 Astrocytes

NPCs were differentiated into astrocytes following a protocol adapted from Tcw *et al.*, 2017. $3x10^4$ carefully dissociated NPCs were seeded on Matrigel-coated plates in astrocytes medium (Table 5). Upon confluency, cells were detached using Accutase and $3x10^4$ cells were plated in new Matrigel-coated wells. After 30 days of differentiation, identity and maturity of the astrocytes were confirmed with immunostainings of typical astrocytes markers (GFAP, S100β, connexin 43, EAAT1, ALDH1L1). Astrocytes were used until day 60. Additionally, astrocytes were expanded and frozen in astrocyte medium supplemented with 20% FBS and 10 % DMSO between days 20 and 35 of differentiation. Astrocytes were thawed in a 37°C water bath, transferred into pre-warmed DMEM/F12 and centrifuged. The astrocytes pellet was resuspended in fresh astrocyte medium and seeded onto Matrigel-coated plates.

2.2.1.5 Neurons: Neuronal differentiation and cultivation

For neuronal differentiation, NPCs from passages 5 to 12 were plated onto polymer imaging µ-dishes (Ibidi) coated with 20% poly-L-ornithine in PBS and 43 µg/mL laminin in DMEM/F12, both overnight at 37°C. On the next day, the medium was changed to Neuronal Medium (day 1) (Table 5). Cells were differentiated for 21 days, with half of the medium changed every 3 to 4 days, and kept in 37°C, 5% CO_2 incubator. In order to remove proliferating cells, the cultures were treated with the mitotic inhibitor cytarabine (Biomol) at 1µM from day 5 to day 6 or 7.

2.2.2 Biochemical methods

2.2.2.1 Lipid peroxidation ELISA

The levels of the lipid peroxidation marker 8-isoprostane were measured in fibroblasts and NPCs culture supernatants, using the 8-isoprostane ELISA Kit (Cayman Chemicals), according to the manufacturer's instructions. Fibroblasts or NPCs were plated in serum-free medium. When confluent, cells were detached and counted, and supernatants were collected and frozen with 1:1000 antioxidant butylated hydroxytoluene to protect lipids from degradation. Supernatants were measured in triplicate in the ELISA plate. Absorbance was measured at a wavelength of 420 nm using the VarioSkan (Thermo Fisher Scientific). 8-isoprostane concentrations were calculated using a 0.8 pg/mL to 5 ng/mL standard curve and normalised to the number of cells.

2.2.2.2 Glutathione (GSH/GSSG)

Reduced and oxidized forms of glutathione were measured with the GSH/GSSG-Glo™ assay (Promega) according to the manufacturer's instructions. $5x10^2$ fibroblasts were seeded in duplicates in 96-wells plates. The next day, cells were lysed with either total or oxidized glutathione lysis reagent for 5 min on a plate shaker, at room temperature (RT). Luciferin generation and detection reagents were subsequently added, and incubated at RT for 30 and 15 min, respectively, before recording luminescence using the VarioSkan.

2.2.3 Metabolic analysis

2.2.3.1 Mitochondrial Respiratory Function Analysis: Seahorse XF Flux analysis

Mitochondrial respiration was analysed using Seahorse XFp Flux analyser (Agilent Technologies). The analysis relies on the measurement of oxygen consumption rates (OCR), which reflect the final reduction of oxygen to water during OXPHOS. Sensor probes containing polymer-embedded fluorophores detect OCR in a small volume of medium above the cell monolayer. During the measurement, an integrated drug delivery system injects relevant compounds to measure specific aspects of mitochondrial respiration. In the

Seahorse XFp Mito Stress Test Kit used here, oligomycin, FCCP and rotenone/antimycin A (Biomol) were injected sequentially, to a final concentration of 1 µM for oligomycin, 2 µM (fibroblasts, astrocytes) or 1 µM (NPCs) for FCCP, and 0.5 µM for rotenone/ antimycin A. The OCR after injection of each compound allows the calculation of **six respiratory parameters** (Figure 3). Before any injection, **basal respiration (1)** reflects the baseline level of mitochondrial respiration to meet normal ATP demand. Oligomycin inhibits complex V of the ETC, ATP synthase, thereby leading to a decrease of OCR, corresponding to ATP synthesis (**ATP-related OCR (2)**). The remaining oxygen consumption after ATP synthase inhibition corresponds to **proton leak (3)**. The injection of FCCP facilitates the movement of protons back to the matrix, thereby dissipating the proton gradient, which would usually be harnessed to produce ATP. Respiration is uncoupled from ATP synthesis. To maintain the proton gradient, the ETC increases electron flow, which mimics physiological energy demand and reveals the maximal capacity of OXPHOS (**maximal respiration (4)**). **Spare respiratory capacity (5)** (SCR) represents the absolute increase in OCR between baseline and maximal respiration. SCR reflects a cell's adaptation faculties in response to increased energy demand or stress. Rotenone and antimycin A inhibit complex I and complex II, respectively. At this stage, mitochondrial respiration is completely inhibited, and the remaining oxygen consumption reflects **non-mitochondrial respiration (6)** (Figure 3).

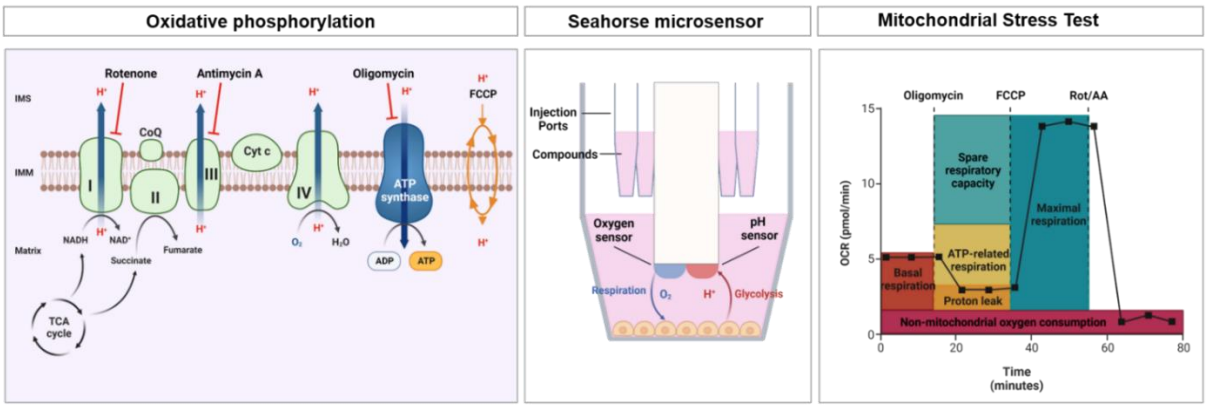

Figure 3: Measure of mitochondrial respiration with the Seahorse XFp Flux Analyser. (Left) Several inhibitors are used to inhibit different parts of the respiratory chain and reveal different respiratory parameters. Oligomycin inhibits the ATP synthase, FCCP uncouples respiration, and a mixture of rotenone and antimycin A inhibits complex I and III. **(Middle)** Seahorse measurements rely on optical microsensors integrated into the cartridge. In the sensor, two fluorophores measure oxygen (O_2) and protons (H^+) concentrations in real time in live cells and the oxygen consumption rate (OCR) and extracellular acidification rate (ECAR) are calculated. **(Right)** Typical OCR curve obtained with the Agilent Seahorse XF Cell Mito Stress Test, illustrating respiratory states. Created with BioRender.com

The day before the assay, $3x10^4$ (fibroblasts, astrocytes) or $8x10^4$ (NPCs) cells were grown in XFp 8-well miniplates with appropriate coating. The sensor cartridges were hydrated with Seahorse XF Calibrant and placed overnight in a non-CO_2, 37°C incubator. On the day of the assay, cells were covered in Seahorse XF Assay medium (Table 5) and placed in a non-CO_2,

37°C incubator for 30 min. The injection ports of the sensor cartridge were loaded with the test compounds and the XFp flux analyser started calibration. After calibration, the miniplate containing the cells was placed inside the machine and the Mito Stress Test protocol was initiated. Data acquisition and analysis were performed with the Wave software (Agilent). At the end of the assay, cells were fixed in 4% paraformaldehyde (PFA) and the nuclei were stained with Hoechst to normalise the respiration data.

2.2.3.2 Total ATP content quantification

For the quantification of cellular ATP content, $1x10^5$ fibroblasts and astrocytes or $1x10^6$ NPCs were pelleted and stored at -20 °C. The ATP content was measured by CellTiter-Glo®Cell Viability Kit (Promega) according to the manufacturer's instructions. Cell pellets were resuspended in PBS, heated at 100 °C for 2 min to inactivate ATPases, and kept on ice. Triplicates of sample or standard were applied to a black 96-well-plate with CellTiter-Glo®Reagent. Luminescence was measured with the VarioSkan using the SkanIT software. The relative light unit (RLU) was used to calculate the ATP content using a 1 nM to 10 µM standard curve. Concentrations were normalised to protein content, in µg/mL, using a BCA assay (Thermo Fisher Scientific).

2.2.3.3 Substrate availability (NAD/NADH)

To measure substrate availability, $5x10^2$ fibroblasts or $5x10^3$ NPCs were seeded in duplicates 96-wells plates. NAD/NADH ratio was measured with NAD/NADH-Glo™ assay (Promega), according to manufacturer's instructions. Cells were lysed in a base solution containing dodecyl trimethylammonium bromide. For NAD^+ detection, 0.4 N HCl was added to the lysis solution, and the plate was heated at 60 °C for 15 min. Then, NAD^+ and NADH wells were buffered with Trizma® and HCl/Trizma® solutions respectively. NAD/NADH-Glo™ detection reagent was added and incubated for 30 min before recording luminescence using the VarioSkan and the SkanIt software.

2.2.4 Microscopy techniques

2.2.4.1 Immunocytochemical staining

For immunocytochemical staining, astrocytes and NPCs were grown on Geltrex- and Matrigel-coated glass coverslips, respectively, while neurons were differentiated for 21 days in Ibidi dishes. Cells were fixed in 4% PFA and stored in PBS at 4°C. Unspecific binding sites were blocked by applying a serum-containing blocking buffer for 20 min (Table 5). Primary antibodies (Table 6) were incubated overnight at 4°C in antibody solution (Table 5). After washing with PBS, cells were incubated with antibody solution containing fluorochrome-conjugated secondary antibodies (Table 7) and 1:1000 Hoechst to counterstain nuclei

(Sigma-Aldrich), and placed in the dark for 2 hours at RT. Coverslips were mounted on glass slides using Dako Fluorescing Mounting Medium. For Ibidi dishes, the mounting medium was applied on the cells, and covered with a glass coverslip.

Table 6: Primary antibodies used for immunocytochemistry

Antibody	Host	Dilution	Manufacturer
ALDHL1 (ab87117)	rabbit	1:500	Abcam; Cambridge, UK
EAAT1 (ab416-1001)	rabbit	1:200	Abcam; Cambridge, UK
GFAP (C53893)	mouse	1:400	Sigma-Aldrich; St. Louis, Missouri
MAP-2 (ab5392)	chicken	1:500	Abcam; Cambridge, UK
NeuN (ab177487)	rabbit	1:1000	Abcam; Cambridge, UK
PSD95 (K28/43)	mouse	1:250	UC Davis/NIH NeuroMab Facility; Davis, California
PAX6	mouse	1:10	deposited to the DSHB by Kawakami, A. (DSHB Hybridoma Product PAX6)
S100β (S2532)	mouse	1:1000	Sigma-Aldrich; St. Louis, Missouri
SOX2 (ab97959)	rabbit	1:1000	Abcam; Cambridge, UK
β-III-Tubulin (G712A)	mouse	1:2000	Promega; Madison, USA
VGLUT-1 (ab180188)	rabbit	1:250	Abcam; Cambridge, UK
Connexin 43 (14-4759-82)	mouse	1:500	Invitrogen by Life Technologies; Carlsbad, California

Table 7: Secondary antibodies used for immunocytochemistry

Antibody	Host	Dilution	Manufacturer
Alexa Fluor® 488 anti-rabbit (A11008)	goat	1:1000	Gibco by Life Technologies; Carlsbad, USA
CY3® anti-mouse (A10521)	goat	1:1000	Gibco by Life Technologies; Carlsbad, USA
CY5® anti-chicken (ab97147)	goat	1:1000	Abcam; Cambridge, UK

2.2.4.2 Fluorescent live-cell imaging

Live-cell imaging experiments were performed using an inverted Zeiss Axio Observer Z.1 microscope equipped with a Fluar 40/1.3 objective lens (Zeiss). All recordings were performed with an AxioCam MRm CCD camera (Zeiss) and using a 40X oil immersion objective. The Lambda DG-4 high-speed wavelength switcher (Sutter Instruments) was used for illumination and image acquisition and the microscope was controlled using the ZEN 2012 imaging software. For the analysis, regions of interest were manually drawn around cells using ImageJ (version 2.9.2). Macros were used for background subtraction, and, where applicable, to calculate ratios, in order to ensure the repeatability of the analysis. Additionally, cell size was measured in Fura-2/AM-loaded cells.

2.2.4.2.1 Analysis of mitochondrial membrane potential with JC-1

The mitochondrial membrane potential (MMP) was measured using the ratiometric fluorophore JC-1 (5,5',6,6'-tetrachloro-1,1',3,3'-tetraethylbenzimidazolylcarbocyanineiodide). JC-1 is a membrane-permeable cationic dye, which enters mitochondria in a potential-dependent manner. When accumulating in mitochondria with high MMP, JC-1 forms red fluorescent aggregates with an emission maximum at 596 nm. Conversely, in mitochondria with lower MMP, JC-1 remains monomeric and emits green fluorescence at 530 nm. The ratio of red to green fluorescence intensity represents MMP, and is not influenced by mitochondrial morphology, dye cellular distribution or concentration.

2.2.4.2.2 Analysis of cytosolic and mitochondrial Ca^{2+} levels with Fura-2/AM and Rhod-2/AM

Cytosolic Ca^{2+} levels were assessed with Fura-2-acetomethyesther (Fura-2/AM). The ester group (AM) ensures that the dye can enter the cell, and is subsequently removed by cellular esterases, regenerating the Fura-2 Ca^{2+} indicator. Fura-2 excitation wavelength shifts upon Ca^{2+} binding, from 380 nm in the unbound state, to 340 nm in the Ca^{2+}-bound state, while peak emission remains steadily around 510nm. The ratio between emitted fluorescence after excitation at 340 nm and at 380 nm ($F_{ratio}340/380$) reflects the amount of intracellular Ca^{2+}.
Measurement of mitochondrial Ca^{2+} was carried out using the dye Rhod-2/AM. Rhod-2/AM is cell permeant thanks to its ester group. Its positive charge will cause it to accumulate in negatively charged mitochondria. Rhod-2 fluorescence emission at 580 nm increases with increasing Ca^{2+} levels, making it an intensity-based Ca^{2+} sensor.

2.2.4.2.3 Experimental procedure for live-cell imaging

One day prior to the live-cell experiment, $1.5x10^5$ fibroblasts, $1.5x10^5$ astrocytes or $2x10^6$ NPCs were plated on uncoated, Matrigel- or Geltrex-coated glass coverslips, respectively. For neurons, $3.5x10^4$ NPCs were plated, and differentiated for 21 days on PLO/laminin-coated Ibidi dishes. On the day of the experiment, the dyes were mixed at a ratio of 1:2 with the non-ionic poloxamer Pluronic F-127 to ensure good solubilisation, and diluted in OptiMEM. For MMP measurement, cells were loaded with JC-1/Pluronic. The JC-1 concentration used was 300 nM in fibroblasts and astrocytes, and 1 µM in NPCs and neurons. For calcium measurements, cells were loaded with 2 µM Fura-2/AM/Pluronic and 2 µM Rhod-2/AM/Pluronic. Cells were then incubated at 37 °C for 30 min. The cells were washed and covered with Ringer's solution containing glucose (300 mosmol/kg).

JC-1 fluorescence was measured at 537/42 nm (green) and 620/60 nm (red), after excitation at 480/36 nm. In neurons, neurites and somas appeared on different focus planes, and were imaged separately.

Fura-2 fluorescence was measured at 510 nm after excitation at 340 or 380 nm. Rhod-2 fluorescence was measured at 576 nm after excitation at 556 nm. In neurons, in addition to basal cytosolic Ca^{2+} measurements, spontaneous Ca^{2+} peaks were recorded over 20 min with 2 Hz frequency using the Fluar 20X/0.75 objective lens. Spikes were analysed with the software IGOR Pro 9 (WaveMetrics).

2.2.5 Flow cytometry analyses

Flow cytometry was used to detect cytosolic and mitochondrial ROS, and mitochondrial content using specific fluorescent dye. DCFDA (2',7'-dichlorofluorescein diacetate) was used to detect cytosolic hydrogen peroxide and peroxyl radicals, mitochondrial superoxide was detected with MitoSOX, and mitochondrial mass was investigated using MitoTracker Green. Fibroblasts, NPCs, and astrocytes were first harvested and centrifuged.

For DCFDA staining, cells were resuspended in FACS buffer (DPBS supplemented with 2% FBS) with 10 µM DCFDA. After 20 min at 37 °C, cells were washed with cold DPBS.

For MitoSOX staining, cells were washed and resuspended in Hank's Balanced Salt Solution (HBSS) with 5 µM MitoSOX, and incubated at 37 °C for 30 min. Then, cells were washed with FACS buffer.

For MitoTracker Green staining, cells were resuspended in RPMI 1640 medium containing 2 mM L-glutamine and 1 µM MitoTracker Green, and incubated at 37°C for 1 hour. Mitochondrial depolarisation was prevented by adding 1.5 µM cyclosporin A.

Immediately before measurement, cells were washed again in FACS buffer and filtered into FACS tubes. Fluorescence was measured in single cells with the violet (405 nm), blue (488 nm) and red (640 nm) lasers of the BD Biosciences FACS Celesta™. The cytometer was run by the Diva software v7.0 (BD Biosciences), and set to record $2x10^4$ events for fibroblasts and astrocytes, and $1x10^5$ events for NPCs. The analysis was performed with FlowJo software (V10.8., Tree Star).

2.2.6 Electrophysiological measurements

Whole-cell patch-clamp recordings were performed on induced neurons during their 4th week of differentiation. Micropipettes were made of borosilicate glass (Science Products) by means of a horizontal pipette puller (Zeitz Instruments) and fire-polished to obtain a series resistance of 3-5 MΩ. Micropipettes were filled with intracellular solution (Table 5). A reference electrode was dipped into the recording chamber, containing the neurons in bath solution (Ringer's solution with glucose, Table 5). The micropipette was brought into contact

with a cell using a micromanipulator (Scientifica). Gentle suction was applied to establish a tight seal ("gigaohm seal") between the pipette tip and the membrane. The whole-cell configuration was achieved by rupturing the sealed membrane patch by further suction. The resting membrane potential (RMP) and capacitance were recorded directly after reaching the whole-cell configuration. The liquid-liquid junction potential was calculated to be 4 mV (LJP calculator of the pClamp software suite, Axon Instruments) but not corrected. The series resistance was assessed but not compensated. For voltage-clamp recordings, membrane potential was held at -80 mV and depolarised in steps of 10 mV to evoke voltage-activated Na^+- and K^+-channels. Spontaneous postsynaptic currents were recorded while holding the membrane potential at –80 mV. In current-clamp mode, manually adjusted currents were injected to hyperpolarise the membrane potential to about -80 mV or –50 mV, and to record spontaneous action potentials.

Additionally, an 8-channels pressurised perfusion system (ALA Scientific) was employed for the acute application of compounds during recordings. GABA (10 µM) and glutamate (10 µM) solutions were prepared, passed through a 0.45 µm filter and placed into syringe reservoirs. The flow speed was controlled by adjusting the pressure and the valve controller allowed the delivery of the compounds. Air bubbles were pushed out of the tubing before each experiment. During recording, a constant flow of Ringer's solution or compounds diluted therein was applied. Recordings were performed at RT using an EPC-10 amplifier (HEKA Electronic). Data were analysed using Patchmaster Next (HEKA Electronic). Cells with RMP of 0 mV and above or without inward Na^+ currents were excluded from the analysis.

2.2.7 Statistical analysis

Graphical depiction and statistical analysis were conducted with Graph Pad Prism 9.5.1 (GraphPad Software). For all experiments, except patch-clamp recordings, the means of two to three technical replicates were calculated and two to three biological replicates were averaged. A technical replicate refers to the same experimental procedure being repeated multiple times on the same sample. Biological replicates refer to independent samples. Measurements were conducted pairwise allowing direct comparison. Statistical outliers were detected and eliminated using ROUT-Method, except for the number of events in spontaneous activity experiments (post-synaptic currents and action potentials). Results of spontaneous activity were compared by Fisher's exact test. All results showed variance homogeneity and were compared using paired Student's *t*-Test. Results were presented as mean ± SEM. *p*-value limit for statistical significance was set to ≤ 0.05. Significant differences were indicated with * (p<0,05), ** (p<0,005), *** (p<0,0005) and **** (p<0,0001).

3 Results

To better understand the neurobiological mechanisms behind Major Depressive Disorder (MDD), cellular and mitochondrial functions were studied in a human cellular model consisting of cells derived from a cohort of 16 MDD patients and 16 matched non-depressed controls. Dermal fibroblasts were first characterised (Kuffner et al., 2020), then induced pluripotent stem cells (iPSCs) were generated. These iPSCs were subsequently differentiated into neural progenitors (NPCs) and induced neurons, which were also investigated (Triebelhorn et al., 2022).

In this study, a deeper exploration into the potential role of mitochondrial dysfunction in MDD was undertaken. Two specific patients were closely examined: one diagnosed with a mitochondriopathy (referred to as "Mito"), and a MDD patient who was not responsive to antidepressant treatments (referred to as "Non-R"). Results for these case study patients were compared with those of age and sex-matched healthy controls: Non-R with Control 17 (Ctl17) and Mito with Control 18 (Ctl18). Additionally, these findings were compared with changes that were observed between the larger MDD and control cohorts (Kuffner et al., 2020; Triebelhorn et al., 2022).

3.1 Fibroblasts from the Non-R and the Mito patient show altered bioenergetic properties

To investigate the activity of the oxidative phosphorylation system (OXPHOS) as a crucial function of mitochondrial metabolism, the oxygen consumption rate (OCR) was measured in the fibroblasts of patients and sex- and age-matched healthy controls. Figure 4A and Figure 4B show representative Seahorse measurements obtained with the Agilent Seahorse XF Cell Mito Stress Test and represent the OCR at different respiratory states in Non-R and Mito patients, respectively.

In the MDD cohort, OCR was significantly decreased across most assessed parameters (Figure 4C). Likewise, Mito patient’s fibroblasts exhibited a lower OCR in most parameters, except for basal respiration and proton leak (Figure 4C). Intriguingly, the Non-R patient showed generally higher OCR. Maximal respiration, spare respiratory capacity, and proton leak were particularly increased in this patient, compared to its matched control, and to the broader MDD and control cohorts (Figure 4C).

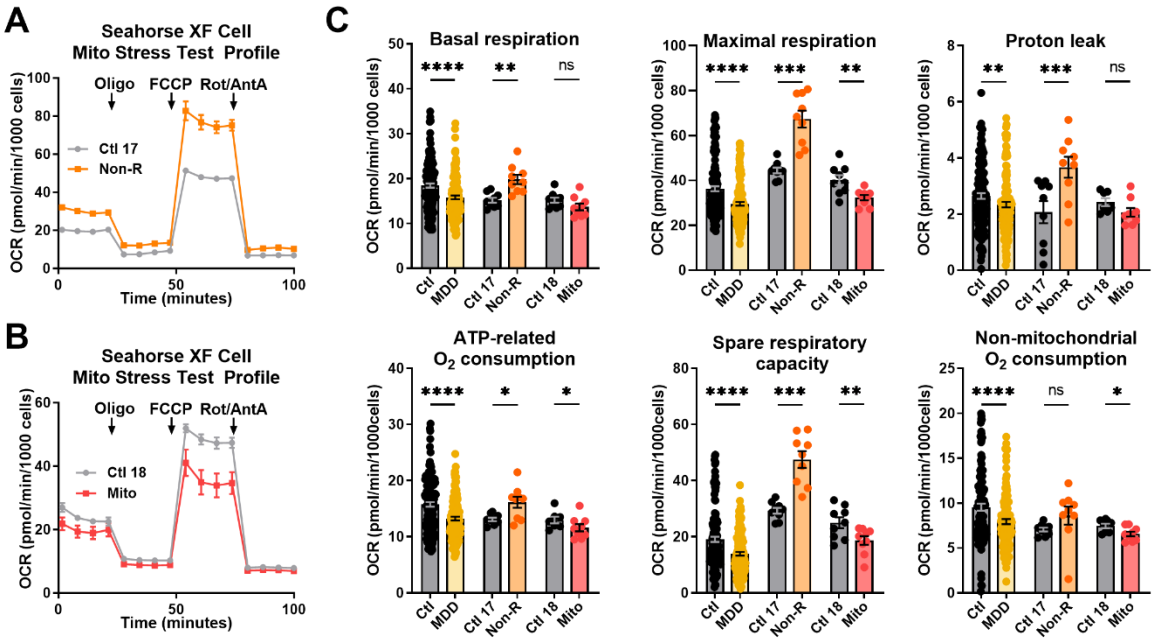

Figure 4: Mitochondrial respiration in fibroblasts. The oxygen consumption rate (OCR) was measured following the Agilent XF Mito Stress Test protocol consisting of sequential injections of oligomycin (Oligo), carbonyl cyanide-4-(trifluoromethoxy)-phenylhydrazone (FCCP) and rotenone/antimycin A (Rot/AntA) to reveal different respiratory parameters. Representative OCR curves are shown for **(A)** Ctl 17 and Non-R and **(B)** Ctl 18 and Mito. **(C)** Key respiratory parameters were compared between fibroblasts from patients and corresponding controls. Data are presented as mean OCR values ± SEM and were analysed using paired t-tests.

To further characterise the bioenergetics properties in our patients' cells, the concentration of ATP, the primary product of the ETC, NAD coenzyme oxidation ratio, as a measure of substrate availability, and mitochondrial content were assessed. While significant variations in OXPHOS activity were apparent in patients' fibroblasts, no substantial differences in ATP levels, the NAD/NADH ratio, and mitochondrial content were observed (Figure 5).

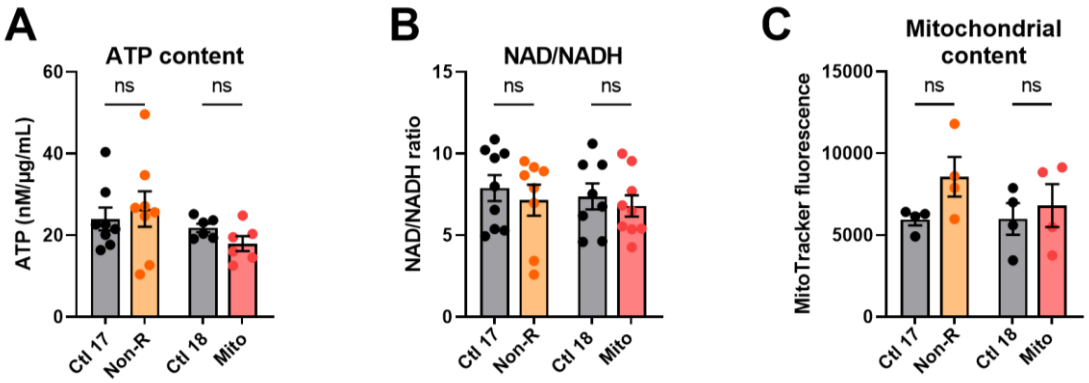

Figure 5: Bioenergetics parameters in fibroblasts. (A) ATP content was measured using a luminescent assay and normalised to protein amount. Bar plot shows nM ATP per µg/mL proteins ± SEM **(B)** Substrate availability was estimated by measuring the NAD/NADH ratio with a colorimetric assay. Bar plots represent mean NAD/NADH ratio ± SEM **(C)** Mitochondrial content was measured using flow cytometry and is indicated by MitoTracker Green mean fluorescence ± SEM, $2x10^4$ events were recorded for each replicate. All data were analysed using paired t-tests.

The mitochondrial membrane potential (MMP) serves as an indirect measure of the mitochondria's metabolic activity and capacity, reflecting the accumulation of protons in the intermembrane space. It was assessed using the potential-dependent ratiometric dye JC-1. Fibroblasts from both the MDD patients and the Mito patient showed a lower MMP compared to their respective controls (Figure 6A). However, despite the markedly increased respiration in the Non-R patient, the MMP remained unchanged (Figure 6A).

Cellular Ca^{2+} homeostasis, which is crucial to mitochondrial function, is influenced by energy-intensive active transport processes, and relies on both chemical and electrical gradients. This homeostasis plays an essential role in signalling, enzyme function, and metabolism. Using the live-cell imaging dyes Fura-2/AM and Rhod-2/AM, cytosolic and mitochondrial Ca^{2+} levels were investigated. Consistent with results from the MDD cohort, no significant changes in cytosolic Ca^{2+} levels were observed in the case study patients (Figure 6B). However, alongside increased respiration, a significant increase in mitochondrial Ca^{2+} was detected in the Non-R patient, while there was no change in the Mito patient (Figure 6C). Additionally, as found in the MDD cohort, there was a significant reduction in the size of the fibroblasts of both case study patients, when assessed in Fura-2/AM loaded cells (Figure 6D). This finding is consistent with the hypothesis of a bioenergetics dysregulation in patients' cells, which could also lead to morphological changes.

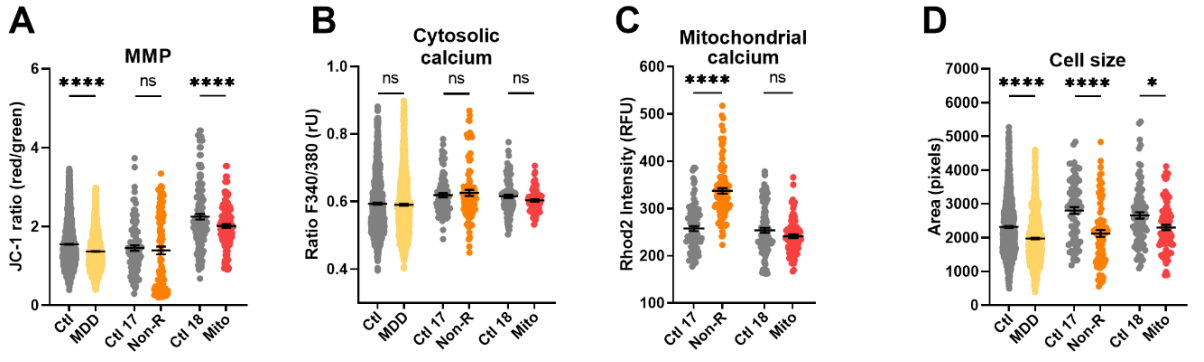

Figure 6: Mitochondrial membrane potential, calcium, and cell size in fibroblasts. (A) MMP was measured with the JC-1 dye and is indicated by the fluorescence ratio between JC-1 aggregates (red) over JC-1 monomers (green). Dot plot shows mean red/green ratios ± SEM. **(B)** Cytosolic calcium was measured as the Fura-2 fluorescence ratio F340/380, and is represented as mean ratio ± SEM **(C)** Mitochondrial calcium levels were measured using Rhod-2/AM/AM and is presented as mean fluorescence intensity, in relative fluorescent unit ± SEM **(D)** Cell size is analysed by assessing area (pixels) of Fura-2/AM-loaded cells. Dot plot shows the number of pixels ± SEM. All data were analysed using paired t-tests.

3.2 Redox homeostasis is partly affected in Non-R and Mito patient's fibroblasts

Mitochondria play a pivotal role in maintaining cellular redox homeostasis as primary producers of ROS at complex I and III of the ETC. While ROS are critical for signalling functions (Sies & Jones, 2020), excessive amounts can lead to oxidative stress and

molecular damage, such as lipid peroxidation (Scholz et al., 2003). The cells' redox balance is maintained with the help of the antioxidant system, including glutathione.

To investigate ROS levels in our case study patients' cells, cytosolic ROS and mitochondrial superoxide were measured using the DCFDA and MitoSOX dyes, respectively, in flow cytometry. There was no noticeable difference in cytosolic ROS, however, a significant increase in mitochondrial superoxide was observed in fibroblasts from the Non-R patient (Figure 7A and B), consistent with a hyperactive ETC, as previously noted in respirometry experiments (Figure 4C). Lipid peroxidation, reflected by 8-isoprostane concentration, was significantly increased in the Mito patient's fibroblasts (Figure 7C). Concurrently, the GSH/GSSG ratio was significantly decreased, indicating higher glutathione oxidation (Figure 7D). This suggests a potential oxidative stress and lower antioxidant capacity in the Mito patient's cells.

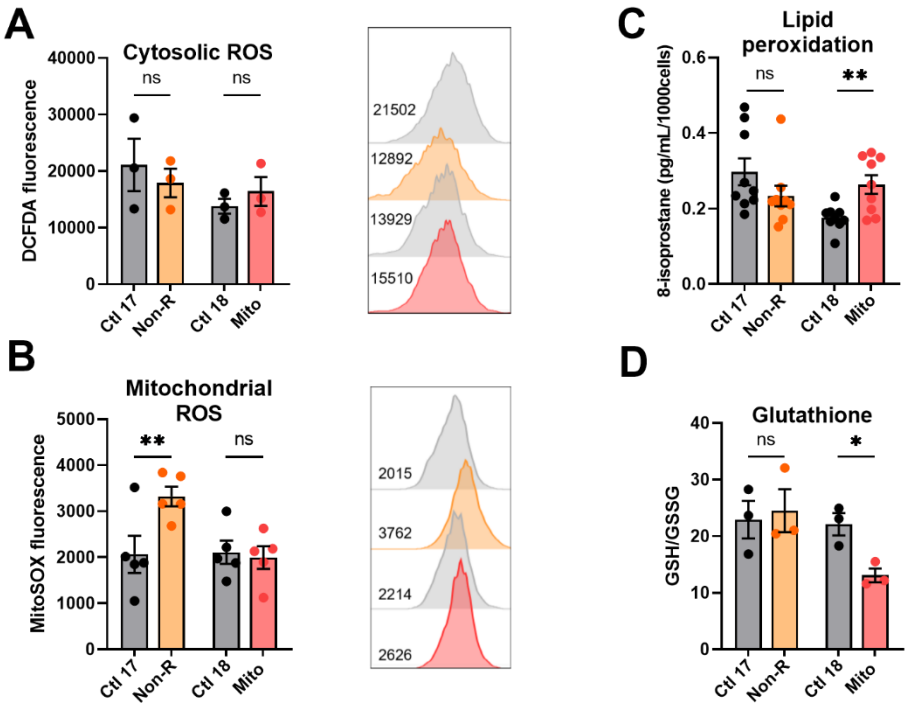

Figure 7: Oxidative stress indicators in fibroblasts. (A) Cytosolic reactive oxygen species (ROS) and **(B)** mitochondrial superoxide levels were measured using flow cytometry and are indicated by DCFDA and MitoSOX mean fluorescence, respectively. Bar plots show mean fluorescence ± SEM. $2x10^4$ events were recorded for each replicate. On the right of each graph, with matching colour coding and order, are representative histograms showing fluorescence (x-axis) and cell count (y-axis). Numbers indicate mean fluorescence. **(C)** Lipid peroxidation was estimated by measuring 8-isoprostane concentration in cell culture supernatants, and normalised to the number of cells. The bar plot shows mean 8-isoprostane concentration in pg/mL/1000 cells ± SEM. **(D)** Antioxidant system function was estimated with the ratio of reduced (GSH) to oxidised (GSSG) glutathione using a luminescent assay. The bar plot represents the mean GSH/GSSG ratios ± SEM. All data were analysed using paired t-tests.

A broader analysis of cellular and mitochondrial lipids using an untargeted lipidomics approach did not reveal any marked alterations in the lipid composition of Mito or Non-R patient fibroblasts (data not shown).

3.3 Induced neural progenitor cells of patients show altered bioenergetics properties

To further investigate bioenergetics properties of neural cells, the patients' primary skin fibroblasts were reprogrammed to iPSCs by transient episomal transduction, and differentiated to neural progenitor cells (NPCs). Immunocytochemical stainings with the neural progenitor markers SOX2 and PAX6 confirmed that our differentiation protocol yielded NPCs (Figure 8).

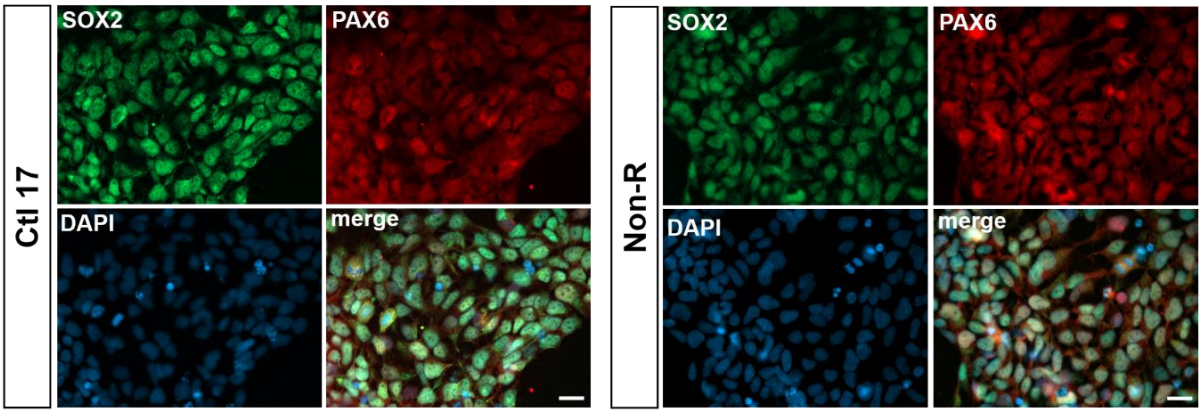

Figure 8: Neural progenitor cells markers. Example images show that SOX2 and PAX6 are co-expressed by a majority of the NPCs differentiated from Ctl 17 and the Non-R patient. Scale bar indicates 20 µm. Quantifications are presented in **Table 8**.

The percentages of cells positively labelled with the respective antibodies, presented in Table 8, indicate that most cells co-expressed both neural progenitor markers.

Table 8: Generation of SOX2 and PAX6 positive iPSC-derived NPCs. Numbers represent proportion of SOX2 and PAX6 positive cells in the analysed cell lines in percent.

Cell line	SOX2 positive (%)	PAX6 positive (%)
Ctl 17	90.4	95.0
Non-R	90.5	94.6
Ctl 18	90.9	95.4
Mito	93.4	96.0

After fibroblasts, mitochondrial respiration was measured in the iPSC-derived NPCs from the Non-R and Mito patients and their controls. Figure 9A and B show representative Seahorse Mito Stress Test measurements in Non-R and Mito patient, and their controls, respectively. NPCs from the MDD cohort had significantly lower respiration in all parameters measured (Figure 9C). In line with findings in fibroblasts, an increase in several respiratory parameters, including basal and maximal respiration, proton leak, and ATP-related oxygen consumption, was observed in NPCs from the Non-R patient. Conversely, NPCs from the Mito patient had

a reduced OCR, characterised by significant decreases in maximal respiration and spare respiratory capacity (Figure 9C).

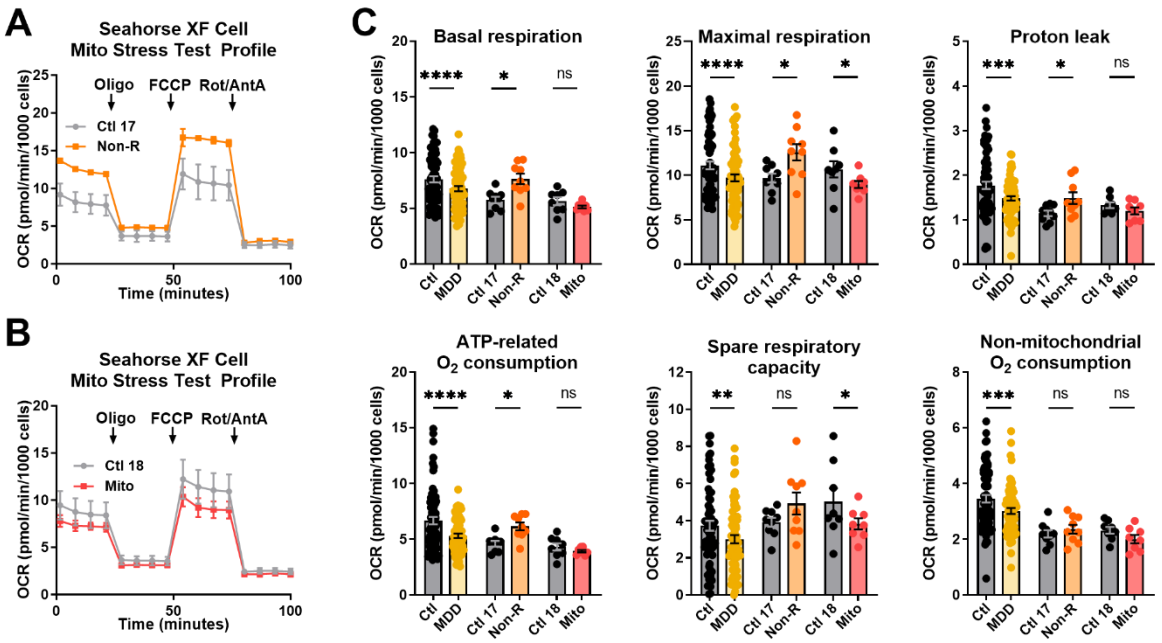

Figure 9: Mitochondrial respiration in neural progenitor cells. The oxygen consumption rate (OCR) was measured following the Agilent XF Mito Stress Test protocol consisting of sequential injections of oligomycin (Oligo), carbonyl cyanide-4-(trifluoromethoxy)-phenylhydrazone (FCCP), and rotenone/antimycin A (Rot/AntA) to reveal different respiratory parameters. Representative OCR curves are shown for **(A)** Ctl 17 and Non-R and **(B)** Ctl 18 and Mito. **(C)** Key respiratory parameters were compared between fibroblasts from patients and corresponding controls. Data are presented as mean OCR values ± SEM and were analysed using paired t-tests.

Following this, further bioenergetics parameters were measured. In NPCs from both patients, no significant differences in cellular ATP levels and mitochondrial content were observed compared to their respective controls, as shown in Figure 10A and C. Notably, an increase in the NAD/NADH ratio was observed in both patients, yet, statistical significance was reached only in the case of the Mito patient (Figure 10B). This suggests potential alterations in substrate availability and a rather oxidative environment in both patients' NPCs.

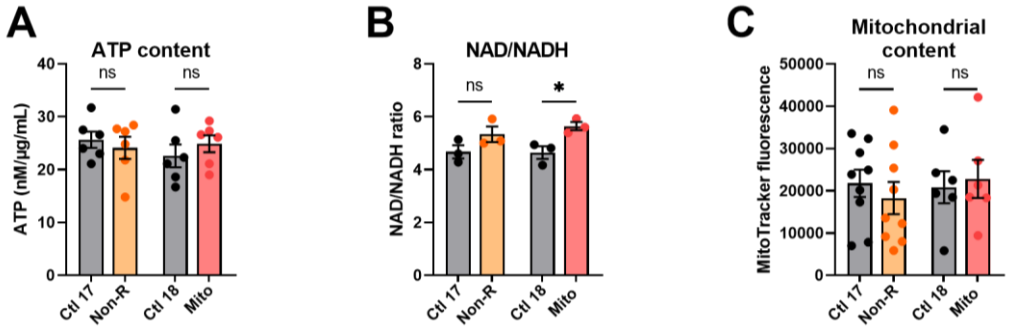

Figure 10: Bioenergetics in neural progenitor cells. (A) ATP content was measured using a luminescent assay and normalised to protein amount. Bar plot shows nM ATP per µg/mL proteins ± SEM **(B)** Substrate availability was estimated by measuring the NAD/NADH ratio with a colorimetric assay. Bar plots represent mean NAD/NADH ratio ± SEM **(C)** Mitochondrial content was measured using flow cytometry and is indicated by MitoTracker Green mean fluorescence ± SEM, $2x10^4$ events were recorded for each replicate. All data were analysed using paired t-tests.

MMP in the Non-R patient and the MDD cohort NPCs did not differ significantly from their respective controls (Figure 11A). However, a significant increase was observed between the Mito patient and its control. Cytoplasmic Ca^{2+} levels in NPCs were higher in both the Mito patient and the MDD cohort, while they did not differ between the Non-R patient and Ctl 17 (Figure 11B). In contrast, mitochondrial Ca^{2+} levels were higher in the Non-R patient's NPCs and lower in the Mito patient's. (Figure 11C). Consistent with observations in fibroblasts, NPCs were significantly smaller in the Mito, Non-R, and MDD patients, compared to their respective controls (Figure 11D).

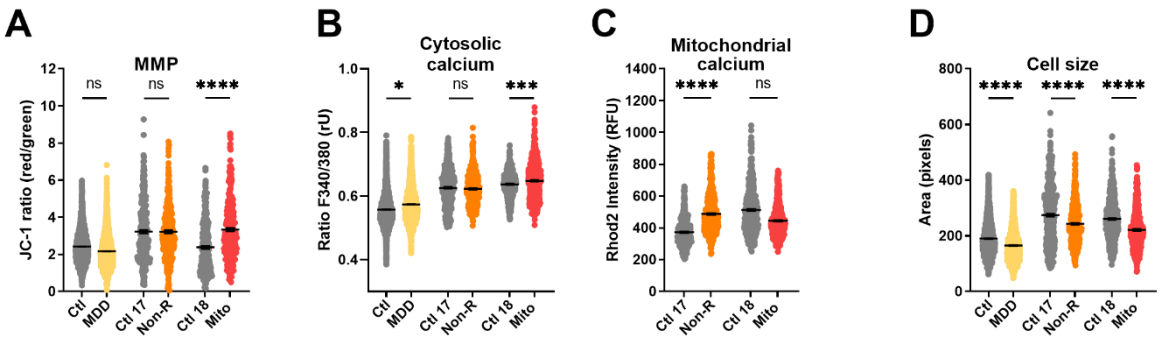

Figure 11: Mitochondrial membrane potential, calcium levels and cell size in neural progenitor cells. (A) MMP was measured with the JC-1 dye and is indicated by the fluorescence ratio between JC-1 aggregates (red) over JC-1 monomers (green). Dot plot shows mean red/green ratios ± SEM. **(B)** Cytosolic calcium was measured as the Fura-2 fluorescence ratio F340/380, and is represented as mean ratio ± SEM **(C)** Mitochondrial calcium levels were measured using Rhod-2/AM and are presented as mean fluorescence intensity, in relative fluorescent unit ± SEM **(D)** Cell size is analysed by assessing area (pixels) of Fura-2/AM-loaded cells. Dot plot shows the number of pixels ± SEM. All data were analysed using paired t-tests.

While there was no clear difference in cellular ROS between NPCs of patients and controls (Figure 12A), as observed in fibroblasts, NPCs from the Mito patient showed a significant increase in mitochondrial superoxide (Figure 12B). Despite a high interindividual variability between the controls, potentially attributable to the age difference (see page 23 for patients' information) (Mecocci et al., 1999; Praticò, 2002), it appeared that lipid peroxidation was decreased in the NPCs of the Non-R patient and increased in the Mito patient (Figure 12C).

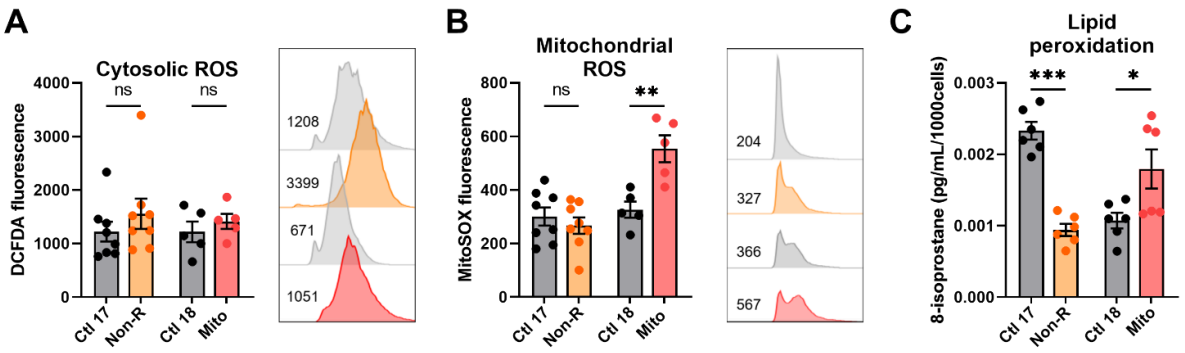

Figure 12: Oxidative stress indicators in neural progenitor cells. (A) Cytosolic reactive oxygen species (ROS) and **(B)** mitochondrial superoxide levels were measured using flow cytometry and are indicated by DCFDA and MitoSOX mean fluorescence, respectively. Bar plots show mean fluorescence ± SEM. $1x10^5$ events were recorded for each replicate. On the right of each graph, with matching colour coding and order, are representative histograms showing fluorescence (x-axis) and cell count (y-axis). Numbers indicate mean fluorescence. **(C)** Lipid peroxidation was estimated by measuring 8-isoprostane concentration in cell culture supernatants, and normalised to the number of cells. The bar plot shows mean 8-isoprostane concentration in pg/mL/1000 cells ± SEM. All data were analysed using paired t-tests.

3.4 Extending the cellular model of MDD to astrocytes

In order to extend our cellular MDD model to another pathology-relevant type of brain cell, the differentiation of NPCs to astrocytes was established, adapting a protocol developed by Tcw *et al.* (Tcw et al., 2017). To validate the differentiation and maturation of the astrocytes, the expression of specific markers was assessed by immunostaining. The markers used were glial fibrillary acidic protein (GFAP), S100 calcium-binding protein β (S100β), glutamate transporter excitatory amino acid transporter 1 (EAAT-1), aldehyde dehydrogenase 1 family member L1 (ALDH1L1), and connexin 43 (Cx43). After 30 days of differentiation, all markers were expressed, as shown in Figure 13A.

The functionality of the mature astrocytes was confirmed by the presence of spontaneous and ATP-elicited Ca^{2+} transients (Figure 13B) (Tcw et al., 2017). Indeed, some Fura-2/AM-loaded cells exhibited spontaneous Ca^{2+} spikes, and most cells responded to a pulse of 100µM ATP with a Ca^{2+} increase, which seemed to propagate as a wave within the culture (Figure 13C). These observations suggested that the obtained astrocytes were capable of responding to external cues with intracellular and intercellular signalling, and expressed functional ATP receptors, altogether suggesting they are able to engage in gliotransmission (Parpura & Zorec, 2010).

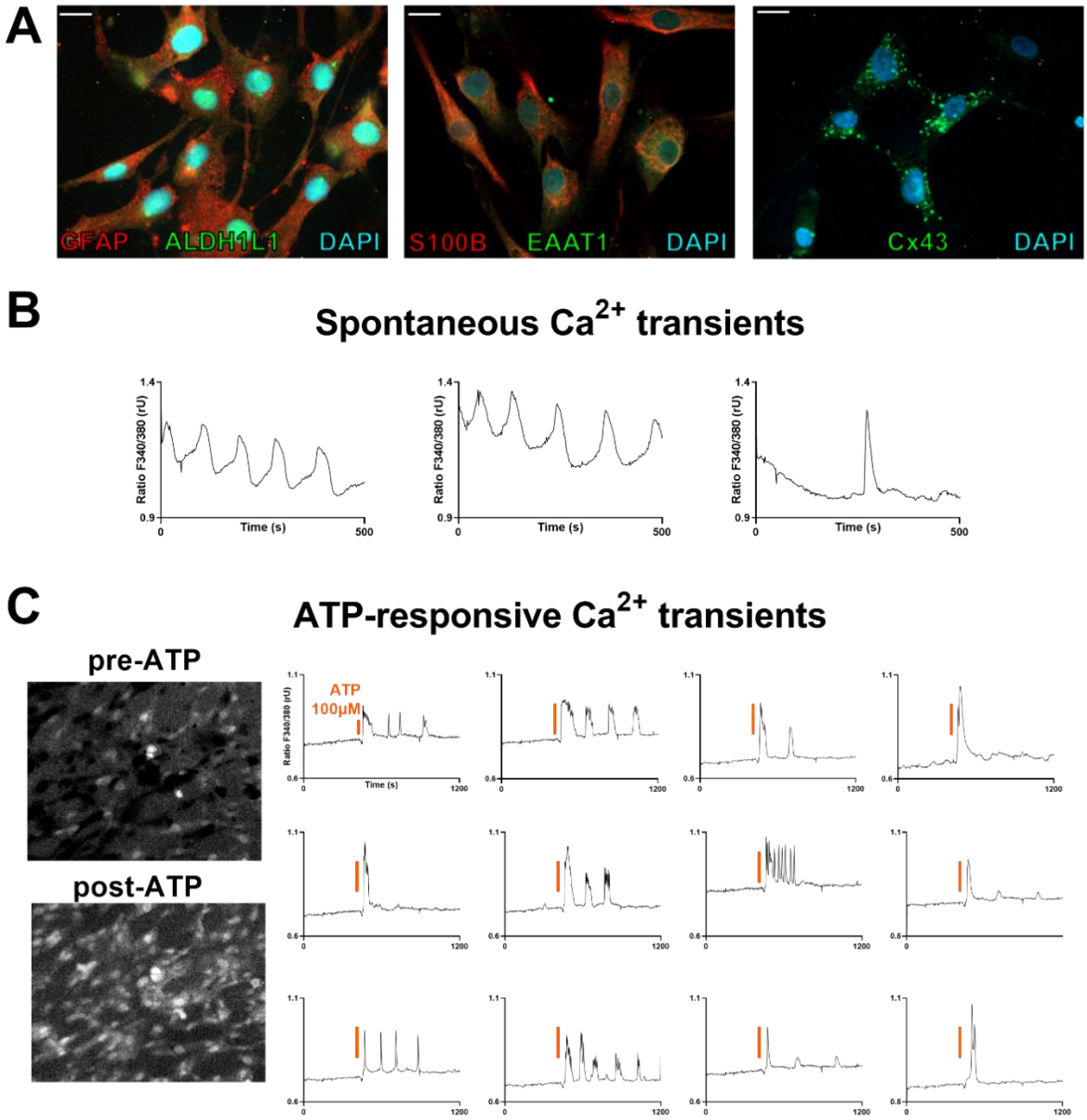

Figure 13: Validation of iPSC-derived astrocytes. (A) Immunofluorescence stainings indicated the expression of mature astrocyte markers, including GFAP, ALDH1L1, S100β, EAAT1 and connexin 43 (Cx43). The scale bar represents 20 µm. Representative traces of Fura-2 fluorescence show that astrocytes exhibited **(B)** spontaneous and **(C)** ATP-responsive calcium transients, both characterising mature and functional astrocytes. ATP was applied to a final concentration of 100 µM, at a time point indicated by the orange bars. On the left, representative Fura-2 ratio images show brighter cells post-ATP treatment, indicating increased intracellular calcium levels.

In addition to the Mito and Non-R patients and their respective controls, astrocytes from subjects of the MDD and control cohort were generated (n=3) to serve as a reference in the present study.

3.5 Induced astrocytes of patients show altered bioenergetics properties and oxidative stress

Mitochondrial functions were investigated in astrocytes by measuring respiration, ATP concentration and mitochondrial content.

Figure 14A and B show representative Seahorse XF Cell Mito Stress Test profiles representing the OCR in different respiratory states in Non-R and Mito patients, respectively. MDD astrocytes displayed significantly reduced basal and maximal respiration as well as ATP-related and non-mitochondrial oxygen consumption (Figure 14C), consistent with findings previously reported in fibroblasts and NPCs. Contrastingly, the basal and maximal respiration of Non-R astrocytes were reduced compared to its control. In astrocytes of the Mito patient, no notable decrease was detected (Figure 14C). These findings suggest that the OXPHOS in astrocytes from both Mito and Non-R patients may be impacted in a differential, cell-dependent manner.

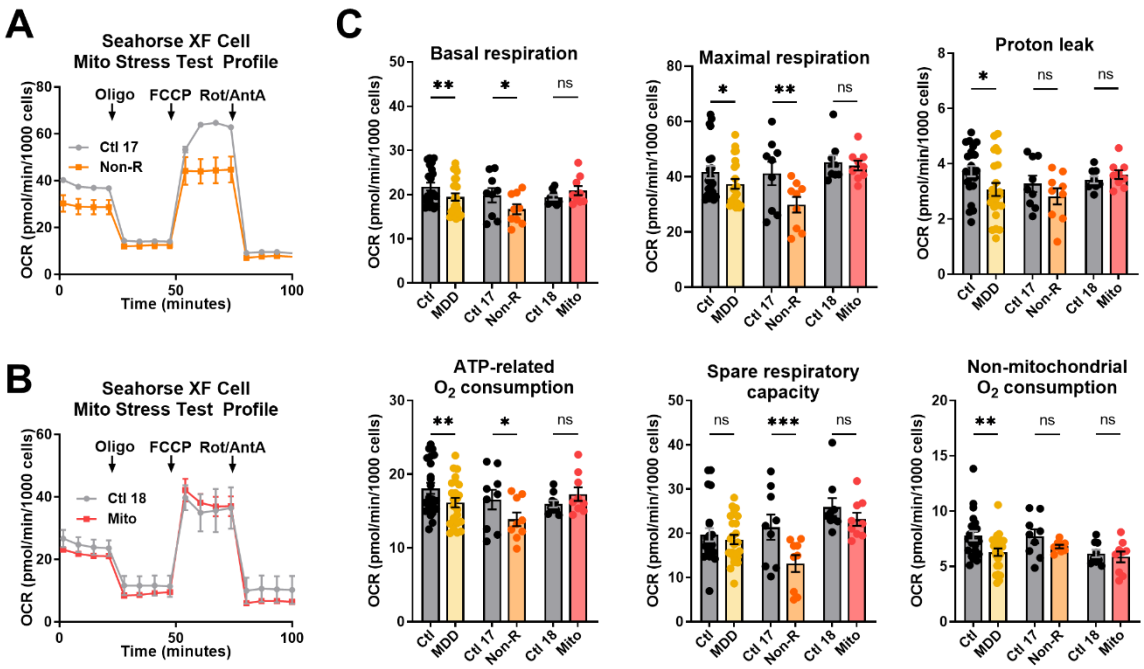

Figure 14: Mitochondrial respiration in astrocytes. The oxygen consumption rate (OCR) was measured following the Agilent XF Mito Stress Test protocol consisting of sequential injections of oligomycin (Oligo), carbonyl cyanide-4-(trifluoromethoxy)-phenylhydrazone (FCCP) and rotenone/antimycin A (Rot/AntA) to reveal different respiratory parameters. Representative OCR curves are shown for **(A)** Ctl 17 and Non-R and **(B)** Ctl 18 and Mito. **(C)** Key respiratory parameters were compared between fibroblasts from patients and corresponding controls. Data are presented as mean OCR values ± SEM and were analysed using paired t-tests.

Despite unchanged respiration, Mito patient's astrocytes showed significantly decreased ATP concentrations. In contrast, ATP levels did not change in the MDD and Non-R patients' astrocytes (Figure 15A). As in the other cell types, there was no significant difference in the mitochondrial content in astrocytes (

Figure 15B).

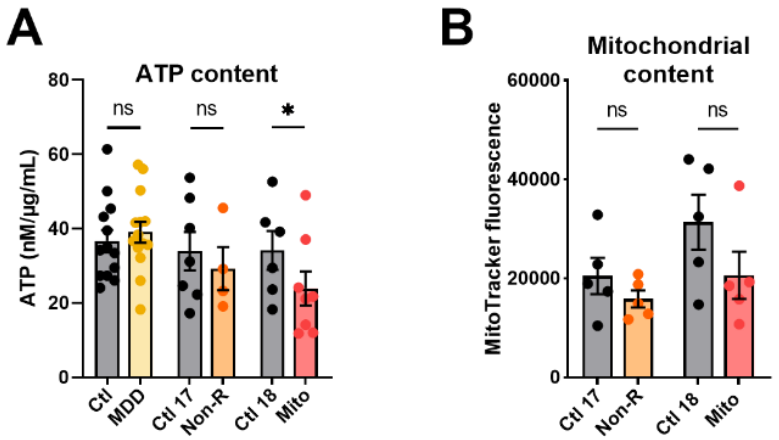

Figure 15: ATP and mitochondrial content in astrocytes. (A) ATP content was measured using a luminescent assay and normalised to protein amount. Bar plot shows nM ATP per µg/mL proteins ± SEM **(B)** Mitochondrial content was measured using flow cytometry and is indicated by MitoTracker Green mean fluorescence ± SEM. $2x10^4$ events were recorded for each replicate. All data were analysed using paired t-tests.

Representing a further measure of bioenergetics functions, the MMP was decreased in astrocytes from MDD patients and the Mito patient, but significantly increased in the Non-R patient (Figure 16A). Regarding Ca^{2+} homeostasis, the MDD cohort astrocytes displayed slightly, yet significantly reduced cytosolic Ca^{2+} levels, whereas there was a marked increase in the Non-R astrocytes, and a significant elevation in the Mito astrocytes (Figure 16B). Consistently with a decreased MMP, mitochondrial Ca^{2+} levels were lower in the MDD cohort and Mito patient's cells. In contrast, despite a higher MMP, Non-R astrocytes showed decreased levels of mitochondrial Ca^{2+} as well (Figure 16C).

In line with prior findings, the cell size of MDD and Non-R astrocytes was decreased. Unexpectedly, astrocytes from the Mito patient exhibited a larger size than their control (Figure 16D).

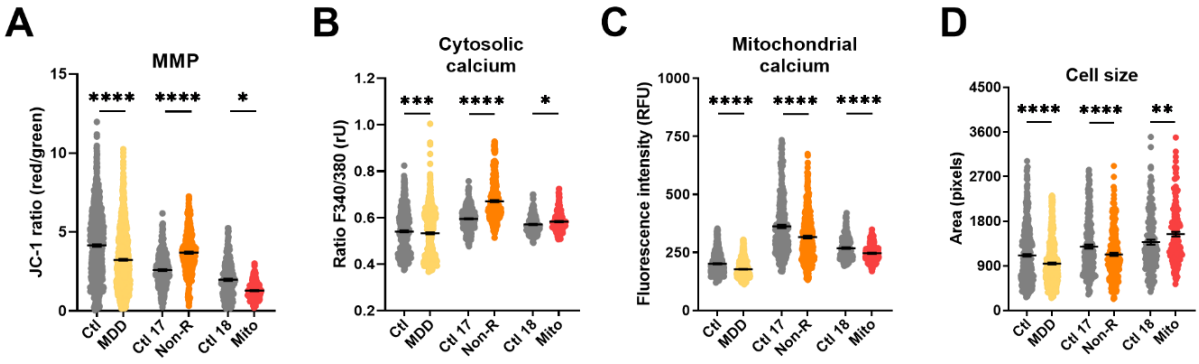

Figure 16: Mitochondrial membrane potential, calcium levels and cell size in astrocytes. (A) MMP was measured with the JC-1 dye and is indicated by the fluorescence ratio between JC-1 aggregates (red) over JC-1 monomers (green). Dot plot shows mean red/green ratios ± SEM. **(B)** Cytosolic calcium was measured as the Fura-2 fluorescence ratio F340/380, and is represented as mean ratio ± SEM **(C)** Mitochondrial calcium levels were measured using Rhod-2/AM and are presented as mean fluorescence intensity, in relative fluorescent unit ± SEM **(D)** Cell size is analysed by assessing area (pixels) of Fura-2/AM-loaded cells. Dot plot shows the number of pixels ± SEM. All data were analysed using paired t-tests.

Finally, ROS levels were measured in both case study patients and their matched controls. Cellular ROS showed considerable variability between groups and were altered in opposite directions in the patients' astrocytes. A decrease was observed in Non-R astrocytes, while an increase was noted in the Mito patient's astrocytes (Figure 17A). Mitochondrial superoxide content remained constant across groups (Figure 17B).

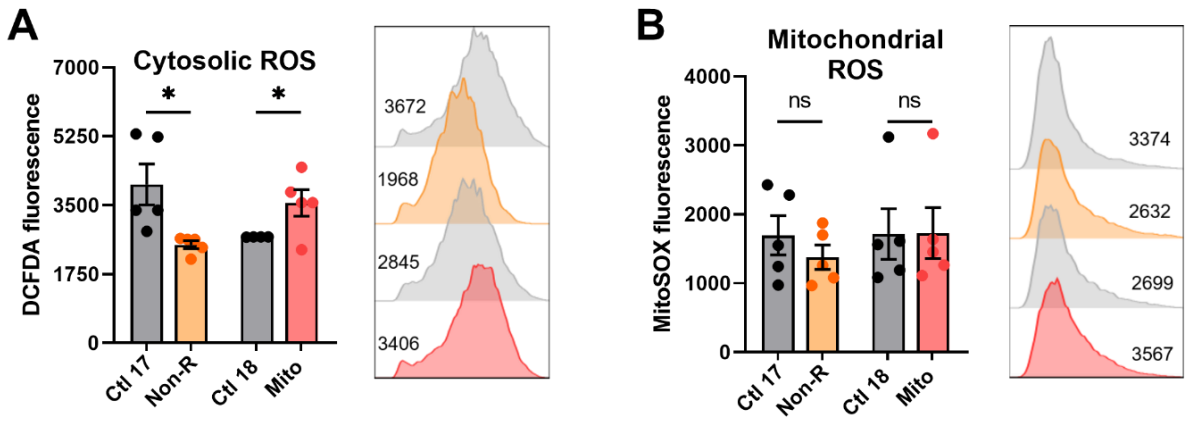

Figure 17: Cytosolic and mitochondrial reactive oxygen species in astrocytes. (A) Cytosolic reactive oxygen species (ROS) and **(B)** mitochondrial superoxide levels were measured using flow cytometry and are indicated by DCFDA and MitoSOX mean fluorescence, respectively. Bar plots show mean fluorescence ± SEM. $2x10^4$ events were recorded for each replicate. On the right of each graph, with matching colour coding and order, are representative histograms showing fluorescence (x-axis) and cell count (y-axis). Numbers indicate mean fluorescence. All data were analysed using paired t-tests.

3.6 Differentiation of neurons

After 21 days of differentiation, iPSC-derived neurons were characterised using immunocytochemistry, as shown in Figure 18A. The neurite network was evidenced with the detection of Microtubule-Associated Protein 2 (MAP2), which plays a role in stabilising dendrites, and β-III-tubulin (β-III-Tub), which is part of the axonal and dendritic cytoskeleton (Dehmelt & Halpain, 2005; Roskams et al., 1998). The neuronal marker NeuN stains post-mitotic nuclei, and its co-expression with the nuclear dye Hoechst demonstrated a highly pure neuronal culture (Mullen et al., 1992). The pre-synaptic marker vesicular glutamate transporters 1 (VGLUT1) and the postsynaptic density protein 95 (PSD95) attested the presence of mature synaptic terminals in the induced neurons. Additionally, PSD95 serves in the localisation of glutamate receptors and VGLUT1 loads glutamate into synaptic vesicles, making both proteins distinctive markers of glutamatergic neurons (Figure 18) (Martineau et al., 2017; Prange et al., 2004). Further visualisation of neuronal morphology was achieved by high-resolution electron microscopy, revealing densely interconnected networks of neurites and protrusions (Figure 18B).

The functionality of the induced neurons was investigated using patch-clamp recordings and Ca^{2+} imaging.

A perfusion system was used to subject neurons to GABA or glutamate (both 10 µM). A membrane potential depolarisation was recorded (Figure 18C), testifying the expression of functional $GABA_A$ and glutamate receptors (AMPA, NMDA or kainate). In physiological settings, a depolarising effect of GABA would suggest neuronal immaturity. However, given the high intracellular chloride concentration used here, $GABA_A$ channel activation leads to chloride efflux, and therefore depolarisation.

Spontaneous activity was detected in the induced neurons by monitoring Ca^{2+} levels. Electrical activity in neurons cause the opening of voltage-dependent Ca^{2+} channels, and thereby a rise in intracellular Ca^{2+} (Catterall, 2000). Such rises were detected in the neurons, further confirming successful differentiation (Figure 18D).

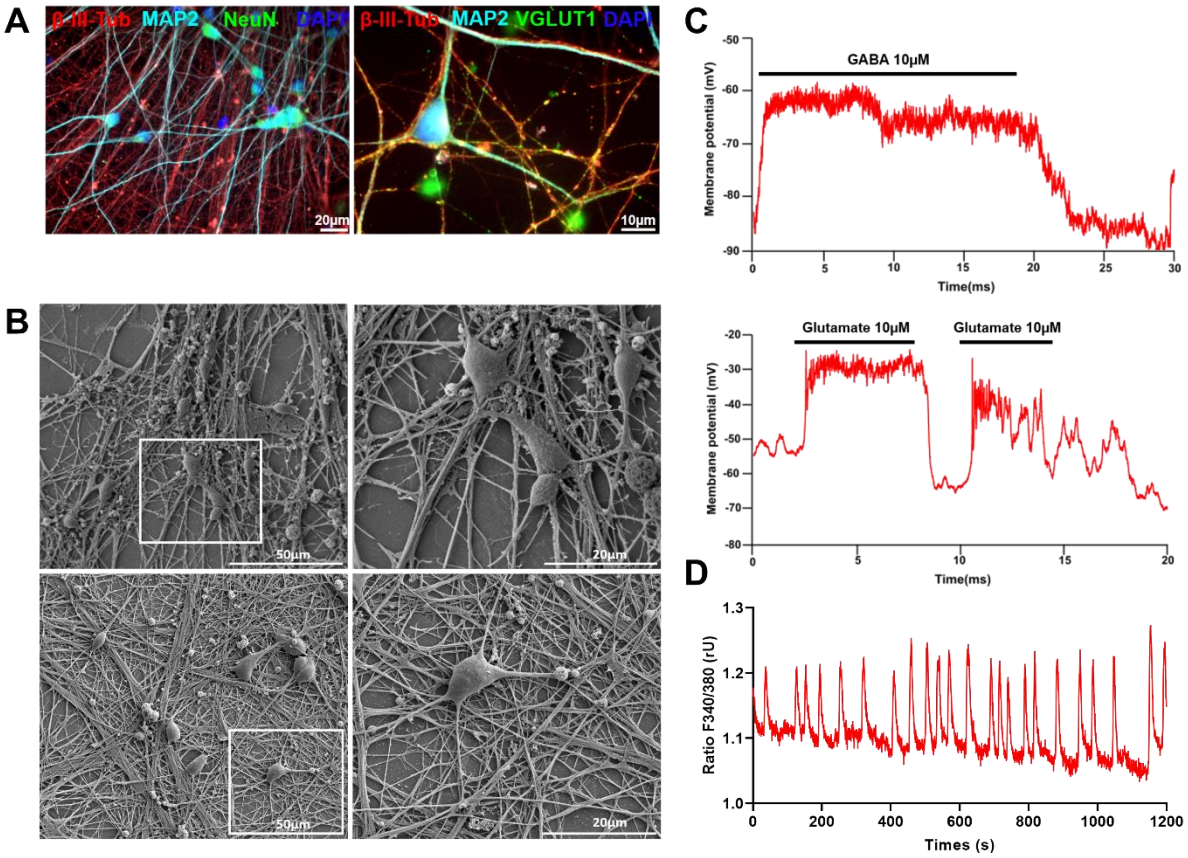

Figure 18: Validation of iPSC-derived neurons. (A) Immunofluorescence stainings on neurons revealed the induced neurons expressed specific neuronal markers. The neurons expressed the typical cytoskeleton proteins β-III-tubulin (β-III-Tub) and Microtubule-Associated Protein 2 (MAP2), as well as the postmitotic neuronal nuclear marker NeuN. Immunostaining for vesicular glutamate transporters 1 (VGLUT1) and the postsynaptic density protein 95 (PSD95) indicates that the majority of induced neurons exhibit a glutamatergic phenotype. Scale bar indicates 20 µM. **(B)** Electron micrographs provide high-resolution visualisation of neuronal morphology. Scale bars indicate 50 µm (left) and 20 µm (right) **(C)** GABA and glutamate response were recorded in current-clamp without injection of current. Membrane potential was measured while applying 10 µM GABA (above) or glutamate (below) using a micro-perfusion system. Bars represent application duration. **(D)** Live-cell imaging in Fura-2/AM-loaded neurons revealed oscillations in intracellular Ca^{2+} concentrations, demonstrating the spontaneous activity of induced neurons. All experiments were performed on day 21 of neuronal differentiation.

3.7 Neurons of patients show altered MMP and Ca^{2+} homeostasis

Mitochondrial functions in neurons were first investigated by evaluating JC-1 fluorescence ratio as a measure of MMP. Since mitochondria residing in the somas or in the neurites appeared in different focal planes, JC-1 fluorescence was imaged separately by focusing on the appropriate structures. The MMP of the Non-R neuronal mitochondria in the somas was decreased compared to the control (Figure 16A), whereas Mito mitochondria showed increased MMP, especially in the neurites (Figure 19A and B).

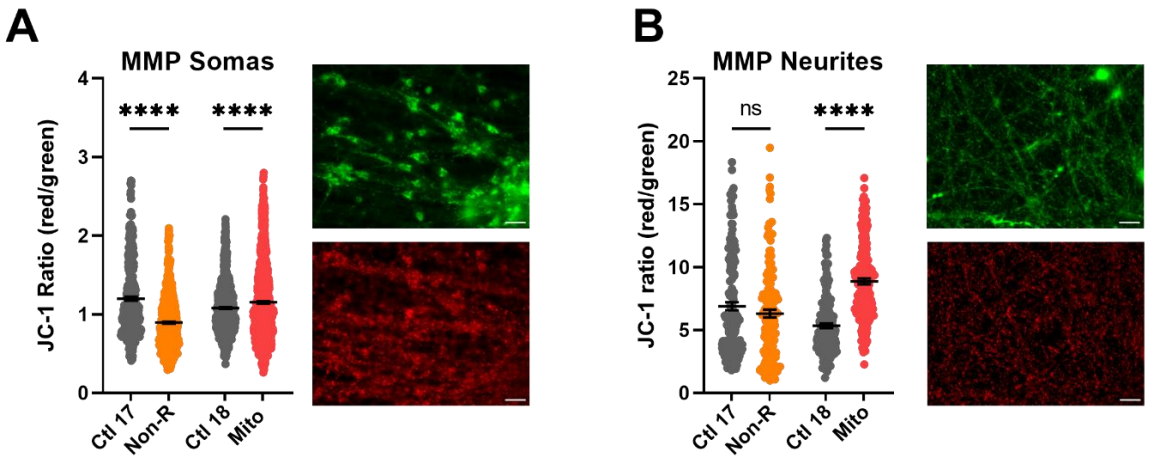

Figure 19: Mitochondrial membrane potential in neurons. MMP was measured with the JC-1 dye and is indicated by the fluorescence ratio between JC-1 aggregates (red) over JC-1 monomers (green). Mitochondria from **(A)** somas and **(B)** neurites appeared on different focal planes and were therefore imaged separately. Representative images show red and green JC-1 fluorescence in the relevant structure. Scale bar indicates 20 µm. Dot plot shows mean red/green ratios ± SEM. All data were analysed using paired t-tests.

To further investigate neuronal mitochondrial function, Ca^{2+} homeostasis was measured. Remarkably, the levels of cytosolic Ca^{2+} were decreased in both patients' neurons (Figure 20A). In addition, levels of mitochondrial Ca^{2+} were decreased in the Mito patient's neurons (Figure 20A and B), and they exhibited a significantly smaller size (Figure 20C).

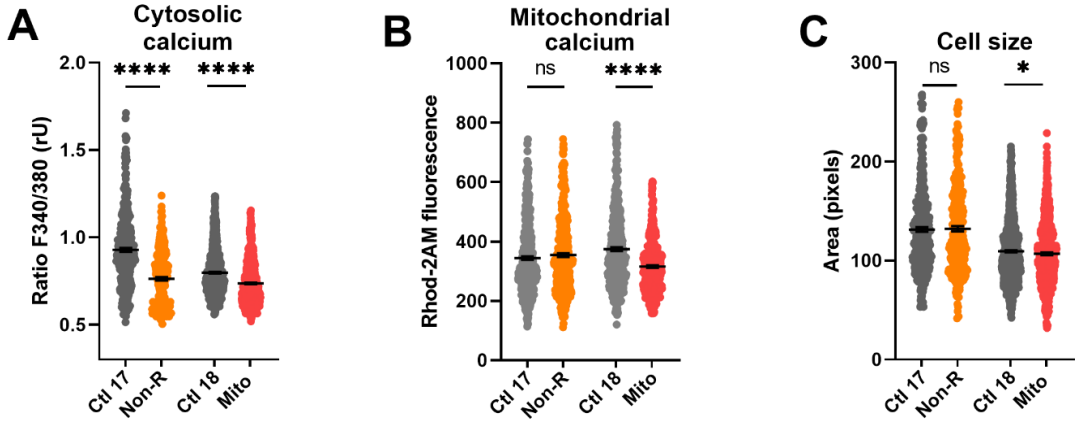

Figure 20: Calcium and cell size in neurons. (A) Cytosolic calcium was measured as the Fura-2 fluorescence ratio F340/380, and is represented as mean ratio ± SEM **(B)** Mitochondrial calcium levels were measured using Rhod-2/AM and are presented as mean fluorescence intensity, in relative fluorescent unit ± SEM **(C)** Cell size is analysed by assessing area (pixels) of Fura-2/AM-loaded cells. Dot plot shows the number of pixels ± SEM. All data were analysed using paired t-tests.

3.8 Functional properties and the activity of patient-derived neurons are altered

Electrical activity is a hallmark of neuronal function. To investigate the biophysical properties of neurons, whole-cell patch-clamp recordings were performed on patient-derived and control neurons.

Resting membrane potential (RMP) of the Mito patient's neurons was significantly depolarised (less negative) than that of the control, as was the case in neurons from the MDD cohort (Figure 21A). Interestingly, the Non-R neurons showed a significantly hyperpolarised (more negative) RMP (Figure 21A). It should be noted that the case study patients' neurons had a more negative RMP than the MDD cohort neurons used in the previous study (Triebelhorn et al., 2022). Optimising the differentiation protocol might have led to a more mature and developed neuronal phenotype. Membrane capacitance is a measure of a cell's ability to store charges across its membrane, and it is directly proportional to the surface area of the cell. Consistently with the MDD cohort, and with findings in fibroblasts, NPCs, and astrocytes, neurons from the case study patients had a lower capacitance, indicating small soma size (Figure 21B).

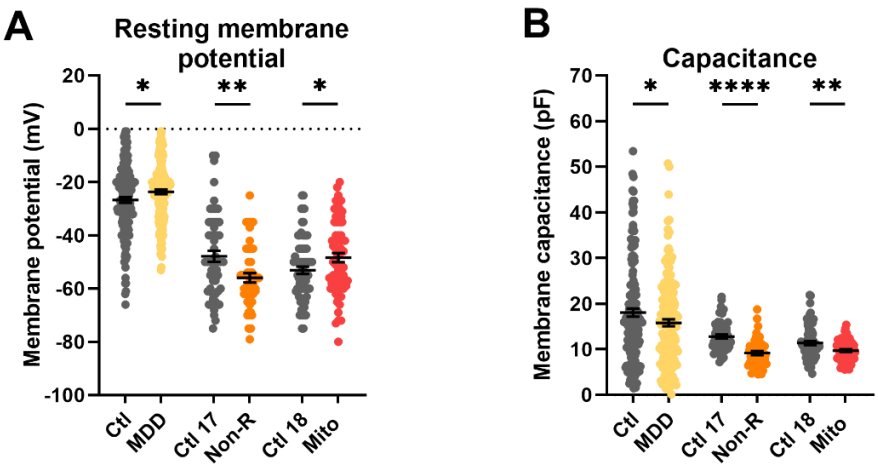

Figure 21: Resting membrane potential and capacitance. (A) Resting membrane potential (RMP) and **(B)** capacitance were recorded immediately after reaching the whole-cell configuration. RMP was measured in current-clamp mode without current injection. Dot plot shows mean RMP in mV ± SEM and mean capacitance in pF ± SEM. All data were analysed using paired t-tests.

In addition to these neuronal passive biophysical properties, active electrophysiological parameters were measured, including sodium (Na^+) and potassium (K^+) currents. This was done by holding the membrane potential at -80 mV (Vhold) and depolarising it in steps of 10 mV to induce the opening of voltage-gated Na^+ and K^+ channels (Figure 22A). The resulting currents were recorded and plotted against the potential, resulting in a current-voltage (IV) curve (Figure 22B). Given the high size variability observed, the currents measurements were normalised to the membrane capacitance by calculating current density (pA/pF). The

voltage-gated Na^+ channels of Mito and MDD neurons showed a significantly higher current density, whereas Na^+ current densities in Non-R neurons did not differ from those of its control (Figure 22C). Remarkably, the current density of voltage-gated K^+ currents was significantly higher in neurons of both the Mito and Non-R patients relative to their controls (Figure 22D).

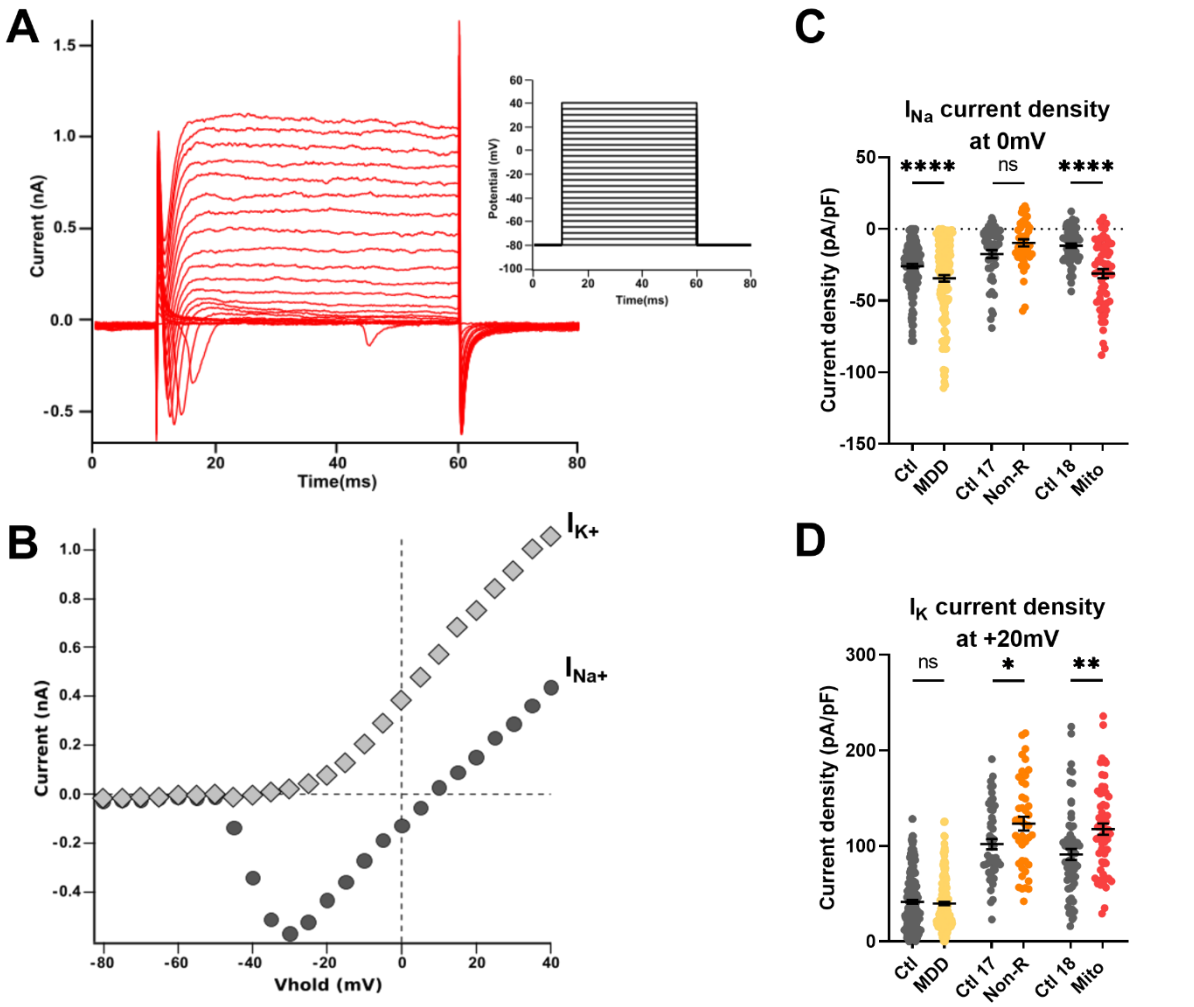

Figure 22: Sodium and potassium currents. (A) Sodium (I_{Na}) and potassium (I_K) currents were recorded in voltage-clamp mode while holding the membrane potential at -80 mV (Vhold) and depolarising in steps of 10 mV to provoke the opening of voltage-gated Na^+ and K^+ channels. Example traces show depolarising steps and the evoked Na^+ and K^+ current, and **(B)** the resulting IV curve. Currents measurements were normalised to the membrane capacitance to account for cell size variability (current density, pA/pF). Dot plots show (C) mean I_{Na} current density at 0 mV pA/pF ± SEM and (D) mean I_K current density at +20 mV in pA/pF ± SEM. All data were analysed using paired t-tests.

Furthermore, the current-clamp mode was used to adjust the basal membrane potential to approximately -50 mV or -80 mV by current injection, and record the potential fluctuations, which occasionally lead to spontaneous action potentials (APs). In this parameter as well, the patients neurons showed opposite trends. A high proportion of Mito neurons (76%) were spontaneously active at -50 mV, which represented a significant increase compared to Ctl 18 with 49% of active cells (Figure 23A). Similarly, despite an overall low spontaneous activity, a

higher proportion of MDD neurons were active than control neurons (Ctl 11% vs. MDD 22%) (Figure 23A). Additionally, active cells in the Mito patient's neurons had a higher number of APs. In contrast, the Non-R patient's neurons had significantly lower spontaneous activity at -50 mV than the corresponding controls (Ctl 17 79% vs. Non-R 50%) (Figure 23A). This was accompanied by a decreased number of APs in the active cells of the Non-R patient (Figure 23A). This patient also presented lower spontaneous activity at -80 mV than Ctl 17 (Ctl 17 88% vs Non-R 59%) (Figure 23B).

The recorded spontaneous APs were analysed individually in order to extract the amplitude and full width of the spikes at half of the maximum amplitude, expressed in seconds (full width half maximum, FWHM) (Figure 23C).The APs from Mito neurons were significantly larger and showed shorter FWHM time than those of Ctl 18 (Figure 23D). The amplitudes and FWHM time of Non-R APs were smaller (Figure 23D).

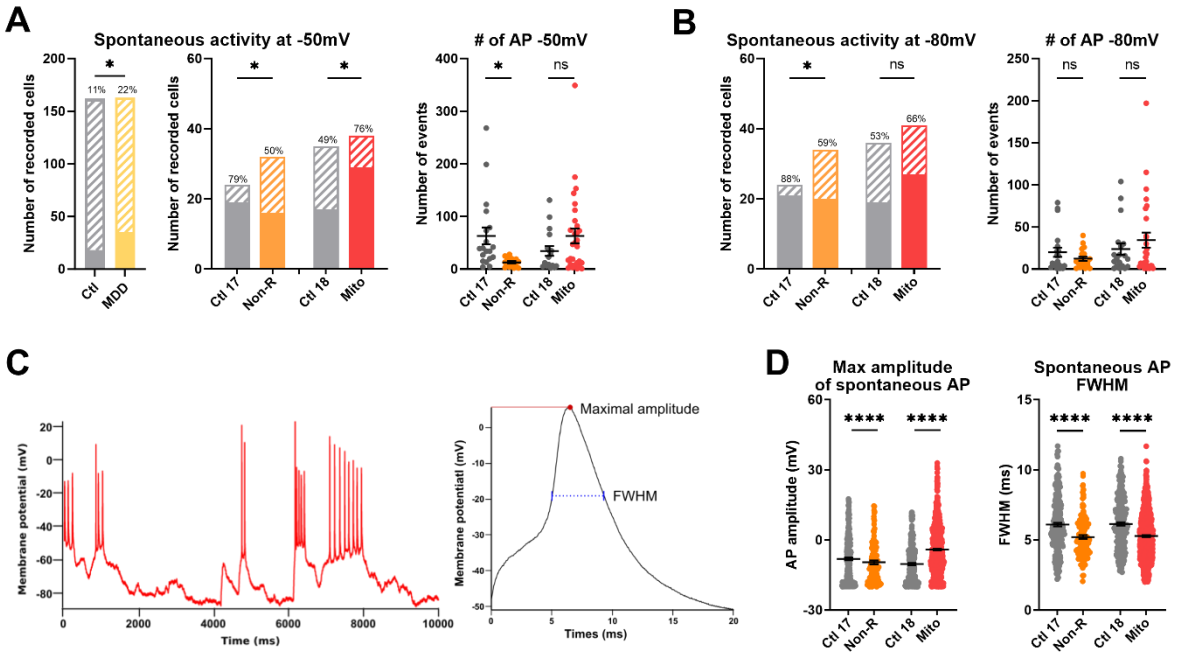

Figure 23: Spontaneous action potential in neurons. Spontaneous action potentials (APs) were recorded in current-clamp while holding the membrane potential at -50 mV or -80 mV. Spontaneous activity bar graphs show the proportion of active cells (solid colour), inactive cells (pattern) and the percentage of active cells at **(A)** -50 mV and **(B)** -80 mV. The number of APs in each recording was counted manually. The dot plots show the mean number of recorded APs ± SEM. **(C)** The example traces show spontaneous APs at a holding potential of -80 mV (left) and a single AP illustrating the measured parameters maximal amplitude and full width at half maximum (FWHM, right). **(D)** Spontaneous APs at -80 mV were analysed individually to extract the maximal amplitude and the FWHM. Graphs show mean AP amplitude in mV ± SEM and mean FWHM in ms ± SEM. Spontaneous activity percentages were analysed with Fisher's exact test, while all other data were analysed using paired t-tests.

To further characterise spontaneous network activity, voltage-clamp experiments at a holding potential of -80 mV were used to record spontaneous postsynaptic currents (PSCs), which can be considered a measure of synaptic input. Only 30% of Non-R neurons displayed PSCs, while the proportion was 81% in Ctl 17 (Figure 24A). In contrast, a large proportion of Mito neurons (72%) received synaptic input, although there was no significant difference

compared with synaptic activity in Ctl 18 (56%) (Figure 24A). Interestingly, the PSCs of Mito neurons differed in various parameters. They were significantly smaller in amplitude, showed a longer rise time from 10 to 90% of the maximal amplitude, and a prolonged time constant of decay compared to their control (Figure 24B). In Non-R neurons, in spite of a markedly smaller proportion of active cells, PSCs displayed significantly a longer rise times and larger amplitudes (Figure 24B).

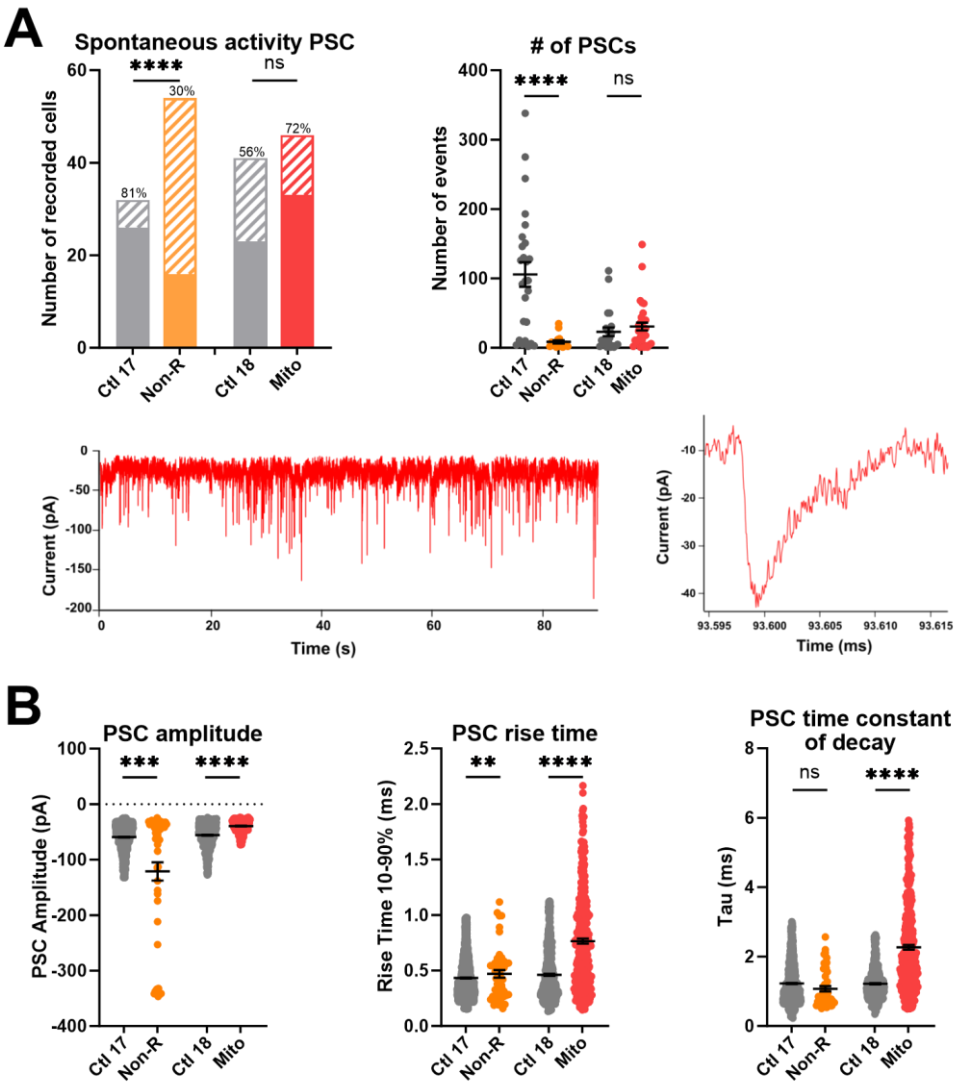

Figure 24: Spontaneous postsynaptic currents. Postsynaptic currents (PSCs) were analysed at a holding potential of -80 mV**. (A)** The proportion of active cells (solid colour), inactive cells (pattern) and the percentage of active cells were calculated (left), the PSCs were counted and plotted as the mean number of recorded PSCs ± SEM (right). Example traces show spontaneous PSCs (left) and one single PSC, as visualised when analysed with the IGOR Pro software (right). **(B)** Single PSCs were analysed to extract the maximal amplitude (pA ± SEM), the rise time from 10 to 90% of the maximal amplitude (ms ± SEM), and the time constant of decay Tau (ms ± SEM). Spontaneous activity percentages were analysed with Fisher's exact test, while all other data were analysed using paired t-tests.

The electrical activity of the cultured neurons triggered Ca^{2+} signals that were recorded by live-cell imaging using the Ca^{2+}-sensitive dye Fura-2/AM. Each peak was then analysed in the same way as APs and PSCs. The amplitudes of the Ca^{2+} transients were not different in

a physiologically relevant manner between the groups, although a statistically significant decrease was observed in the Non-R patient's neurons (Figure 25B). The rise time was unchanged in the Non-R patient, although the time constant of decay was increased (Figure 25C and D). In contrast, both the rise time and the time constant of decay were longer in the Mito neurons, suggesting prolonged Ca^{2+} signals (Figure 25C and D).

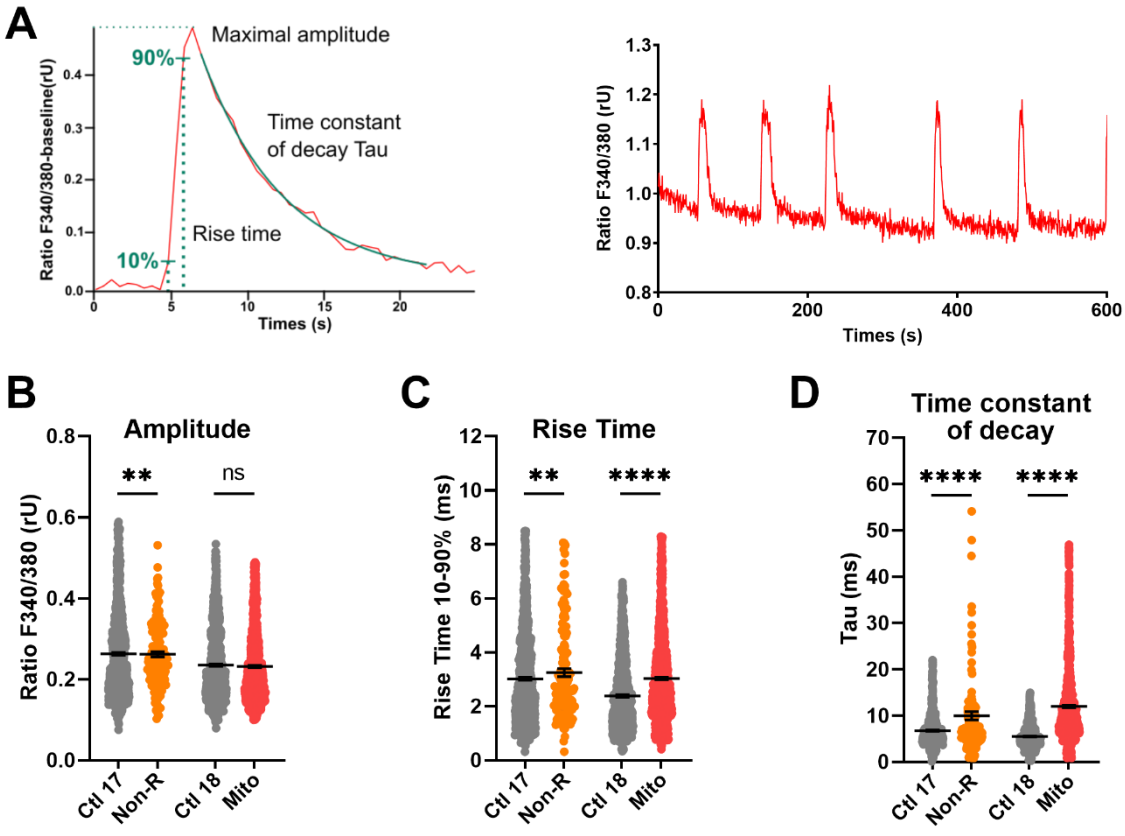

Figure 25: Kinetics of calcium peaks in neurons. Spontaneous calcium transients were analysed in Fura-2/AM-loaded cells. **(A)** Example traces show a baseline subtracted calcium peak, illustrating maximal amplitude, rise time between 10 and 90% of maximal amplitude and the exponential fit used to calculate the time constant of decay Tau (left), and representative calcium transients in a neuron (right). **(B)** Graphs show the maximum amplitude of the calcium peaks (ratio 340 nm/380 nm ± SEM), the rise time and the time constant of decay Tau (ms ± SEM). All data were analysed using paired t-tests.

A comprehensive overview of the alterations reported in this study, as well as corresponding results in the MDD cohort from previous studies (Kuffner et al., 2020; Triebelhorn et al., 2022) are provided in Table 9.

Table 9: Overview of results. Arrows represent increases (↗) and decreases (↘), and asterisks reflect the significance of the difference. Equal signs (=) represent an unchanged parameter.

	Non-R			Mito			MDD Cohort		
	Fibroblasts	NPCs	Astrocytes	Fibroblasts	NPCs	Astrocytes	Fibroblasts	NPCs	Astrocytes
Respiration	↗	↗	↘	↘	↘	=	↘	↘	↘
ATP	=	=	=	=	=	↘ *	↘ *	=	=
NAD/NADH	=	=		=	↗ *				
Mito. content	=	=	=	=	=	=			
MMP	=	=	↗ ****	↘ ****	↗ ****	↘ *	↘ ****	=	↘ ****
Cytosolic Ca^{2+}	=	=	↗ ****	=	↗ ***	↗ *	=	↗ *	↘***
Mitochondrial Ca^{2+}	↗ ****	↗ ****	↘ ****	=	=	↘ ****			↘ ****
Cell size	↘ ****	↘****	↘ ****	↘ *	↘ ****	↗ **	↘ ****	↘****	↘ ****
Cytosolic ROS	=	=	↘ *	=	=	↗ *			
Mito. ROS	↗ **	=	=	=	↗ **	=			
Lipid peroxidation	=	↘ **		↗ **	↗ *				
GSH/GSSG	=			↘ *					
	Neurons								
MMP somas	↘ ****			↗ ****					
MMP neurites	=			↗ ****					
Cytosolic Ca^{2+}	↘ ****			↘ ****					
Mitochondrial Ca^{2+}	=			↘ ****					
Cell size	=			↘ *					
RMP	↗ ** (hyperpolarised)			↘ * (depolarised)			↘ * (depolarised)		
Capacitance	↘ ****			↘ **			↘ *		
$I_{Na+\ 0mV}$ curr. density	=			↘ ****			↘ ****		
$I_{K+\ 20mV}$ curr. density	↗ *			↗ **			=		
Spontaneous activity	-50 mV	-80 mV	PSCs	-50 mV	-80 mV	PSCs	-50 mV		
	↘*	↘*	↘****	↗ *	=	=	↗ *		
Number of events	-50 mV	-80 mV	PSCs	-50 mV	-80 mV	PSCs			
	↘*	=	↘****	=	=	=			
Spont. AP amplitude	↘ ****			↗ ****					
Spont. AP FWHM	↘ ****			↘ ****					
PSC amplitude	↗ ***			↘ ****					
PSC rise time	↗ **			↗ ****					
PSC decay time (Tau)	=			↗ ****					

4 Discussion

Despite decades of research, the biological mechanisms underlying MDD remain a persistent enigma. Historically, early theories attributed MDD symptoms to humoral imbalances, but in the 20th century, the discovery of monoamine alterations in depression marked a turning point and revolutionised the treatment of this condition. As research evolved, it began to incorporate modern genetics methods, neuroimaging and even started considering the gut-brain axis, leading to the development of many theories. Despite the strides made by these advances, no single theory has prevailed and successfully provided a comprehensive explanation for depression. Instead, each discovery has added layers of complexity to our understanding.

One promising area of research that emerged in the late 20th century is the potential link between mitochondria and depression. This connection is rooted in both mitochondria's involvement in many mechanisms identified in depression, and early observations in patients with mitochondrial disorders. While there has been increasing research in this area, our understanding of the role of mitochondria in depression is still evolving.

Building on previous work with an MDD patients cohort, in the present study, we focused on mitochondrial (dys)function in atypical patients, with the aim to gain a more comprehensive understanding of ways in which mitochondria can influence cellular function and potentially contribute to the development of depression.

4.1 Bioenergetics alterations in patients

Mitochondria play pivotal roles in cellular physiology, with their primary and most crucial function being the production of the body's main energy currency: ATP. OXPHOS is the metabolic pathway that yields the highest amount of ATP from a single molecule of glucose. While glycolysis produces 2 ATP molecules from one glucose molecule, OXPHOS produces approximately 28 ATP molecules from the same initial glucose molecule. However, these numbers can vary depending on several factors affecting OXPHOS. These factors include the efficiency of the ETC, proton leak, cellular conditions, like the availability of oxygen and substrates, the presence of uncoupling proteins, and alternative pathways. Notably, some cells favour glycolysis for energy production, even when oxygen is readily available.

As described previously, several studies reported alterations of mitochondrial respiration in peripheral cells from patients and in some cases, reduced ATP concentrations (Gardner et al., 2003; Hroudová et al., 2013; Karabatsiakis et al., 2014). In the cohort of MDD patients used as a reference here, both respiration and ATP levels were decreased in fibroblasts, compared to non-depressed controls (Kuffner et al., 2020), and lower respiration was observed in neural progenitor cells (NPCs) (Triebelhorn et al., 2022). In cells from the two

case studies patients investigated here, significant alterations in respiration were observed as well.

4.1.1 Antidepressant non-responder patient

Since MDD is known to involve mitochondrial alterations and reduced bioenergetics (Klinedinst & Regenold, 2015; Manji et al., 2012), findings of a significantly increased mitochondrial respiration in fibroblasts and NPCs from the non-responder (Non-R) patient were unexpected. The unchanged mitochondrial content suggests that this heightened respiration resulted from increased activity rather than an increase in the number of mitochondria. However, this high OXPHOS activity was not accompanied by an elevated ATP concentration, suggesting an uncoupling of the ETC and the ATP synthase.

4.1.1.1 Proton leak

Notably, proton leak was markedly increased in fibroblasts and elevated in NPCs from the Non-R patient, which could partly account for this uncoupling. The fact that ETC hyperactivity was not accompanied by a higher MMP also speaks for a contribution of proton leak. Basal proton leak occurs physiologically and may contribute to regulating metabolic rate. Composition and integrity of the phospholipid bilayer of mitochondrial membranes can influence proton conductivity. However, analysis of the lipid composition in isolated mitochondria using an untargeted lipidomics approach did not reveal any significant alterations in fibroblasts (data not shown). Moreover, Brookes *et al.* reported that only about 5 % of proton leak is mediated by lipid bilayers (Brookes et al., 1997). These findings prompted Brand *et al.* to identify a mitochondrial protein responsible for proton leak and they demonstrated that the adenine nucleotide translocase (ANT) is a major catalyst of basal proton leak in mitochondria (Brand et al., 2005). It could be hypothesised that ANT expression or activity was altered in the Non-R patient's fibroblasts and NPCs, resulting in a high proton leak and to the dissipation of the proton gradient, which caused a compensatory increase in ETC activity, in a failed attempt to maintain the MMP and ATP production.

Importantly, the observed changes in respiration in the Non-R patient do not align with the mitochondrial hypothesis of MDD, which postulates that mitochondrial dysfunction is characterised in part by decreased respiration. The specificity of this antidepressant-resistant MDD patient suggests a need for a more nuanced view on this theory, one that encompasses an over activation of certain mitochondrial functions, thus creating a detrimental imbalance.

4.1.1.2 Astrocytes specificity

In contrast to fibroblasts and NPCs, mitochondrial respiration in the astrocytes from the Non-R patient was generally reduced. One possible explanation for this contrast may be found in

another differing observation between fibroblasts and NPCs on one hand, and astrocytes on the other. It is known that Ca^{2+} stimulates respiration by activating key enzymes in the TCA cycle. In line with this, respiratory activity and mitochondrial Ca^{2+} levels showed a consistent trend in this patient's cells: both increased in fibroblasts and NPCs but decreased in astrocytes. Interestingly, recent studies have revealed unique aspects of mitochondrial Ca^{2+} homeostasis in astrocytes when compared to other cell types. Astrocytes do not seem to rely on the mitochondrial uniporter (MCU) for Ca^{2+} influx (Huntington & Srinivasan, 2021), whereas the Na^{+}/Ca^{2+}/lithium exchanger (NCLX) plays a particularly important role in Ca^{2+} efflux in astrocytes (Palty et al., 2010). It is therefore conceivable that the Non-R patient's cells expressed higher amounts of NCLX, resulting in a particularly enhanced Ca^{2+} efflux from astrocytic mitochondria, and, consequently, reduced mitochondrial Ca^{2+} and ETC activity in astrocytes. In contrast, the elevated mitochondrial Ca^{2+} observed in fibroblasts and NPCs from the Non-R patient could result from modulations of MCU expression, a mechanism that would not affect astrocytic mitochondrial Ca^{2+} level.

4.1.2 Mitochondriopathy patient

4.1.2.1 Bioenergetics impairments

In the case study patient suffering from a mild mitochondriopathy (Mito), fibroblasts and NPCs showed significantly reduced oxygen consumption rates, mirroring the observations made in the MDD cohort (Kuffner et al., 2020; Triebelhorn et al., 2022). Decreased mitochondrial respiration is a hallmark of mitochondrial disorders. However, exome sequencing of fibroblasts from the Mito patient detected no known pathogenic disease-associated variants in nuclear genes (data not shown). Likewise, mitochondrial genome sequencing did not identify any mutations linked to mitochondrial diseases. Nevertheless, it is important to note that the analysis of sequence data may not provide a comprehensive assessment of all genes. Limitations of this method include the detection of low-grade mosaics, of repeat expansions, of balanced changes (translocations and inversions), and in the calling accuracy of larger Indels. Furthermore, in exome sequencing, variants in non-enriched regions (untranslated regions, introns, promoter and enhancer regions) cannot be detected. Additionally, given the potential for heteroplasmy in mitochondria, where mutated mtDNA can exist in only a subset of the total mtDNA population within a tissue, it is impossible to entirely rule out mitochondrial mutations (Wallace & Chalkia, 2013). It is conceivable that a sporadic mutation in one of the mitochondrial genes in a subset of cells, or an environmental factor, such as certain pharmaceutical drugs (Vuda & Kamath, 2016) or air pollution (Breton et al., 2019) is responsible for the phenotype observed in this patient.

Despite the decrease in respiration, the ATP content in fibroblasts and NPCs from the Mito patient remained stable. This suggests a compensatory glycolytic activity that offsets the cost

of energy-intensive processes (Distelmaier et al., 2015). Moreover, the mitochondrial mass was not altered in this patient's cells, indicating that decreased respiration resulted solely from lower OXPHOS activity.

4.1.2.2 Astrocytes specificity

As in the Non-R patient, astrocytes from the Mito patient displayed distinct characteristics. While in the MDD cohort, astrocytic respiration was consistently decreased, astrocytes from the Mito patient exhibited unchanged respiration, relative to the matched control. This finding is particularly intriguing considering that both mitochondrial Ca^{2+} levels and MMP were decreased. Typically, these factors would suggest a decreased OXPHOS activity, with mitochondrial Ca^{2+} acting as a cause, and MMP as a consequence. Moreover, ATP concentration was significantly decreased in astrocytes from this patient.

Astrocytes predominantly use glycolysis for energy production (Rose et al., 2020). A decrease in ATP might result from diminished glycolysis, even when OXPHOS appears unaffected. Furthermore, in the Mito patient astrocytes, there was a notable increase in cytosolic ROS detected by DCFDA. ROS inhibit various glycolytic enzymes, including glyceraldehyde 3-phosphate dehydrogenase (GAPDH), pyruvate kinase M2, and phosphofructokinase-1. Hyslop *et al.* demonstrated that upon exposure to ROS, there was a decrease in ADP phosphorylation, leading to reduced ATP levels. This decrease was attributed to GAPDH inhibition, resulting in a slower glycolytic rate. In an additional experiment where oligomycin was used to inhibit complex V of the ETC, the ATP synthase, Hyslop and colleagues found that ROS-induced reduction in mitochondrial ATP production was due to the direct inhibition of ATP synthase rather than to a decreased respiratory chain capacity (Hyslop et al., 1988). It is plausible that elevated ROS in this patient's astrocytes hindered ATP production by concurrently inhibiting glycolysis and the ATP synthase complex in the ETC. This would account for the observed reduction in ATP levels.

While an unchanged respiration rate might at first glance indicate healthy mitochondrial functions in astrocytes, when put in a broader context, a mitochondrial dysfunction becomes apparent. Typically, decreased ATP levels and lower MMP would trigger a compensatory rise in the rate of OXPHOS. The absence of an OXPHOS increase suggests that the mitochondria are struggling to meet energy demands efficiently. In this context, the observed lower mitochondrial Ca^{2+} levels likely result from the decreased MMP, which in turn leads to reduced Ca^{2+} import into the mitochondrial matrix.

4.2 Calcium homeostasis and redox homeostasis

Within the complex landscape of cellular physiology, calcium (Ca^{2+}) and redox homeostasis are essential and interconnected regulators of cell health. Ca^{2+} homeostasis ensures that intracellular Ca^{2+} concentrations are maintained within a narrow range, a balance that is vital for numerous cellular processes, from signal transduction to energy metabolism. Redox homeostasis maintains the balance between oxidants and antioxidants, which is crucial in preventing oxidative stress and preserving cellular integrity.

Changes in cytosolic Ca^{2+} levels were not evident in the MDD cohort relative to controls in fibroblasts (Kuffner et al., 2020). However, an increase was detected in NPCs from depressed patients (Triebelhorn et al., 2022). Several studies have suggested a connection between Ca^{2+} homeostasis and depression. For instance, a genome-wide meta-analysis of depression by Howard *et al.* found an association between depression and two genes coding for Ca^{2+} channels (Howard et al., 2019). Additionally, there is genetic evidence for a causal effect of depression on lower vitamin D concentrations, potentially causing a lower intestinal absorption of Ca^{2+} and reduced Ca^{2+} transport inside cells (Mulugeta et al., 2020).

Research on Ca^{2+} homeostasis alterations in mitochondrial diseases (MDs) has been limited. Visch *et al.* observed that patients with an isolated complex I deficiency exhibited reduced mitochondrial Ca^{2+} uptake after physiological stimulation and lower cytosolic Ca^{2+} removal rate due to lower activity of membrane Ca^{2+} transporters (Visch et al., 2006). Additionally, Moudy *et al.* found that fibroblasts from MELAS patients had elevated Ca^{2+} levels and could not normally sequester Ca^{2+} influxes (Moudy et al., 1995).

Since the investigation of redox markers was initiated in this study, there is currently no data available from the MDD and control cohorts. However, many studies have documented changes in redox homeostasis and increased oxidative stress in depression. Reported oxidative disturbances in depressed patients include elevated lipid peroxidation products, oxidative DNA damage and reduced serum vitamin C. Interestingly, some studies also identified a correlation between the severity of depression and oxidative stress indicators (reviewed in Ng et al., 2008).

Patients with MDs have also shown imbalances in redox homeostasis and increased oxidative stress. Specifically, complex I deficiency in various MDs has been linked to increased superoxide production and induction of superoxide dismutase (Pitkanen & Robinson, 1996). This deficiency also led to an excessive formation of hydroxyl radicals and aldehydic lipid peroxidation products in skin fibroblasts from patients (Luo et al., 1997).

Overall, existing literature underscores the importance of exploring Ca^{2+} and redox homeostasis in our depressed AD-non responder patient, and mitochondriopathy patient.

4.2.1 Calcium homeostasis

Ca^{2+} is pivotal in cellular physiology, modulating numerous signalling pathways, making it the most versatile intracellular second messenger. The concentration gradient of cytosolic Ca^{2+} relative to extracellular Ca^{2+} levels is tightly regulated, and is crucial for triggering Ca^{2+}-dependent signalling cascades. Extracellular Ca^{2+} levels are typically 20,000 times higher than cytosolic concentration, a difference maintained by energy consuming Ca^{2+} transport (Hopp, 2021). Within the cell, rises in cytosolic Ca^{2+} are buffered by Ca^{2+}-binding proteins and sequestration in organelles. The endoplasmic reticulum (ER) is the primary Ca^{2+} storage site, and its close interaction with mitochondria facilitates significant Ca^{2+} exchanges (Pizzo & Pozzan, 2007). At rest, the mitochondrial matrix maintains a Ca^{2+} concentration of about 100 nM, balanced with the cytosol. When cytosolic Ca^{2+} rises, mitochondria can quickly uptake Ca^{2+}, reaching concentrations up to 100 µM (Filadi et al., 2017). In this study, Ca^{2+} homeostasis was explored through two linked aspects: cytosolic and mitochondrial Ca^{2+}.

The main change observed over the different patients and different cell types was a rise in cytosolic Ca^{2+} levels. An effect of altered membrane composition on Ca^{2+} channels properties and activity was ruled out after lipidomics analysis did not reveal any changes in membrane lipid composition (data not shown; (Tillman & Cascio, 2003)). Elevated cytosolic Ca^{2+} levels could originate from a release of the ER store, or a decreased binding to Ca^{2+}-binding proteins (Yáñez et al., 2012).

When intracellular Ca^{2+} levels rise, transporters and pumps, such as the Plasma Membrane Ca^{2+} ATPase (PMCA), use ATP to extrude Ca^{2+} out of the cell, thus maintaining viability. Interestingly, in this study, most instances of increased cytosolic Ca^{2+} were accompanied by decreased respiration. The Km for ATP binding to the PMCA suggest that theoretically, a large drop in ATP would be needed for its inhibition. However, Mankad *et al.* demonstrated that in the case of altered mitochondrial respiration, even when global ATP concentrations are maintained by compensatory glycolytic rate, PMCA becomes particularly dependent on local ATP supply, and sensitive to small ATP fluctuations (Mankad et al., 2012). Castro *et al.* additionally demonstrated that when ATP is scarce, the cation pump Na^+/K^+ ATPase is prone to “steal” ATP from PMCA, leading to its inhibition and to the accumulation of intracellular Ca^{2+} (Castro et al., 2006). In the context of the present work, it is plausible that in patients cells exhibiting higher Ca^{2+} levels, perturbations in respiration may have reduced PMCA activity. This could be attributed to the prioritisation of other cation pumps, leading, in turn, to a moderate accumulation of cytosolic Ca^{2+}.

While an overload of Ca^{2+} can induce apoptosis and necrosis, a moderate elevation has subtler effects, including the enhanced activation of specific enzymes such as the Ca^{2+} calmodulin-dependent kinases (CaMKs) and phosphatases. These enzymes can, in turn, influence various cellular processes (Ishida et al., 2003). Notably, CaMKs are known to

phosphorylate several transcription factors, with cAMP response element-binding protein (CREB) being among the most extensively studied (Ishida et al., 2003). Thus, elevated cytosolic Ca^{2+} can indirectly regulate gene transcription.

Cytosolic Ca^{2+} dynamics can also affect mitochondrial Ca^{2+} and vice versa. For instance, when cytosolic Ca^{2+} concentrations rise, mitochondria can enhance their Ca^{2+} uptake. Conversely, under stress conditions, such as oxidative stress, mitochondria may release Ca^{2+} into the cytosol as a protective mechanism against apoptosis. A concurrent increased cytosolic Ca^{2+} and decreased mitochondrial Ca^{2+} was observed in astrocytes from both patients. Yet, it did not correspond with increased ROS in mitochondria. Therefore, the unique characteristics of astrocytes concerning mitochondrial Ca^{2+} influx and efflux, as described above, seem to be more plausible explanations for these observed alterations.

The patterns between cytosolic and mitochondrial Ca^{2+} was not consistent, making it challenging to draw definitive conclusions relating both parameters, especially since mitochondrial Ca^{2+} measurements were missing in fibroblasts and NPCs from the MDD cohort. Nonetheless, it is noteworthy that mitochondrial Ca^{2+} levels were altered in all cells derived from the patients, and that the variations consistently mirrored changes in mitochondrial respiration. This observation aligns with the activating role of Ca^{2+} on OXPHOS, and underscores the central role of mitochondria in the cellular anomalies observed in these patient's cells.

4.2.2 Redox homeostasis

Redox homeostasis is fundamental to a wide range of cellular processes. On the one hand, moderate levels of ROS are essential for cell signalling. For instance, hydrogen peroxide oxidation of specific amino acid residues alters protein activity, localisation, and interactions (Rhee et al., 2000). On the other hand, disruption of the balance by excessive ROS accumulation leads to oxidative stress, which can have detrimental effects on cell health and is implicated in the pathogenesis of numerous diseases (Valko et al., 2007). Mitochondria are major sources of ROS, primarily at complexes I and III of the ETC. They also contain antioxidant systems to detoxify ROS, such as manganese superoxide dismutase, and thus play an important role in maintaining redox homeostasis.

Here, different aspects of redox homeostasis were investigated. Mitochondrial and cytosolic ROS were measured in fibroblasts, NPCs and astrocytes. Lipid peroxidation was estimated in supernatants from fibroblasts and NPCs cultures. Finally, the glutathione antioxidant system was examined in fibroblasts.

4.2.2.1 Antidepressant non-responder patient

In fibroblasts from the Non-R patient, mitochondrial superoxide was markedly increased, suggesting oxidative stress in these organelles. This aligns with the very high OXPHOS rate observed in these cells, since complex I of the respiratory chain produces most of the superoxide (Murphy, 2009). High OXPHOS could itself be a result of the markedly increased mitochondrial Ca^{2+} measured in these cells. Interestingly, the oxidative stress appeared to be exclusive to mitochondria, since cytosolic ROS levels and the peroxidation of membrane lipids were not increased, and the glutathione antioxidant system was not affected in fibroblasts. A study by Takashi and Asada demonstrated that superoxide diffuses very slowly through phospholipid bilayers (M.-A. Takahashi & Asada, 1983). This suggests that in these fibroblasts, the outer mitochondrial membrane effectively compartmentalised most of the superoxide within mitochondria. Any minor amount that did cross into the cytosol were likely efficiently neutralised by local antioxidant systems, preventing any detrimental effects. However, it is important to note that having both high ROS and Ca^{2+} levels in mitochondria is a dangerous combination. Elevated mitochondrial ROS can sensitise mitochondria to apoptotic Ca^{2+}-induced mPTP opening (Drahota et al., 2012). Conversely, elevated mitochondrial Ca^{2+} can further increase ROS production, creating a positive feedback loop, which could potentially amplify mitochondrial dysfunction. Taken together, these findings emphasise again the pivotal role of mitochondria in the cellular anomalies detected in this patient's cells.

In NPCs and astrocytes derived from the Non-R patient, findings differ with the fibroblasts, with no increase in ROS. In fact, lipid peroxidation was reduced in NPCs, and there was a decrease in cytosolic ROS in astrocytes. However, it is important to note the high interindividual variability. On a closer look, it appears that these parameters might be elevated in the control group, rather than reduced in the Non-R patient. The levels in the Non-R patient were comparable to those in the Mito control. The high interindividual variability represents a major limitation in case studies, especially when, as in this instance, no cohort results are available.

4.2.2.2 Mitochondriopathy patient

In fibroblasts from the Mito patient, the increased lipid peroxidation coupled with a decreased GSH/GSSG ratio suggests a compromised antioxidant defence system. Lipid peroxidation can lead to membrane instability and potential cellular dysfunction. GSH is a primary cellular antioxidant, and its decrease can impair the cell's ability to neutralise reactive species.

In NPCs, the dual increase of mitochondrial superoxide and lipid peroxidation suggests elevated oxidative stress. Complex I-mediated superoxide production is mainly regulated by the rate of reverse electron transport (RET). RET occurs when reduced ubiquinone transfers

electrons back through complex I to flavin mononucleotides. RET is driven by a high ubiquinol/ubiquinone ratio alongside a high proton-motive force (Murphy, 2009). In short, RET is characterised by lower respiration, high MMP and results in high superoxide. Interestingly, this corresponds exactly to the changes observed in the Mito patient's NPCs. Therefore, RET is a likely explanation for high mitochondrial ROS in this patient. Continued RET results in high oxidative stress, and was associated with cell death during reperfusion following an ischemic episode (Chouchani et al., 2014). Oxidative stress was also evident in astrocytes from the Mito patient, which exhibited elevated cytosolic ROS.

In conclusion, the distinct redox homeostasis profiles across the cell types derived from the Mito patient highlight the cell-specific responses to oxidative stress. Moreover, these various alterations associated with redox homeostasis are indicative of a general cellular dysfunction in the Mito patient.

4.3 Focus on neurons

The ground-breaking discovery of a simplified protocol to derive induced pluripotent stem cells (iPSCs) from patients by Shinya Yamanaka and Kazutoshi Takahashi in 2006 has revolutionised biomedical research (K. Takahashi & Yamanaka, 2006). Prior to this, obtaining live human neurons necessitated invasive procedures and opening a patient's skull. Now, the iPSCs technology enables to generate iPSCs-derived neurons from easily accessible cells, from patients and healthy donors. In the present study, we utilised iPSC technology to produce mature cortical-like neurons from two case-study patients and their matched controls. The physiology of the neurons was investigated through two complementary approaches: live-cell imaging and patch-clamp measurements. The first approach provided insights into the MMP in somas and neurites, soma size, basal Ca^{2+} homeostasis, and the dynamics of spontaneous Ca^{2+} activity. The second approach allowed to measure both active and passive biophysical properties of the neurons, including resting membrane potential (RMP), currents densities, spontaneous action potentials (APs) and postsynaptic currents (PSCs).

4.3.1 Mitochondrial membrane potential and calcium

4.3.1.1 Mitochondrial membrane potential

Neurons are highly polarised and complex cells, which primarily rely on OXPHOS in mitochondria to meet their substantial ATP demand during neuronal transmission. OXPHOS is recognised as the main source of energy during neuronal activity and synaptic transmission (Seager et al., 2020). Here, we were not able to measure mitochondrial respiration due to the geometry of Seahorse XFp Miniplate wells, which prevented an even

distribution of neurons. However, since MMP is established by the proton gradient generated during OXPHOS, it can serve as an indicator of OXPHOS function.

Measuring MMP in both somas and neurites showed that MMP can be differentially regulated in these compartments. Specifically, in the Non-R patient, MMP was decreased solely in somas. Neuronal mitochondria have to respond to compartment specific needs. In the soma, mitochondrial energy production is primarily needed for the synthesis of proteins and lipids required for neuronal function. While it is challenging to infer mitochondrial functions based on MMP variations alone, the alterations observed in neurons from the Non-R patient suggest mitochondria do not function optimally. Assuming that decreased MMP reflects decreased OXPHOS rates and subsequent ATP production, it is plausible that biosynthetic pathways could be compromised in the somas of the Non-R patient neurons. Moreover, the soma is where most of the inputs from dendrites are integrated before an AP is generated. Insufficient ATP in the soma could affect the neuron's ability to integrate these signals effectively, potentially altering its responsiveness to synaptic inputs (Magee, 2000).

Additionally, when their MMP is low, neuronal mitochondria are transported in the retrograde direction, towards the cell body (K. E. Miller & Sheetz, 2004). An accumulation of depolarised, deenergised mitochondria in the soma could therefore also reflect an exhaustion of mitochondria residing in distal parts of the neurons.

In the Mito patient however, MMP variations were consistent, with a marked elevation both in somas and in neurites. While this elevated MMP might indicate a higher OXPHOS rate, it could also suggest alterations in the ETC complexes. For instance, a less active ATP synthase would lead to the accumulation of protons in the intermembrane space. As previously mentioned, a very high MMP has the potential to trigger RET, leading to a surge in ROS production (Murphy, 2009). Neurons are highly vulnerable to oxidative stress due to their high lipid content and weaker antioxidant defence. Thus, in neurons, RET could have serious consequences.

4.3.1.2 Basal calcium

Ca^{2+} ions are fundamental to neuronal function, not only serving as essential messengers in various cellular processes and signalling pathways but also playing a crucial role in mediating neuronal transmission within the nervous system.

Mitochondria play a major role in buffering intracellular Ca^{2+} during synaptic transmission. Early work by Jouaville *et al.* identified Ca^{2+} as a key mediator enabling mitochondria to match ATP production to the energy demand resulting from neuronal transmission. Indeed, they demonstrated that the concentration of ATP is proportional to the rise in mitochondrial Ca^{2+}, provided that oxidative substrates are available (Jouaville et al., 1999). While mitochondrial Ca^{2+} levels were unaffected in neurons from the Non-R patient, there was a

significant decrease in the Mito patient, despite an increased MMP. Taken together, these findings suggest that neurons from the Mito patient might struggle with the dynamic regulation of ATP synthesis, a process vital for their function.

Interestingly, this apparent alteration in Ca^{2+} uptake capacity by mitochondria did not result in accumulation of cytosolic Ca^{2+}. Instead, intracellular Ca^{2+} was markedly decreased in neurons from both the Non-R and the Mito patient. Given the central role of Ca^{2+} in neuronal function, such a decrease could have profound implications. At chemical synapses, the process of neurotransmitter release is Ca^{2+}-dependent. When an AP reaches the synaptic terminal, Ca^{2+} influx triggers the fusion of synaptic vesicles with the presynaptic membrane, releasing neurotransmitters into the synaptic cleft. A decreased baseline concentration of cytosolic Ca^{2+} might result in a lower probability of neurotransmitter release. This can also influence the timing of release, potentially leading to slower postsynaptic responses. Furthermore, reduced Ca^{2+} can alter the Ca^{2+}-dependent short term plasticity mechanisms, such as paired-pulse facilitation and depression (Neher & Sakaba, 2008).

4.3.1.3 Calcium dynamics

The drop in basal Ca^{2+} in neurons from both case study patients relative to their controls prompted us to investigate how neurotransmission could be affected in those patients. To do so, Ca^{2+} peaks were monitored using the fluorescent Ca^{2+} indicator Fura-2 over 20 min periods. The Ca^{2+} dynamics in the patients' cells were analysed through the amplitude of the Ca^{2+} peaks, the rise and the decay time of the signal.

Amplitude of the Ca^{2+} peaks did not change, but both rise time and time constant of decay were significantly longer in both patients. Prolonged Ca^{2+} signals could affect the timing and amount of neurotransmitter release, potentially leading to altered synaptic strength and plasticity (Südhof, 2012). Whether or not the prolonged Ca^{2+} signals lead to a higher amount of Ca^{2+} in the cytosol depends on the origin of the Ca^{2+} signal. The Ca^{2+} signal could originate from extracellular Ca^{2+} influx (e.g., through voltage-gated Ca^{2+} channels or NMDA receptors), or from the release of Ca^{2+} from intracellular stores. Given the 1-10 ms rise time and 1-60 ms decay time, and considering intracellular release is typically slower (Schiegg et al., 1995), the data suggests that the Ca^{2+} signal originated from extracellular Ca^{2+} entry (Ali & Kwan, 2020). While this would typically mean more Ca^{2+} entered the neurons, decreases in cytosolic Ca^{2+} levels were observed in patient-derived neurons, suggesting an enhanced buffering capacity. Considering that mitochondrial Ca^{2+} levels remained unchanged, an upregulation in Ca^{2+}-binding proteins like parvalbumin or calbindin could be responsible for this increased buffering. Enhanced expression or activity of these proteins might counteract the increased Ca^{2+} entry, resulting in reduced concentrations of free Ca^{2+} in the cytosol in resting conditions.

4.3.2 Electrophysiology

Electrophysiology represents a fundamental approach in neuroscientific research, enabling the quantification and analysis of neuronal electrical activities. Through the measurement of ion currents and voltage changes across neuronal membranes, the patch-clamp technique provides a direct assessment of neuronal biophysical properties and excitability. Alterations in electrophysiological parameters can be indicative of altered neuronal health or perturbed cellular homeostasis. Neuronal transmission and maintenance are highly energy-intensive processes. This is reflected in the high metabolic rate of the brain, which, despite accounting for only about 2% of body weight, consumes approximately 20% of the body's total energy (Clarke & Sokoloff, 1999). Considering this, it is obvious that perturbations in the brain's energy metabolism can have drastic implications. In line with this, mitochondrial function changes in NPCs from MDD patients were accompanied by pronounced alterations of electrophysiological properties in neurons derived from these NPCs (Triebelhorn et al., 2022). Here, the neurons derived from the Non-R and Mito case study patients displayed significant variations in many electrophysiological parameters.

4.3.2.1 Membrane's resting potential and capacitance, and ionic currents

The resting membrane potential (RMP) is the electrical voltage difference across a cell's membrane, primarily maintained by the differential distribution of potassium (K^+) ions on each side, facilitated by ion channels and pumps. RMP is typically about -70 mV in neurons *in vivo*, and approximately -45 to -60 mV in cultured neurons (Johansson et al., 1992; Lamas et al., 2002). Another parameter giving insights into a neuronal membrane's electrical properties is membrane capacitance, which reflects the membrane's ability to store electrical charges. This ability is directly linked to its surface area, and therefore to cell size (M.-H. Kim & von Gersdorff, 2010). Capacitance was remarkably decreased in neurons from all patients. Together with the depolarised RMP observed in the MDD cohort and the Mito patient, these findings indicate a compromised energy supply due to mitochondrial dysfunction. This is underscored by the substantial energy demands of maintaining RMP and the pivotal role of mitochondrial biogenesis in axonal growth (Vaarmann et al., 2016). To adjust for variations in soma size, Na^+ and K^+ currents were normalised to the membrane capacitance. The resulting parameter is called current density, and provides insights into neuronal excitability and AP generation and propagation. Specifically, Na^+ drives rapid depolarisation, while K^+ facilitates subsequent repolarisation. A striking feature of neurons from both patients, is the markedly increased density of K^+ currents, pointing to efficient post-AP repolarisation. Furthermore, the MDD cohort and Mito patient-derived neurons displayed elevated Na^+ current densities, suggesting a quicker depolarisation during AP, which could influence AP threshold and signal transmission.

4.3.2.2 Spontaneous action potentials

Excitability is determined by the proximity of the RMP to the AP threshold, and by the strength of the input relative to the membrane's resistance and capacitance, which together dictate the capacity of a current to generate a voltage change. On the other hand, Na^+ and K^+ current densities influence depolarisation and repolarisation. Together these parameters determine the frequency and dynamics of spontaneous APs.

In the Non-R patient, a hyperpolarised RMP with constant Na^+ current density made reaching the AP threshold challenging. Consistently, spontaneous activity was significantly lower, both at -50 and -80 mV, and there was a lower frequency of APs in active cells. Additionally, the APs observed were smaller and narrower. Overall, these observations point to a significant shift in excitability and neuronal transmission in the Non-R patient.

In neurons from the Mito patient and the MDD cohort, a depolarised RMP was closer to the threshold for AP generation, and increased Na^+ currents further promoted depolarisation. This led to a high proportion of neurons showing spontaneous APs at -50 mV. In the Mito patient, the resulting APs were taller, yet narrower, as seen in their maximal amplitude and half-maximum width. This is consistent with a faster depolarisation and repolarisation indicated by changes in Na^+ and K^+ currents. Such enhanced excitability can influence the overall activity patterns within neural circuits and might be associated with pathological conditions.

4.3.2.3 Spontaneous postsynaptic currents

Spontaneous postsynaptic currents (PSCs) provide valuable insights into the functional properties and dynamics of neural networks, including connectivity, neurotransmission and plasticity. At a holding potential of -80 mV, AMPA-type glutamate receptors, permeable to Na^+ and K^+, are involved in PSCs. The activation of these receptors leads to an influx of Na^+ ions into the cell, producing a negative (inward) current.

PSCs were drastically altered in neurons from the Non-R patient. A much smaller fraction of cells had spontaneous PSCs relative to the control and those that did have them, showed a significant drop in event frequency. The PSCs had extended rise time, potentially linked to the increased amplitude. This points to a modified network excitability, aligning with the infrequent spontaneous APs observed. These observations could be indicative of lower synaptic density, synaptic degeneration or altered properties of postsynaptic AMPA receptors, such as desensitisation or altered subunit composition.

In neurons from the Mito patient, while there were no differences in the synaptic activity, spontaneous PSCs kinetics were significantly altered. Lower amplitude combined with longer rise time and decay time suggest PSCs that are both smaller and wider. This could indicate changes in neurotransmitter release, either due to reduced neurotransmitter content per

vesicle, or fewer vesicles being released. The latter seems plausible given the decreased Ca^{2+} levels in Mito neurons. The prolonged rise time could be due to changes in synaptic structure, like wider synaptic cleft. Collectively, the synaptic currents changes could lead to less efficient synaptic transmission and slower synaptic dynamics.

4.3.2.4 Conclusions

4.3.2.4.1 Antidepressant non-responder patient

In neurons from the Non-R patient, analysis of the electrophysiological properties revealed decreased excitability and synaptic transmission.

Reduced excitability can influence the growth and retraction of dendritic spines, the primary sites for excitatory synapses. This can affect the neuronal network's connectivity patterns. In line with this, neuroimaging studies have shown changes in interregional connectivity in depressed patients (Helm et al., 2018).

Altered synaptic transmission can result in altered synaptic plasticity, a hallmark of MDD (Vose & Stanton, 2017). The changes observed in our experimental conditions suggest impairments specifically in postsynaptic AMPA receptors. In line with this, Mao *et al.* reported a downregulation of surface AMPA receptor in a rat model of depression (Mao et al., 2022). Interestingly, Vadodaria *et al.* reported altered neurite growth and morphology in neurons derived from serotonin reuptake inhibitors (SSRI) non-responder depressed patients. These changes were associated with lowered expression of key Protocadherin alpha genes (Vadodaria et al., 2019). Such alterations in the Non-R patient could influence network activity and explain the observed decreases in spontaneous APs and PSCs.

Moreover, the brain's cortical region is densely innervated by serotonin neurons and has a high expression of serotonergic receptors (Puig & Gulledge, 2011). Considering our findings, cortical-like neurons from the Non-R patient might be less responsive to serotonergic signals due to their hyperpolarisation. This could mean that these neurons are less receptive to the increased serotonergic signalling resulting from AD treatment, potentially explaining the Non-R patient's lack of response to such treatments. To validate this hypothesis, further investigations would be necessary. One approach could involve using pharmacological agents or optogenetic tools (e.g. chloride-conducting channel rhodopsins) to induce hyperpolarisation in cortical-like neurons from a healthy donor and then recording the postsynaptic response to serotonin.

4.3.2.4.2 Mitochondriopathy patient

In neurons from the Mito patient, we observed two main alterations: increased excitability and lower efficiency of synaptic transmission.

Hyperexcitability is a common feature of mitochondrial disorders, especially in MELAS (Sproule & Kaufmann, 2008) and Myoclonus Epilepsy associated with Ragged-Red Fibres (MERRF) (Lorenzoni et al., 2014). Supporting this, mice models with induced mitochondrial dysfunction by conditional knock-out of critical mitochondrial proteins showed increased excitability in both glutamatergic neurons (De La Rossa et al., 2022) and serotonergic neurons (Kato et al., 2018). While these studies did not identify the exact cause of hyperexcitability, both suggested a potential disruption in Ca^{2+} homeostasis, with defective Ca^{2+} accumulation in mitochondria following depolarisation. This aligns with the decreased mitochondrial Ca^{2+} levels observed in the Mito patient's neurons.

Synaptic mitochondria are critical in assisting synaptic transmission, aiding neurotransmitter synthesis, storage and the ATP-driven packaging of these neurotransmitters into vesicles. Mitochondria also contribute to vesicle cycling, largely due to their key role in maintaining intra-synaptic Ca^{2+} balance (Guo et al., 2017). There is a growing body of evidence linking mitochondrial dysfunction to synaptic transmission failures in Alzheimer's disease. Notably, patients with early-stage Alzheimer's disease show synaptic mitochondria issues even before significant synaptic damage occurs (Guo et al., 2017). Given this, it is plausible that the synaptic transmission alterations observed in the Mito patient stem from impairments of neuronal mitochondria.

4.4 Decreased cell size

When recording fluorescence in Fura-2/AM-loaded fibroblasts, we consistently observed that more patients' cells fitted the visual field that control cells. Detailed analysis by carefully drawing regions of interest around the cytoplasm confirmed that patients' fibroblasts were smaller. This encouraged a review of Fura-2 images from the previous studies, revealing that fibroblasts and NPCs from the entire MDD cohort were smaller compared to non-depressed controls (Triebelhorn et al., 2022). Systematic measurement confirmed this size reduction in patients across all cell types. Additionally, membrane capacitance, considered as another way to measure neuron size, was also decreased in MDD patients and in the two case study patients (Triebelhorn et al., 2022). The only exception observed were larger astrocytes in the Mito patient, which also differed from other cells by exhibiting elevated cellular ROS. This size increase may be a defence against oxidative stress, where increased cytoplasm volume dilutes ROS. Additionally, oxidative stress can trigger the production of protective proteins, such as heat shock proteins and antioxidant enzymes, thus contributing to cellular hypertrophy (Reeg et al., 2016). All other patients' astrocytes are consistently smaller than the corresponding controls, so overall, cell size remains a robust surrogate marker for patients' cells.

Interestingly, in an iPS model where mitochondrial translocator protein 18-KDa (TSPO) was knocked-out, cells were also notably smaller. Specifically, the absence of TSPO led to reduced sizes in iPS-derived NPCs, astrocytes and neurons. This size reduction was accompanied by decreased mitochondrial respiration and MMP in NPCs and astrocytes (Wetzel et al., 2024, under review). Similarly, when TSPO was silenced in human microglia, the cells were smaller and had lower MMP (Bader et al., 2023). These findings, in conjunction with ours, suggest a relationship between mitochondrial dysfunction and reduced cell size.

Cell size is influenced by growth, division, genetic regulation, and environmental conditions. Cells typically enlarge in preparation for division. However, in our study, cell cycle was synchronised by simultaneously splitting both patients and control cells.

While most cellular components scale with cell size, mitochondrial content and function do not. For instance, OXPHOS and MMP are the highest in medium-sized cells. This discrepancy in mitochondrial function suggests an optimal cell size for maximising cellular health and proliferation potential (Miettinen & Björklund, 2017). Additionally, the mevalonate pathway, responsible for producing components like cholesterol for the plasma membrane, impacts how mitochondria function and scale (Miettinen et al., 2014).

Growth factors are also essential regulators of cell size. Many of their receptors are tyrosine kinases that require ATP for activation. Moreover, growth factor-induced changes in cell size often coincide with increased biosynthetic activities, which are energy-intensive (Ward & Thompson, 2012). Cytoskeleton plays a central role in regulating cell shape and is therefore able to influence cell size. Specifically, actin filaments form a dense network under the plasma membrane that provides mechanical support and determines cell shape. Pedersen *et al.* have reported that cell shrinkage is associated with an increase, and cell swelling with a decrease in F-actin content (Pedersen et al., 2001). Interestingly, there seems to be a link between mitochondrial dysfunction and actin polymerisation. Notably, a study by Chakrabarti *et al.* revealed that actin polymerises in response to mitochondrial dysfunction (Chakrabarti et al., 2022). Considering these findings, it is conceivable that in our patients' cells, mitochondrial dysfunction led to increased actin polymerisation, resulting in cell shrinkage.

Overall, while further investigations are necessary to precisely pinpoint the reason for smaller size in patients' cells, it is evident that mitochondrial dysfunction, leading to reduced energy output, is a likely factor. Future research might explore the activity of the mevalonate pathway in patient's cells or attempt to replicate the size reduction by modifying mitochondrial functions in control cells.

4.5 Limitations

While this study provides valuable insights into the role of mitochondrial (dys)function in MDD, it is essential to acknowledge its limitations. The present section outlines the potential constraints and boundaries of the research.

4.5.1 Interindividual variability

Interindividual variability in measurements from human patient-derived cells can stem from many factors including genetics, epigenetics, environmental, and lifestyle.

Although one might expect consistent data from healthy, non-depressed controls, discrepancies were noted between Ctl 17 and Ctl 18 in our study, particularly in oxidative stress parameters. This inconsistency might be attributed to the 25-year age gap between the Ctl 17/Non-R and the Ctl 18/Mito pairs. Increased oxidative stress with age is well documented (Cui et al., 2012), specifically with increased steady-state concentrations of lipid peroxidation products (Praticò, 2002) and oxidative DNA damage (OH8dG; (Mecocci et al., 1999)). This underscores the importance of age-matching controls and patients. Additionally, established sex differences in mitochondrial function emphasise the importance of sex-matching in control/patient pairs (Demarest & McCarthy, 2015).

Given the variability between individual subjects, we aimed to relate our case study data to data obtained from a larger cohort of MDD patients and controls. However, due to the depth and breadth of the case studies, cohort data was not always available for comparison.

4.5.2 Generalisability

Interindividual variability is an intrinsic limitation of case studies, limiting their broad generalisability, and we acknowledge that our findings are based on individual observations and should not be seen as universally representative of mitochondrial diseases and treatment-resistant depression.

While generalisation in case study research is debated, some argue that case studies can offer "theoretical generalisation". This means that a case study can help in refining or building theories that can then be tested in larger samples for broader applicability (Roller, 2020). We feel that our study aligns with this perspective. Data from the Non-R patient challenges the theory that mitochondrial dysfunction in MDD is solely about reduced functions. Instead, it suggests a harmful imbalance of mitochondrial and cellular parameters. Meanwhile, the Mito patient data offers detailed insights into mitochondrial dysfunctions and their impact on many cellular functions, shedding light on potential new MDD-related mitochondrial impairments.

4.5.3 Information about case study patients

A limitation of our study is the incomplete understanding of the conditions affecting our case study patients.

For the Mito patient, despite thorough clinical investigations, there is no clear diagnosis for the specific mitochondriopathy yet. While ongoing investigations continue, it is possible that the mitochondriopathy results from an unidentified pathology. However, this provides an opportunity to investigate the comorbidity of MDD with another condition affecting mitochondrial functions, as seen in mitochondrial diseases, Parkinson's, Alzheimer's, diabetes, and cardiovascular diseases (Arnaud et al., 2022).

For the Non-R patient, the origin of antidepressant resistance was not determined through genetic testing. While pharmacogenomics can pinpoint genetic variations affecting drug response and have shown long-term cost-effectiveness in the U.S. (Groessl et al., 2018), such tests are not covered by public health insurance in Germany. They are available only as self-paid services, posing a significant cost to patients. For instance, a test for 16 frequently prescribed active substances costs around 400€, with an added 100€ for sample collection at a doctor's office (STADApharm GmbH, 2016).

5 Summary and conclusion

This study provided a detailed analysis of two case study patient in order to elucidate the intricate pathomechanisms underlying the development of major depressive disorder (MDD).

The antidepressant non-responder patient (Non-R) presented intriguing findings. In the Non-R patient's fibroblasts and NPCs, we observed an important increase in OXPHOS activity. However, this was not accompanied by a rise in MMP, suggesting a potential proton leak, possibly via the adenine nucleotide translocase on the outer mitochondrial membrane. The unexpected reduced respiration in astrocytes was thought to be due to the unique ways astrocytic mitochondria handle calcium. Specifically, we hypothesised that heightened activity or expression of the NCLX calcium transporter might cause an excessive mitochondrial calcium efflux to the cytosol. This could lead to reduced activation of the tricarboxylic acid cycle enzymes, resulting in decreased OXPHOS. In the Non-R patient's fibroblasts, we speculated that high mitochondrial calcium induced an increased OXPHOS activity, leading to a rise in mitochondrial ROS. This combination of high mitochondrial calcium and ROS could initiate a damaging positive feedback loop, further indicating mitochondrial dysfunction in this patient. In neurons, evidence suggested compromised synaptic transmission. First, a decreased MMP in the soma indicated reduced OXPHOS activity and ATP production, potentially affecting the integration of synaptic inputs in the soma. Second, lowered basal calcium levels and extended calcium peak durations might affect synaptic transmission by affecting neurotransmitter release and short-term plasticity

mechanisms. Third, spontaneous postsynaptic currents were markedly reduced. Such an impairment in synaptic functions could be attributed to altered mitochondrial functions and changes in postsynaptic AMPA receptors. The Non-R patient's neurons also displayed decreased excitability, attributed to the hyperpolarisation of the resting membrane potential (RMP), leading to fewer spontaneous action potentials. This altered network activity might be linked to altered neurite growth. Overall, these changes might make the patient's cortical neurons less responsive to signals from neurons innervating the cortex, such as serotonergic neurons. This could potentially explain the patient's non-responsiveness to serotonin-increasing antidepressant treatments.

In the patient with a mild mitochondriopathy (Mito), fibroblasts and NPCs displayed reduced mitochondrial respiration typical of mitochondrial disorders. However, astrocyte respiration was unchanged, again contrasting with other cells. Despite stable respiration, ATP levels were decreased, possibly due to ROS-mediated inhibition of ATP synthase and glycolysis. Moreover, the unchanged respiration, despite decreased MMP and ATP, suggested mitochondria failed to meet the astrocytes' energy demand. Oxidative stress was elevated in Mito patient's cells, varying by cell type, with signs including increased lipid peroxidation, and both cytosolic and mitochondrial ROS. In NPCs, the combination of high MMP, low respiration and elevated ROS suggested reverse electron transport, potentially impacting cell function and neuronal differentiation. Neurons from the Mito patient showed high MMP in both soma and neurites, indicating either enhanced OXPHOS or alteration in the electron transport chain. Both scenarios could lead to increased ROS production, particularly harmful for neurons. These neurons also exhibited hyperexcitability, linked to a depolarised RMP and increased sodium current density. This hyperexcitability might also arise from impaired calcium uptake into mitochondria during transmission, consistent with observed reductions in mitochondrial calcium. Given calcium's role in dynamically regulating mitochondrial ATP synthesis in response to energy demand, the decreased mitochondrial calcium implied that Mito neurons struggled adjusting to the energy demands of neurotransmission. This was further supported by reduced cytosolic calcium and prolonged calcium peak durations, leading to diminished and slower synaptic currents. We postulate that mitochondrial dysfunction in the Mito patient's neurons contributed to synaptic degradation. Overall, the Mito patient's cells showed clear signs of mitochondrial dysfunction.

Finally, cells from both patients were overall smaller in size. Given mitochondria's role in determining optimal cell size, this could be a marker for mitochondrial dysfunction.

The Non-R patient's data offers a new perspective on MDD. It challenges the long-held belief that mitochondrial dysfunction in MDD is merely about reduced functions, hinting instead at a detrimental imbalance in mitochondrial and cellular dynamics. On the other hand, the Mito

patient's data provides a deeper dive into mitochondrial dysfunctions, illuminating their broader impact on cellular functions and potentially highlighting MDD-associated mitochondrial issues. Together, findings in these case study patients bring a new dimension to our understanding of MDD.

6 References

Ahmad, T., Aggarwal, K., Pattnaik, B., Mukherjee, S., Sethi, T., Tiwari, B. K., Kumar, M., Micheal, A., Mabalirajan, U., Ghosh, B., Sinha Roy, S., & Agrawal, A. (2013). Computational classification of mitochondrial shapes reflects stress and redox state. *Cell Death & Disease*, *4*(1), e461. https://doi.org/10.1038/cddis.2012.213

Alberts, B. (2015). *Molecular biology of the cell* (Sixth edition). Garland Science, Taylor and Francis Group.

Alevizos, B., Alevizos, E., Leonardou, A., & Zervas, I. (2012). Low dosage lithium augmentation in venlafaxine resistant depression: An open-label study. *Psychiatrike = Psychiatriki*, *23*(2), 143–148.

Ali, F., & Kwan, A. C. (2020). Interpreting in vivo calcium signals from neuronal cell bodies, axons, and dendrites: A review. *Neurophotonics*, *7*(1), 011402. https://doi.org/10.1117/1.NPh.7.1.011402

American Psychiatric Association. (2022). *Diagnostic And Statistical Manual Of Mental Disorders, Fifth Edition, Text Revision*.

Anderson, S., Bankier, A. T., Barrell, B. G., de Bruijn, M. H. L., Coulson, A. R., Drouin, J., Eperon, I. C., Nierlich, D. P., Roe, B. A., Sanger, F., Schreier, P. H., Smith, A. J. H., Staden, R., & Young, I. G. (1981). Sequence and organization of the human mitochondrial genome. *Nature*, *290*(5806), Article 5806. https://doi.org/10.1038/290457a0

Arnaud, A. M., Brister, T. S., Duckworth, K., Foxworth, P., Fulwider, T., Suthoff, E. D., Werneburg, B., Aleksanderek, I., & Reinhart, M. L. (2022). Impact of Major Depressive Disorder on Comorbidities: A Systematic Literature Review. *The Journal of Clinical Psychiatry*, *83*(6), 43390. https://doi.org/10.4088/JCP.21r14328

Bader, S., Würfel, T., Jahner, T., Nothdurfter, C., Rupprecht, R., Milenkovic, V. M., & Wetzel, C. H. (2023). Impact of Translocator Protein 18 kDa (TSPO) Deficiency on Mitochondrial Function and the Inflammatory State of Human C20 Microglia Cells. *Cells*, *12*(6), 954. https://doi.org/10.3390/cells12060954

Barnhart, D., Voytenko, V., Lemke, A., Tobey, D., Biondolillo, K., & Bornhoff, A. (2018). *Psychosocial Factors in Treatment-Resistant Depression: An Umbrella Review*. https://doi.org/10.13140/RG.2.2.15330.58560

Berlim, M. T., & Turecki, G. (2007). What is the meaning of treatment resistant/refractory major depression (TRD)? A systematic review of current randomized trials. *European Neuropsychopharmacology: The Journal of the European College of Neuropsychopharmacology*, *17*(11), 696–707. https://doi.org/10.1016/j.euroneuro.2007.03.009

Berridge, M. J., Lipp, P., & Bootman, M. D. (2000). The versatility and universality of calcium signalling. *Nature Reviews Molecular Cell Biology*, *1*(1), 11–21. https://doi.org/10.1038/35036035

Beurel, E., Toups, M., & Nemeroff, C. B. (2020). The Bidirectional Relationship of Depression and Inflammation: Double Trouble. *Neuron*, *107*(2), 234–256. https://doi.org/10.1016/j.neuron.2020.06.002

Bowers, W. A. (1990). Treatment of depressed in-patients. Cognitive therapy plus medication, relaxation plus medication, and medication alone. *The British Journal of Psychiatry: The Journal of Mental Science*, *156*, 73–78. https://doi.org/10.1192/bjp.156.1.73

Brand, M. D., Affourtit, C., Esteves, T. C., Green, K., Lambert, A. J., Miwa, S., Pakay, J. L., & Parker, N. (2004). Mitochondrial superoxide: Production, biological effects, and activation of uncoupling proteins. *Free Radical Biology and Medicine*, *37*(6), 755–767. https://doi.org/10.1016/j.freeradbiomed.2004.05.034

Brand, M. D., Pakay, J. L., Ocloo, A., Kokoszka, J., Wallace, D. C., Brookes, P. S., & Cornwall, E. J. (2005). The basal proton conductance of mitochondria depends on adenine nucleotide translocase content. *Biochemical Journal*, *392*(Pt 2), 353–362. https://doi.org/10.1042/BJ20050890

Breton, C. V., Song, A. Y., Xiao, J., Kim, S.-J., Mehta, H. H., Wan, J., Yen, K., Sioutas, C., Lurmann, F., Xue, S., Morgan, T. E., Zhang, J., & Cohen, P. (2019). Effects of air pollution on mitochondrial function, mitochondrial DNA methylation, and mitochondrial peptide expression. *Mitochondrion*, *46*, 22–29. https://doi.org/10.1016/j.mito.2019.04.001

Brookes, P. S., Rolfe, D. F., & Brand, M. D. (1997). The proton permeability of liposomes made from mitochondrial inner membrane phospholipids: Comparison with isolated mitochondria. *The Journal of Membrane Biology*, *155*(2), 167–174. https://doi.org/10.1007/s002329900168

Cai, N., Li, Y., Chang, S., Liang, J., Lin, C., Zhang, X., Liang, L., Hu, J., Chan, W., Kendler, K. S., Malinauskas, T., Huang, G.-J., Li, Q., Mott, R., & Flint, J. (2015). Genetic Control over mtDNA and Its Relationship to Major Depressive Disorder. *Current Biology: CB*, *25*(24), 3170–3177. https://doi.org/10.1016/j.cub.2015.10.065

Carafoli, E., Tiozzo, R., Lugli, G., Crovetti, F., & Kratzing, C. (1974). The release of calcium from heart mitochondria by sodium. *Journal of Molecular and Cellular Cardiology*, *6*(4), 361–371. https://doi.org/10.1016/0022-2828(74)90077-7

Casarotto, P. C., Girych, M., Fred, S. M., Kovaleva, V., Moliner, R., Enkavi, G., Biojone, C., Cannarozzo, C., Sahu, M. P., Kaurinkoski, K., Brunello, C. A., Steinzeig, A., Winkel, F., Patil, S., Vestring, S., Serchov, T., Diniz, C. R. A. F., Laukkanen, L., Cardon, I., … Castrén, E. (2021). Antidepressant drugs act by directly binding to TRKB neurotrophin receptors. *Cell*, *184*(5), 1299-1313.e19. https://doi.org/10.1016/j.cell.2021.01.034

Castro, J., Ruminot, I., Porras, O. H., Flores, C. M., Hermosilla, T., Verdugo, E., Venegas, F., Härtel, S., Michea, L., & Barros, L. F. (2006). ATP steal between cation pumps: A mechanism linking Na+ influx to the onset of necrotic Ca2+ overload. *Cell Death & Differentiation*, *13*(10), Article 10. https://doi.org/10.1038/sj.cdd.4401852

Catterall, W. A. (2000). Structure and regulation of voltage-gated Ca2+ channels. *Annual Review of Cell and Developmental Biology*, *16*, 521–555. https://doi.org/10.1146/annurev.cellbio.16.1.521

Chakrabarti, R., Fung, T. S., Kang, T., Elonkirjo, P. W., Suomalainen, A., Usherwood, E. J., & Higgs, H. N. (2022). Mitochondrial dysfunction triggers actin polymerization necessary for rapid glycolytic activation. *Journal of Cell Biology*, *221*(11), e202201160. https://doi.org/10.1083/jcb.202201160

Charlson, F. J., Baxter, A. J., Dua, T., Degenhardt, L., Whiteford, H. A., & Vos, T. (2014). Excess mortality from mental, neurological and substance use disorders in the Global Burden of Disease Study 2010. *Epidemiology and Psychiatric Sciences*, *24*(2), 121–140. https://doi.org/10.1017/S2045796014000687

Cheetham, S. C., Katona, CLE., & Horton, R. W. (1991). CHAPTER 6—POST-MORTEM STUDIES OF NEUROTRANSMITTER BIOCHEMISTRY IN DEPRESSION AND SUICIDE. In R. W. Horton & C. L. E. Katona (Eds.), *Biological Aspects of Affective Disorders* (pp. 191–221). Academic Press. https://doi.org/10.1016/B978-0-12-356510-5.50012-1

Cheng, X.-Y., Biswas, S., Li, J., Mao, C.-J., Chechneva, O., Chen, J., Li, K., Li, J., Zhang, J.-R., Liu, C.-F., & Deng, W.-B. (2020). Human iPSCs derived astrocytes rescue rotenone-induced mitochondrial dysfunction and dopaminergic neurodegeneration in vitro by donating functional mitochondria. *Translational Neurodegeneration*, *9*(1), 13. https://doi.org/10.1186/s40035-020-00190-6

Chinopoulos, C. (2011). Mitochondrial consumption of cytosolic ATP: Not so fast. *FEBS Letters*, *585*(9), 1255–1259. https://doi.org/10.1016/j.febslet.2011.04.004

Chipuk, J. E., Bouchier-Hayes, L., & Green, D. R. (2006). Mitochondrial outer membrane permeabilization during apoptosis: The innocent bystander scenario. *Cell Death & Differentiation*, *13*(8), Article 8. https://doi.org/10.1038/sj.cdd.4401963

Chouchani, E. T., Pell, V. R., Gaude, E., Aksentijević, D., Sundier, S. Y., Robb, E. L., Logan, A., Nadtochiy, S. M., Ord, E. N. J., Smith, A. C., Eyassu, F., Shirley, R., Hu, C.-H., Dare, A. J., James, A. M., Rogatti, S., Hartley, R. C., Eaton, S., Costa, A. S. H., … Murphy, M. P. (2014). Ischaemic accumulation of succinate controls reperfusion injury

through mitochondrial ROS. *Nature*, *515*(7527), Article 7527. https://doi.org/10.1038/nature13909

Clarke, D. D., & Sokoloff, L. (1999). Circulation and Energy Metabolism of the Brain. In *Basic Neurochemistry: Molecular, Cellular and Medical Aspects. 6th edition*. Lippincott-Raven. https://www.ncbi.nlm.nih.gov/books/NBK20413/

Coppen, A. (1967). The biochemistry of affective disorders. *The British Journal of Psychiatry: The Journal of Mental Science*, *113*(504), 1237–1264. https://doi.org/10.1192/bjp.113.504.1237

Cui, H., Kong, Y., & Zhang, H. (2012). Oxidative Stress, Mitochondrial Dysfunction, and Aging. *Journal of Signal Transduction*, *2012*, 646354. https://doi.org/10.1155/2012/646354

Davies, K. M., & Daum, B. (2013). Role of cryo-ET in membrane bioenergetics research. *Biochemical Society Transactions*, *41*(5), 1227–1234. https://doi.org/10.1042/BST20130029

De La Rossa, A., Laporte, M. H., Astori, S., Marissal, T., Montessuit, S., Sheshadri, P., Ramos-Fernández, E., Mendez, P., Khani, A., Quairiaux, C., Taylor, E. B., Rutter, J., Nunes, J. M., Carleton, A., Duchen, M. R., Sandi, C., & Martinou, J.-C. (2022). Paradoxical neuronal hyperexcitability in a mouse model of mitochondrial pyruvate import deficiency. *eLife*, *11*, e72595. https://doi.org/10.7554/eLife.72595

Dehmelt, L., & Halpain, S. (2005). The MAP2/Tau family of microtubule-associated proteins. *Genome Biology*, *6*(1), 204. https://doi.org/10.1186/gb-2004-6-1-204

Demarest, T. G., & McCarthy, M. M. (2015). Sex differences in mitochondrial (dys)function: Implications for neuroprotection. *Journal of Bioenergetics and Biomembranes*, *47*(1–2), 173–188. https://doi.org/10.1007/s10863-014-9583-7

Distelmaier, F., Valsecchi, F., Liemburg-Apers, D. C., Lebiedzinska, M., Rodenburg, R. J., Heil, S., Keijer, J., Fransen, J., Imamura, H., Danhauser, K., Seibt, A., Viollet, B., Gellerich, F. N., Smeitink, J. A. M., Wieckowski, M. R., Willems, P. H. G. M., & Koopman, W. J. H. (2015). Mitochondrial dysfunction in primary human fibroblasts triggers an adaptive cell survival program that requires AMPK-α. *Biochimica et Biophysica Acta (BBA) - Molecular Basis of Disease*, *1852*(3), 529–540. https://doi.org/10.1016/j.bbadis.2014.12.012

Drahota, Z., Endlicher, R., Staňková, P., Rychtrmoc, D., Milerová, M., & Červinková, Z. (2012). Characterization of calcium, phosphate and peroxide interactions in activation of mitochondrial swelling using derivative of the swelling curves. *Journal of Bioenergetics and Biomembranes*, *44*(3), 309–315. https://doi.org/10.1007/s10863-012-9443-2

Duchen, M. R. (2000). Mitochondria and calcium: From cell signalling to cell death. *The Journal of Physiology*, *529*(Pt 1), 57–68. https://doi.org/10.1111/j.1469-7793.2000.00057.x

Echtay, K. S., Roussel, D., St-Pierre, J., Jekabsons, M. B., Cadenas, S., Stuart, J. A., Harper, J. A., Roebuck, S. J., Morrison, A., Pickering, S., Clapham, J. C., & Brand, M. D. (2002). Superoxide activates mitochondrial uncoupling proteins. *Nature*, *415*(6867), 96–99. https://doi.org/10.1038/415096a

El-Hage, W., Leman, S., Camus, V., & Belzung, C. (2013). Mechanisms of antidepressant resistance. *Frontiers in Pharmacology*, *4*. https://doi.org/10.3389/fphar.2013.00146

Evans, C. S., & Holzbaur, E. L. F. (2020). Quality Control in Neurons: Mitophagy and Other Selective Autophagy Mechanisms. *Journal of Molecular Biology*, *432*(1), 240–260. https://doi.org/10.1016/j.jmb.2019.06.031

Fattal, O., Link, J., Quinn, K., Cohen, B. H., & Franco, K. (2007). Psychiatric comorbidity in 36 adults with mitochondrial cytopathies. *CNS Spectrums*, *12*(6), 429–438. https://doi.org/10.1017/s1092852900015303

Fava, M., & Rush, A. J. (2006). Current Status of Augmentation and Combination Treatments for Major Depressive Disorder: A Literature Review and a Proposal for a Novel Approach to Improve Practice. *Psychotherapy and Psychosomatics*, *75*(3), 139–153. https://doi.org/10.1159/000091771

Filadi, R., Theurey, P., Rossi, A., Fedeli, C., & Pizzo, P. (2017). Mitochondrial Ca2+ Handling and Behind: The Importance of Being in Contact with Other Organelles. In T. K. Rostovtseva (Ed.), *Molecular Basis for Mitochondrial Signaling* (pp. 3–39). Springer International Publishing. https://doi.org/10.1007/978-3-319-55539-3_1

Frigerio, F., Casimir, M., Carobbio, S., & Maechler, P. (2008). Tissue specificity of mitochondrial glutamate pathways and the control of metabolic homeostasis. *Biochimica et Biophysica Acta (BBA) - Bioenergetics*, *1777*(7), 965–972. https://doi.org/10.1016/j.bbabio.2008.04.031

Garbett, K. A., Vereczkei, A., Kálmán, S., Wang, L., Korade, Ž., Shelton, R. C., & Mirnics, K. (2015). Fibroblasts from patients with major depressive disorder show distinct transcriptional response to metabolic stressors. *Translational Psychiatry*, *5*, e523. https://doi.org/10.1038/tp.2015.14

Gardner, A., & Boles, R. G. (2011). Beyond the serotonin hypothesis: Mitochondria, inflammation and neurodegeneration in major depression and affective spectrum disorders. *Progress in Neuro-Psychopharmacology & Biological Psychiatry*, *35*(3), 730–743. https://doi.org/10.1016/j.pnpbp.2010.07.030

Gardner, A., Johansson, A., Wibom, R., Nennesmo, I., von Döbeln, U., Hagenfeldt, L., & Hällström, T. (2003). Alterations of mitochondrial function and correlations with personality traits in selected major depressive disorder patients. *Journal of Affective Disorders*, *76*(1), 55–68. https://doi.org/10.1016/S0165-0327(02)00067-8

Gerencser, A. A., Chinopoulos, C., Birket, M. J., Jastroch, M., Vitelli, C., Nicholls, D. G., & Brand, M. D. (2012). Quantitative measurement of mitochondrial membrane potential in cultured cells: Calcium-induced de- and hyperpolarization of neuronal mitochondria. *The Journal of Physiology*, *590*(12), 2845–2871. https://doi.org/10.1113/jphysiol.2012.228387

Gorman, G. S., Chinnery, P. F., DiMauro, S., Hirano, M., Koga, Y., McFarland, R., Suomalainen, A., Thorburn, D. R., Zeviani, M., & Turnbull, D. M. (2016). Mitochondrial diseases. *Nature Reviews Disease Primers*, *2*(1), 16080. https://doi.org/10.1038/nrdp.2016.80

Gray, M. W. (1989). The evolutionary origins of organelles. *Trends in Genetics: TIG*, *5*(9), 294–299. https://doi.org/10.1016/0168-9525(89)90111-x

Green, D. R., & Reed, J. C. (1998). Mitochondria and apoptosis. *Science (New York, N.Y.)*, *281*(5381), 1309–1312. https://doi.org/10.1126/science.281.5381.1309

Groessl, E. J., Tally, S. R., Hillery, N., Maciel, A., & Garces, J. A. (2018). Cost-Effectiveness of a Pharmacogenetic Test to Guide Treatment for Major Depressive Disorder. *Journal of Managed Care & Specialty Pharmacy*, *24*(8), 10.18553/jmcp.2018.24.8.726. https://doi.org/10.18553/jmcp.2018.24.8.726

Gunter, T. E., & Pfeiffer, D. R. (1990). Mechanisms by which mitochondria transport calcium. *American Journal of Physiology-Cell Physiology*, *258*(5), C755–C786. https://doi.org/10.1152/ajpcell.1990.258.5.C755

Guo, L., Tian, J., & Du, H. (2017). Mitochondrial Dysfunction and Synaptic Transmission Failure in Alzheimer's Disease. *Journal of Alzheimer's Disease : JAD*, *57*(4), 1071–1086. https://doi.org/10.3233/JAD-160702

Hamilton, M. (1980). Rating depressive patients. *The Journal of Clinical Psychiatry*, *41*(12 Pt 2), 21–24.

Haworth, R. A., & Hunter, D. R. (1979). The Ca2+-induced membrane transition in mitochondria. II. Nature of the Ca2+ trigger site. *Archives of Biochemistry and Biophysics*, *195*(2), 460–467. https://doi.org/10.1016/0003-9861(79)90372-2

Helm, K., Viol, K., Weiger, T. M., Tass, P. A., Grefkes, C., del Monte, D., & Schiepek, G. (2018). Neuronal connectivity in major depressive disorder: A systematic review. *Neuropsychiatric Disease and Treatment*, *14*, 2715–2737. https://doi.org/10.2147/NDT.S170989

Hertz, L. (2013). The Glutamate–Glutamine (GABA) Cycle: Importance of Late Postnatal Development and Potential Reciprocal Interactions between Biosynthesis and

Degradation. *Frontiers in Endocrinology*, *4*. https://www.frontiersin.org/articles/10.3389/fendo.2013.00059

Hopp, S. C. (2021). Targeting microglia L-type voltage-dependent calcium channels for the treatment of central nervous system disorders. *Journal of Neuroscience Research*, *99*(1), 141–162. https://doi.org/10.1002/jnr.24585

Horn, A., Raavicharla, S., Shah, S., Cox, D., & Jaiswal, J. K. (2020). Mitochondrial fragmentation enables localized signaling required for cell repair. *The Journal of Cell Biology*, *219*(5), e201909154. https://doi.org/10.1083/jcb.201909154

Howard, D. M., Adams, M. J., Clarke, T.-K., Hafferty, J. D., Gibson, J., Shirali, M., Coleman, J. R. I., Hagenaars, S. P., Ward, J., Wigmore, E. M., Alloza, C., Shen, X., Barbu, M. C., Xu, E. Y., Whalley, H. C., Marioni, R. E., Porteous, D. J., Davies, G., Deary, I. J., … McIntosh, A. M. (2019). Genome-wide meta-analysis of depression identifies 102 independent variants and highlights the importance of the prefrontal brain regions. *Nature Neuroscience*, *22*(3), 343–352. https://doi.org/10.1038/s41593-018-0326-7

Hroudová, J., Fišar, Z., Kitzlerová, E., Zvěřová, M., & Raboch, J. (2013). Mitochondrial respiration in blood platelets of depressive patients. *Mitochondrion*, *13*(6), 795–800. https://doi.org/10.1016/j.mito.2013.05.005

Huntington, T. E., & Srinivasan, R. (2021). Astrocytic mitochondria in adult mouse brain slices show spontaneous calcium influx events with unique properties. *Cell Calcium*, *96*, 102383. https://doi.org/10.1016/j.ceca.2021.102383

Hyslop, P. A., Hinshaw, D. B., Halsey, W. A., Schraufstätter, I. U., Sauerheber, R. D., Spragg, R. G., Jackson, J. H., & Cochrane, C. G. (1988). Mechanisms of oxidant-mediated cell injury. The glycolytic and mitochondrial pathways of ADP phosphorylation are major intracellular targets inactivated by hydrogen peroxide. *The Journal of Biological Chemistry*, *263*(4), 1665–1675.

Ichas, F., Jouaville, L. S., Sidash, S. S., Mazat, J. P., & Holmuhamedov, E. L. (1994). Mitochondrial calcium spiking: A transduction mechanism based on calcium-induced permeability transition involved in cell calcium signalling. *FEBS Letters*, *348*(2), 211–215. https://doi.org/10.1016/0014-5793(94)00615-6

Ide, T., Tsutsui, H., Hayashidani, S., Kang, D., Suematsu, N., Nakamura, K., Utsumi, H., Hamasaki, N., & Takeshita, A. (2001). Mitochondrial DNA Damage and Dysfunction Associated With Oxidative Stress in Failing Hearts After Myocardial Infarction. *Circulation Research*, *88*(5), 529–535. https://doi.org/10.1161/01.RES.88.5.529

Inczedy-Farkas, G., Remenyi, V., Gal, A., Varga, Z., Balla, P., Udvardy-Meszaros, A., Bereznai, B., & Molnar, M. J. (2012). Psychiatric symptoms of patients with primary mitochondrial DNA disorders. *Behavioral and Brain Functions*, *8*(1), 9. https://doi.org/10.1186/1744-9081-8-9

Iosifescu, D. V., Bolo, N. R., Nierenberg, A. A., Jensen, J. E., Fava, M., & Renshaw, P. F. (2008). Brain Bioenergetics and Response to Triiodothyronine Augmentation in Major Depressive Disorder. *Biological Psychiatry*, *63*(12), 1127–1134. https://doi.org/10.1016/j.biopsych.2007.11.020

Ishida, A., Shigeri, Y., Taniguchi, T., & Kameshita, I. (2003). Protein phosphatases that regulate multifunctional Ca2+/calmodulin-dependent protein kinases: From biochemistry to pharmacology. *Pharmacology & Therapeutics*, *100*(3), 291–305. https://doi.org/10.1016/j.pharmthera.2003.09.003

Jackson, S. P., & Bartek, J. (2009). The DNA-damage response in human biology and disease. *Nature*, *461*(7267), Article 7267. https://doi.org/10.1038/nature08467

Jastroch, M., Divakaruni, A. S., Mookerjee, S., Treberg, J. R., & Brand, M. D. (2010). Mitochondrial proton and electron leaks. *Essays in Biochemistry*, *47*, 53–67. https://doi.org/10.1042/bse0470053

Jauhar, S., Cowen, P. J., & Browning, M. (2023). Fifty years on: Serotonin and depression. *Journal of Psychopharmacology (Oxford, England)*, *37*(3), 237–241. https://doi.org/10.1177/02698811231161813

Johansson, S., Friedman, W., & Arhem, P. (1992). Impulses and resting membrane properties of small cultured rat hippocampal neurons. *The Journal of Physiology*, *445*, 129–140.

Jones, M. S., & Jones, O. T. (1969). The structural organization of haem synthesis in rat liver mitochondria. *The Biochemical Journal*, *113*(3), 507–514. https://doi.org/10.1042/bj1130507

Jouaville, L. S., Pinton, P., Bastianutto, C., Rutter, G. A., & Rizzuto, R. (1999). Regulation of mitochondrial ATP synthesis by calcium: Evidence for a long-term metabolic priming. *Proceedings of the National Academy of Sciences of the United States of America*, *96*(24), 13807–13812. https://doi.org/10.1073/pnas.96.24.13807

Kamer, K. J., & Mootha, V. K. (2015). The molecular era of the mitochondrial calcium uniporter. *Nature Reviews Molecular Cell Biology*, *16*(9), Article 9. https://doi.org/10.1038/nrm4039

Kamo, N., Muratsugu, M., Hongoh, R., & Kobatake, Y. (1979). Membrane potential of mitochondria measured with an electrode sensitive to tetraphenyl phosphonium and relationship between proton electrochemical potential and phosphorylation potential in steady state. *The Journal of Membrane Biology*, *49*(2), 105–121. https://doi.org/10.1007/BF01868720

Kaplowitz, N., Aw, T. Y., & Ookhtens, M. (1985). The Regulation of Hepatic Glutathione. *Annual Review of Pharmacology and Toxicology*, *25*(1), 715–744. https://doi.org/10.1146/annurev.pa.25.040185.003435

Karabatsiakis, A., Böck, C., Salinas-Manrique, J., Kolassa, S., Calzia, E., Dietrich, D. E., & Kolassa, I.-T. (2014). Mitochondrial respiration in peripheral blood mononuclear cells correlates with depressive subsymptoms and severity of major depression. *Translational Psychiatry*, *4*(6), e397–e397. https://doi.org/10.1038/tp.2014.44

Karlinsky, H., & Shulman, K. I. (1984). The clinical use of electroconvulsive therapy in old age. *Journal of the American Geriatrics Society*, *32*(3), 183–186. https://doi.org/10.1111/j.1532-5415.1984.tb01999.x

Kato, T. M., Kubota-Sakashita, M., Fujimori-Tonou, N., Saitow, F., Fuke, S., Masuda, A., Itohara, S., Suzuki, H., & Kato, T. (2018). Ant1 mutant mice bridge the mitochondrial and serotonergic dysfunctions in bipolar disorder. *Molecular Psychiatry*, *23*(10), Article 10. https://doi.org/10.1038/s41380-018-0074-9

Kendler, K. S. (2016). The Phenomenology of Major Depression and the Representativeness and Nature of DSM Criteria. *The American Journal of Psychiatry*, *173*(8), 771–780. https://doi.org/10.1176/appi.ajp.2016.15121509

Kendler, K. S., Gatz, M., Gardner, C. O., & Pedersen, N. L. (2006). A Swedish national twin study of lifetime major depression. *The American Journal of Psychiatry*, *163*(1), 109–114. https://doi.org/10.1176/appi.ajp.163.1.109

Kim, M.-H., & von Gersdorff, H. (2010). Extending the realm of membrane capacitance measurements to nerve terminals with complex morphologies. *The Journal of Physiology*, *588*(Pt 12), 2011–2012. https://doi.org/10.1113/jphysiol.2010.191270

Kim, M.-Y., Lee, J.-W., Kang, H.-C., Kim, E., & Lee, D.-C. (2011). Leukocyte mitochondrial DNA (mtDNA) content is associated with depression in old women. *Archives of Gerontology and Geriatrics*, *53*(2), e218–e221. https://doi.org/10.1016/j.archger.2010.11.019

Klinedinst, N. J., & Regenold, W. T. (2015). A mitochondrial bioenergetic basis of depression. *Journal of Bioenergetics and Biomembranes*, *47*(1), 155–171. https://doi.org/10.1007/s10863-014-9584-6

Koene, S., Kozicz, T. L., Rodenburg, R. J. T., Verhaak, C. M., De Vries, M. C., Wortmann, S., Van De Heuvel, L., Smeitink, J. A. M., & Morava, E. (2009). Major depression in adolescent children consecutively diagnosed with mitochondrial disorder. *Journal of Affective Disorders*, *114*(1–3), 327–332. https://doi.org/10.1016/j.jad.2008.06.023

Kolovos, S., Kleiboer, A., & Cuijpers, P. (2016). Effect of psychotherapy for depression on quality of life: Meta-analysis. *British Journal of Psychiatry*, *209*(6), 460–468. https://doi.org/10.1192/bjp.bp.115.175059

Kuffner, K., Triebelhorn, J., Meindl, K., Benner, C., Manook, A., Sudria-Lopez, D., Siebert, R., Nothdurfter, C., Baghai, T. C., Drexler, K., Berneburg, M., Rupprecht, R., Milenkovic, V. M., & Wetzel, C. H. (2020). Major Depressive Disorder is Associated with Impaired Mitochondrial Function in Skin Fibroblasts. *Cells*, *9*(4), E884. https://doi.org/10.3390/cells9040884

Kühlbrandt, W. (2015). Structure and function of mitochondrial membrane protein complexes. *BMC Biology*, *13*(1), 89. https://doi.org/10.1186/s12915-015-0201-x

Lamas, A. J., Reboreda, A., & Codesido, V. (2002). Ionic basis of the resting membrane potential in cultured rat sympathetic neurons. *NeuroReport*, *13*(5), 585.

Liu, W., Ge, T., Leng, Y., Pan, Z., Fan, J., Yang, W., & Cui, R. (2017). The Role of Neural Plasticity in Depression: From Hippocampus to Prefrontal Cortex. *Neural Plasticity*, *2017*, 6871089. https://doi.org/10.1155/2017/6871089

Lorenzoni, P. J., Scola, R. H., Kay, C. S. K., Silvado, C. E. S., & Werneck, L. C. (2014). When should MERRF (myoclonus epilepsy associated with ragged-red fibers) be the diagnosis? *Arquivos de Neuro-Psiquiatria*, *72*, 803–811. https://doi.org/10.1590/0004-282X20140124

Luo, X., Pitkänen, S., Kassovska-Bratinova, S., Robinson, B. H., & Lehotay, D. C. (1997). Excessive formation of hydroxyl radicals and aldehydic lipid peroxidation products in cultured skin fibroblasts from patients with complex I deficiency. *The Journal of Clinical Investigation*, *99*(12), 2877–2882. https://doi.org/10.1172/JCI119481

Lyons, T. W., Reinhard, C. T., & Planavsky, N. J. (2014). The rise of oxygen in Earth's early ocean and atmosphere. *Nature*, *506*(7488), 307–315. https://doi.org/10.1038/nature13068

Maes, M., Lambrechts, J., Bosmans, E., Jacobs, J., Suy, E., Vandervorst, C., de Jonckheere, C., Minner, B., & Raus, J. (1992). Evidence for a systemic immune activation during depression: Results of leukocyte enumeration by flow cytometry in conjunction with monoclonal antibody staining. *Psychological Medicine*, *22*(1), 45–53. https://doi.org/10.1017/s0033291700032712

Magee, J. C. (2000). Dendritic integration of excitatory synaptic input. *Nature Reviews Neuroscience*, *1*(3), Article 3. https://doi.org/10.1038/35044552

Mahoney, J., & Goertz, G. (2006). A Tale of Two Cultures: Contrasting Quantitative and Qualitative Research. *Political Analysis*, *14*(3), 227–249. https://doi.org/10.1093/pan/mpj017

Manji, H., Kato, T., Di Prospero, N. A., Ness, S., Beal, M. F., Krams, M., & Chen, G. (2012). Impaired mitochondrial function in psychiatric disorders. *Nature Reviews. Neuroscience*, *13*(5), 293–307. https://doi.org/10.1038/nrn3229

Mankad, P., James, A., Siriwardena, A. K., Elliott, A. C., & Bruce, J. I. E. (2012). Insulin protects pancreatic acinar cells from cytosolic calcium overload and inhibition of plasma membrane calcium pump. *The Journal of Biological Chemistry*, *287*(3), 1823–1836. https://doi.org/10.1074/jbc.M111.326272

Mao, L.-M., Mathur, N., & Wang, J. Q. (2022). Downregulation of surface AMPA receptor expression in the striatum following prolonged social isolation, a role of mGlu5 receptors. *IBRO Neuroscience Reports*, *13*, 22–30. https://doi.org/10.1016/j.ibneur.2022.05.007

Martineau, M., Guzman, R. E., Fahlke, C., & Klingauf, J. (2017). VGLUT1 functions as a glutamate/proton exchanger with chloride channel activity in hippocampal glutamatergic synapses. *Nature Communications*, *8*(1), Article 1. https://doi.org/10.1038/s41467-017-02367-6

Matta Reddy, A., Iqbal, M., Chopra, H., Urmi, S., Junapudi, S., Bibi, S., Kumar Gupta, S., Nirmala Pangi, V., Singh, I., & Abdel-Daim, M. M. (2022). Pivotal role of vitamin D in mitochondrial health, cardiac function, and human reproduction. *EXCLI Journal*, *21*, 967–990. https://doi.org/10.17179/excli2022-4935

Maydych, V. (2019). The Interplay Between Stress, Inflammation, and Emotional Attention: Relevance for Depression. *Frontiers in Neuroscience*, *13*, 384. https://doi.org/10.3389/fnins.2019.00384

Mecocci, P., Fanó, G., Fulle, S., MacGarvey, U., Shinobu, L., Polidori, M. C., Cherubini, A., Vecchiet, J., Senin, U., & Beal, M. F. (1999). Age-dependent increases in oxidative damage to DNA, lipids, and proteins in human skeletal muscle. *Free Radical Biology & Medicine*, *26*(3–4), 303–308. https://doi.org/10.1016/s0891-5849(98)00208-1

Miettinen, T. P., & Björklund, M. (2017). Mitochondrial Function and Cell Size: An Allometric Relationship. *Trends in Cell Biology*, *27*(6), 393–402. https://doi.org/10.1016/j.tcb.2017.02.006

Miettinen, T. P., Pessa, H. K. J., Caldez, M. J., Fuhrer, T., Diril, M. K., Sauer, U., Kaldis, P., & Björklund, M. (2014). Identification of Transcriptional and Metabolic Programs Related to Mammalian Cell Size. *Current Biology*, *24*(6), 598–608. https://doi.org/10.1016/j.cub.2014.01.071

Miller, I. W., Norman, W. H., & Keitner, G. I. (1989). Cognitive-behavioral treatment of depressed inpatients: Six- and twelve-month follow-up. *The American Journal of Psychiatry*, *146*(10), 1274–1279. https://doi.org/10.1176/ajp.146.10.1274

Miller, K. E., & Sheetz, M. P. (2004). Axonal mitochondrial transport and potential are correlated. *Journal of Cell Science*, *117*(13), 2791–2804. https://doi.org/10.1242/jcs.01130

Miller, W. L. (2013). Steroid hormone synthesis in mitochondria. *Molecular and Cellular Endocrinology*, *379*(1–2), 62–73. https://doi.org/10.1016/j.mce.2013.04.014

Mitchell, P. (1961). Coupling of Phosphorylation to Electron and Hydrogen Transfer by a Chemi-Osmotic type of Mechanism. *Nature*, *191*(4784), Article 4784. https://doi.org/10.1038/191144a0

Moncrieff, J., Cooper, R. E., Stockmann, T., Amendola, S., Hengartner, M. P., & Horowitz, M. A. (2022). The serotonin theory of depression: A systematic umbrella review of the evidence. *Molecular Psychiatry*, 1–14. https://doi.org/10.1038/s41380-022-01661-0

Moretti, A., Gorini, A., & Villa, R. F. (2003). Affective disorders, antidepressant drugs and brain metabolism. *Molecular Psychiatry*, *8*(9), 773–785. https://doi.org/10.1038/sj.mp.4001353

Moudy, A. M., Handran, S. D., Goldberg, M. P., Ruffin, N., Karl, I., Kranz-Eble, P., DeVivo, D. C., & Rothman, S. M. (1995). Abnormal calcium homeostasis and mitochondrial polarization in a human encephalomyopathy. *Proceedings of the National Academy of Sciences of the United States of America*, *92*(3), 729–733.

Mullen, R. J., Buck, C. R., & Smith, A. M. (1992). NeuN, a neuronal specific nuclear protein in vertebrates. *Development (Cambridge, England)*, *116*(1), 201–211. https://doi.org/10.1242/dev.116.1.201

Mulugeta, A., Lumsden, A., & Hyppönen, E. (2020). Relationship between Serum 25(OH)D and Depression: Causal Evidence from a Bi-Directional Mendelian Randomization Study. *Nutrients*, *13*(1), 109. https://doi.org/10.3390/nu13010109

Murphy, M. P. (2009). How mitochondria produce reactive oxygen species. *Biochemical Journal*, *417*(Pt 1), 1–13. https://doi.org/10.1042/BJ20081386

Nedergaard, J., Golozoubova, V., Matthias, A., Asadi, A., Jacobsson, A., & Cannon, B. (2001). UCP1: The only protein able to mediate adaptive non-shivering thermogenesis and metabolic inefficiency. *Biochimica Et Biophysica Acta*, *1504*(1), 82–106. https://doi.org/10.1016/s0005-2728(00)00247-4

Neher, E., & Sakaba, T. (2008). Multiple roles of calcium ions in the regulation of neurotransmitter release. *Neuron*, *59*(6), 861–872. https://doi.org/10.1016/j.neuron.2008.08.019

Ng, F., Berk, M., Dean, O., & Bush, A. I. (2008). Oxidative stress in psychiatric disorders: Evidence base and therapeutic implications. *International Journal of Neuropsychopharmacology*, *11*(6), 851–876. https://doi.org/10.1017/S1461145707008401

Palty, R., Silverman, W. F., Hershfinkel, M., Caporale, T., Sensi, S. L., Parnis, J., Nolte, C., Fishman, D., Shoshan-Barmatz, V., Herrmann, S., Khananshvili, D., & Sekler, I. (2010). NCLX is an essential component of mitochondrial Na+/Ca2+ exchange. *Proceedings of*

the National Academy of Sciences, *107*(1), 436–441. https://doi.org/10.1073/pnas.0908099107

Parpura, V., & Zorec, R. (2010). Gliotransmission: Exocytotic release from astrocytes. *Brain Research Reviews*, *63*(1–2), 83–92. https://doi.org/10.1016/j.brainresrev.2009.11.008

Pasdois, P., Parker, J. E., Griffiths, E. J., & Halestrap, A. P. (2011). The role of oxidized cytochrome c in regulating mitochondrial reactive oxygen species production and its perturbation in ischaemia. *Biochemical Journal*, *436*(2), 493–505. https://doi.org/10.1042/BJ20101957

Pedersen, S. F., Hoffmann, E. K., & Mills, J. W. (2001). *The cytoskeleton and cell volume regulation &*.

Picard, M., & Shirihai, O. S. (2022). Mitochondrial signal transduction. *Cell Metabolism*, *34*(11), 1620–1653. https://doi.org/10.1016/j.cmet.2022.10.008

Pitkanen, S., & Robinson, B. H. (1996). Mitochondrial complex I deficiency leads to increased production of superoxide radicals and induction of superoxide dismutase. *The Journal of Clinical Investigation*, *98*(2), 345–351. https://doi.org/10.1172/JCI118798

Pizzo, P., & Pozzan, T. (2007). Mitochondria–endoplasmic reticulum choreography: Structure and signaling dynamics. *Trends in Cell Biology*, *17*(10), 511–517. https://doi.org/10.1016/j.tcb.2007.07.011

Prange, O., Wong, T. P., Gerrow, K., Wang, Y. T., & El-Husseini, A. (2004). A balance between excitatory and inhibitory synapses is controlled by PSD-95 and neuroligin. *Proceedings of the National Academy of Sciences*, *101*(38), 13915–13920. https://doi.org/10.1073/pnas.0405939101

Praticò, D. (2002). Lipid peroxidation and the aging process. *Science of Aging Knowledge Environment: SAGE KE*, *2002*(50), re5. https://doi.org/10.1126/sageke.2002.50.re5

Puig, M. V., & Gulledge, A. T. (2011). Serotonin and prefrontal cortex function: Neurons, networks, and circuits. *Molecular Neurobiology*, *44*(3), 449–464. https://doi.org/10.1007/s12035-011-8214-0

Pyle, A., Hudson, G., Wilson, I. J., Coxhead, J., Smertenko, T., Herbert, M., Santibanez-Koref, M., & Chinnery, P. F. (2015). Extreme-Depth Re-sequencing of Mitochondrial DNA Finds No Evidence of Paternal Transmission in Humans. *PLOS Genetics*, *11*(5), e1005040. https://doi.org/10.1371/journal.pgen.1005040

Quinzii, C. M., & Hirano, M. (2010). Coenzyme Q and Mitochondrial Disease. *Developmental Disabilities Research Reviews*, *16*(2), 183–188. https://doi.org/10.1002/ddrr.108

Rahman, S. (2020). Mitochondrial disease in children. *Journal of Internal Medicine*, *287*(6), 609–633. https://doi.org/10.1111/joim.13054

Reeg, S., Jung, T., Castro, J. P., Davies, K. J. A., Henze, A., & Grune, T. (2016). The molecular chaperone Hsp70 promotes the proteolytic removal of oxidatively damaged proteins by the proteasome. *Free Radical Biology & Medicine*, *99*, 153–166. https://doi.org/10.1016/j.freeradbiomed.2016.08.002

Rhee, S. G., Bae, Y. S., Lee, S.-R., & Kwon, J. (2000). Hydrogen Peroxide: A Key Messenger That Modulates Protein Phosphorylation Through Cysteine Oxidation. *Science's STKE*, *2000*(53), pe1–pe1. https://doi.org/10.1126/stke.2000.53.pe1

Roller, M. R. (2020, December 8). Generalizability in Case Study Research. *Research Design Review*. https://researchdesignreview.com/2020/12/08/generalizability-case-study-research/

Romero-Garcia, S., & Prado-Garcia, H. (2019). Mitochondrial calcium: Transport and modulation of cellular processes in homeostasis and cancer (Review). *International Journal of Oncology*, *54*(4), 1155–1167. https://doi.org/10.3892/ijo.2019.4696

Rose, J., Brian, C., Pappa, A., Panayiotidis, M. I., & Franco, R. (2020). Mitochondrial Metabolism in Astrocytes Regulates Brain Bioenergetics, Neurotransmission and Redox Balance. *Frontiers in Neuroscience*, *14*. https://www.frontiersin.org/articles/10.3389/fnins.2020.536682

Roskams, A. J. I., Cai, X., & Ronnett, G. V. (1998). Expression of neuron-specific beta-III tubulin during olfactory neurogenesis in the embryonic and adult rat. *Neuroscience*, *83*(1), 191–200. https://doi.org/10.1016/S0306-4522(97)00344-8

Rutherford, B. R., Wager, T. D., & Roose, S. P. (2010). Expectancy and the Treatment of Depression: A Review of Experimental Methodology and Effects on Patient Outcome. *Current Psychiatry Reviews*, *6*(1), 1–10. https://doi.org/10.2174/157340010790596571

Scaini, G., Mason, B. L., Diaz, A. P., Jha, M. K., Soares, J. C., Trivedi, M. H., & Quevedo, J. (2021). Dysregulation of mitochondrial dynamics, mitophagy and apoptosis in major depressive disorder: Does inflammation play a role? *Molecular Psychiatry*, 1–8. https://doi.org/10.1038/s41380-021-01312-w

Schaefer, A., Lim, A., & Gorman, G. (2019). Epidemiology of Mitochondrial Disease. In M. Mancuso & T. Klopstock (Eds.), *Diagnosis and Management of Mitochondrial Disorders* (pp. 63–79). Springer International Publishing. https://doi.org/10.1007/978-3-030-05517-2_4

Schiegg, A., Gerstner, W., Ritz, R., & van Hemmen, J. L. (1995). Intracellular Ca2+ stores can account for the time course of LTP induction: A model of Ca2+ dynamics in dendritic spines. *Journal of Neurophysiology*, *74*(3), 1046–1055. https://doi.org/10.1152/jn.1995.74.3.1046

Scholz, H., Yndestad, A., Damås, J. K., Wæhre, T., Tonstad, S., Aukrust, P., & Halvorsen, B. (2003). 8-Isoprostane increases expression of interleukin-8 in human macrophages through activation of mitogen-activated protein kinases. *Cardiovascular Research*, *59*(4), 945–954. https://doi.org/10.1016/S0008-6363(03)00538-8

Schulze, M., Hoja, S., Winner, B., Winkler, J., Edenhofer, F., & Riemenschneider, M. J. (2016). Model Testing of PluriTest with Next-Generation Sequencing Data. *Stem Cells and Development*, *25*(7), 569–571. https://doi.org/10.1089/scd.2015.0266

Seager, R., Lee, L., Henley, J. M., & Wilkinson, K. A. (2020). Mechanisms and roles of mitochondrial localisation and dynamics in neuronal function. *Neuronal Signaling*, *4*(2), NS20200008. https://doi.org/10.1042/NS20200008

Shah, D. I., Takahashi-Makise, N., Cooney, J. D., Li, L., Schultz, I. J., Pierce, E. L., Narla, A., Seguin, A., Hattangadi, S. M., Medlock, A. E., Langer, N. B., Dailey, T. A., Hurst, S. N., Faccenda, D., Wiwczar, J. M., Heggers, S. K., Vogin, G., Chen, W., Chen, C., … Paw, B. H. (2012). Mitochondrial Atpif1 regulates haem synthesis in developing erythroblasts. *Nature*, *491*(7425), 608–612. https://doi.org/10.1038/nature11536

Sies, H., & Jones, D. P. (2020). Reactive oxygen species (ROS) as pleiotropic physiological signalling agents. *Nature Reviews Molecular Cell Biology*. https://doi.org/10.1038/s41580-020-0230-3

Sinyor, M., Schaffer, A., & Levitt, A. (2009). *The Sequenced Treatment Alternatives to Relieve Depression (STAR*D) Trial: A Review*. https://doi.org/10.1177/0706743710055003O3

Sluzewska, A. (1999). Indicators of immune activation in depressed patients. *Advances in Experimental Medicine and Biology*, *461*, 59–73. https://doi.org/10.1007/978-0-585-37970-8_4

Spees, J. L., Olson, S. D., Whitney, M. J., & Prockop, D. J. (2006). Mitochondrial transfer between cells can rescue aerobic respiration. *Proceedings of the National Academy of Sciences of the United States of America*, *103*(5), 1283–1288. https://doi.org/10.1073/pnas.0510511103

Sproule, D. M., & Kaufmann, P. (2008). Mitochondrial encephalopathy, lactic acidosis, and strokelike episodes: Basic concepts, clinical phenotype, and therapeutic management of MELAS syndrome. *Annals of the New York Academy of Sciences*, *1142*, 133–158. https://doi.org/10.1196/annals.1444.011

STADApharm GmbH. (2016). *Labortest für eine individuell optimierte Therapieplanung bei Depressionen Zur Anwendung in der ärztlichen Praxis*. www.stada-diagnostik.de

Südhof, T. C. (2012). Calcium Control of Neurotransmitter Release. *Cold Spring Harbor Perspectives in Biology*, *4*(1), a011353. https://doi.org/10.1101/cshperspect.a011353

Suomalainen, A., Majander, A., Haltia, M., Somer, H., Lönnqvist, J., Savontaus, M. L., & Peltonen, L. (1992). Multiple deletions of mitochondrial DNA in several tissues of a patient with severe retarded depression and familial progressive external ophthalmoplegia. *The Journal of Clinical Investigation*, *90*(1), 61–66. https://doi.org/10.1172/JCI115856

Suzuki, Y., Sugai, T., Fukui, N., Watanabe, J., Ono, S., Inoue, Y., Ozdemir, V., & Someya, T. (2011). CYP2D6 genotype and smoking influence fluvoxamine steady-state concentration in Japanese psychiatric patients: Lessons for genotype-phenotype association study design in translational pharmacogenetics. *Journal of Psychopharmacology (Oxford, England)*, *25*(7), 908–914. https://doi.org/10.1177/0269881110370504

Takahashi, K., & Yamanaka, S. (2006). Induction of Pluripotent Stem Cells from Mouse Embryonic and Adult Fibroblast Cultures by Defined Factors. *Cell*, *126*(4), 663–676. https://doi.org/10.1016/j.cell.2006.07.024

Takahashi, M.-A., & Asada, K. (1983). Superoxide anion permeability of phospholipid membranes and chloroplast thylakoids. *Archives of Biochemistry and Biophysics*, *226*(2), 558–566. https://doi.org/10.1016/0003-9861(83)90325-9

Takeuchi, A., Kim, B., & Matsuoka, S. (2015). The destiny of Ca2+ released by mitochondria. *The Journal of Physiological Sciences*, *65*(1), 11–24. https://doi.org/10.1007/s12576-014-0326-7

Tcw, J., Wang, M., Pimenova, A. A., Bowles, K. R., Hartley, B. J., Lacin, E., Machlovi, S. I., Abdelaal, R., Karch, C. M., Phatnani, H., Slesinger, P. A., Zhang, B., Goate, A. M., & Brennand, K. J. (2017). An Efficient Platform for Astrocyte Differentiation from Human Induced Pluripotent Stem Cells. *Stem Cell Reports*, *9*(2), 600–614. https://doi.org/10.1016/j.stemcr.2017.06.018

Thase, M. E. (1997). Treatment of Major Depression With Psychotherapy or Psychotherapy-Pharmacotherapy Combinations. *Archives of General Psychiatry*, *54*(11), 1009. https://doi.org/10.1001/archpsyc.1997.01830230043006

Tillman, T. S., & Cascio, M. (2003). Effects of membrane lipids on ion channel structure and function. *Cell Biochemistry and Biophysics*, *38*(2), 161–190. https://doi.org/10.1385/CBB:38:2:161

Triebelhorn, J., Cardon, I., Kuffner, K., Bader, S., Jahner, T., Meindl, K., Rothhammer-Hampl, T., Riemenschneider, M. J., Drexler, K., Berneburg, M., Nothdurfter, C., Manook, A., Brochhausen, C., Baghai, T. C., Hilbert, S., Rupprecht, R., Milenkovic, V. M., & Wetzel, C. H. (2022). Induced neural progenitor cells and iPS-neurons from major depressive disorder patients show altered bioenergetics and electrophysiological properties. *Molecular Psychiatry*, 1–11. https://doi.org/10.1038/s41380-022-01660-1

Vaarmann, A., Mandel, M., Zeb, A., Wareski, P., Liiv, J., Kuum, M., Antsov, E., Liiv, M., Cagalinec, M., Choubey, V., & Kaasik, A. (2016). Mitochondrial biogenesis is required for axonal growth. *Development (Cambridge, England)*, *143*(11), 1981–1992. https://doi.org/10.1242/dev.128926

Vadodaria, K. C., Ji, Y., Skime, M., Paquola, A. C., Nelson, T., Hall-Flavin, D., Heard, K. J., Fredlender, C., Deng, Y., Elkins, J., Dani, K., Le, A. T., Marchetto, M. C., Weinshilboum, R., & Gage, F. H. (2019). Altered serotonergic circuitry in SSRI-resistant major depressive disorder patient-derived neurons. *Molecular Psychiatry*, *24*(6), 808–818. https://doi.org/10.1038/s41380-019-0377-5

Valko, M., Leibfritz, D., Moncol, J., Cronin, M. T. D., Mazur, M., & Telser, J. (2007). Free radicals and antioxidants in normal physiological functions and human disease. *The International Journal of Biochemistry & Cell Biology*, *39*(1), 44–84. https://doi.org/10.1016/j.biocel.2006.07.001

van der Bliek, A. M., Sedensky, M. M., & Morgan, P. G. (2017). Cell Biology of the Mitochondrion. *Genetics*, *207*(3), 843–871. https://doi.org/10.1534/genetics.117.300262

Visch, H.-J., Koopman, W. J. H., Zeegers, D., van Emst-de Vries, S. E., van Kuppeveld, F. J. M., van den Heuvel, L. W. P. J., Smeitink, J. A. M., & Willems, P. H. G. M. (2006).

Ca2+-mobilizing agonists increase mitochondrial ATP production to accelerate cytosolic Ca2+ removal: Aberrations in human complex I deficiency. *American Journal of Physiology. Cell Physiology*, *291*(2), C308-316. https://doi.org/10.1152/ajpcell.00561.2005

Vose, L. R., & Stanton, P. K. (2017). Synaptic Plasticity, Metaplasticity and Depression. *Current Neuropharmacology*, *15*(1), 71–86. https://doi.org/10.2174/1570159x14666160202121111

Vreeburg, S. A., Hoogendijk, W. J. G., van Pelt, J., Derijk, R. H., Verhagen, J. C. M., van Dyck, R., Smit, J. H., Zitman, F. G., & Penninx, B. W. J. H. (2009). Major depressive disorder and hypothalamic-pituitary-adrenal axis activity: Results from a large cohort study. *Archives of General Psychiatry*, *66*(6), 617–626. https://doi.org/10.1001/archgenpsychiatry.2009.50

Vuda, M., & Kamath, A. (2016). Drug induced mitochondrial dysfunction: Mechanisms and adverse clinical consequences. *Mitochondrion*, *31*, 63–74. https://doi.org/10.1016/j.mito.2016.10.005

Walker, J. E. (2013). The ATP synthase: The understood, the uncertain and the unknown. *Biochemical Society Transactions*, *41*(1), 1–16. https://doi.org/10.1042/BST20110773

Wallace, D. C., & Chalkia, D. (2013). Mitochondrial DNA Genetics and the Heteroplasmy Conundrum in Evolution and Disease. *Cold Spring Harbor Perspectives in Biology*, *5*(11), a021220. https://doi.org/10.1101/cshperspect.a021220

Ward, P. S., & Thompson, C. B. (2012). Signaling in Control of Cell Growth and Metabolism. *Cold Spring Harbor Perspectives in Biology*, *4*(7), a006783. https://doi.org/10.1101/cshperspect.a006783

Westermann, B. (2012). Bioenergetic role of mitochondrial fusion and fission. *Biochimica et Biophysica Acta (BBA) - Bioenergetics*, *1817*(10), 1833–1838. https://doi.org/10.1016/j.bbabio.2012.02.033

Wetzel, C., Bader, S., Jahner, T., Dörfelt, A., Melchner, D., Cardon, I., Siegmund, H., Brochhausen, C., Rupprecht, R., & Milenkovic, V. (2024). *A comprehensive functional investigation of the human translocator protein 18 kDa (TSPO) in a novel human neuronal cell knockout model: From molecule to depression*. https://doi.org/10.21203/rs.3.rs-4024118/v1

World Health Organization. (2018). *Management of physical health conditions in adults with severe mental disorders: WHO guidelines*. World Health Organization. https://apps.who.int/iris/handle/10665/275718

World Health Organization. (2020). *Global Health Estimates 2019: Disease burden by cause, age, sex, by country and by region, 2000–2019*. https://www.who.int/docs/default-source/gho-documents/ global-health-estimates/ghe2019_yld_global_2000_2019c417f68b- 841d-4a7a-9e5c-f087f9f86e48.xlsx?sfvrsn=dac29788_7

Yan, Y., Shin, S., Jha, B. S., Liu, Q., Sheng, J., Li, F., Zhan, M., Davis, J., Bharti, K., Zeng, X., Rao, M., Malik, N., & Vemuri, M. C. (2013). Efficient and rapid derivation of primitive neural stem cells and generation of brain subtype neurons from human pluripotent stem cells. *Stem Cells Translational Medicine*, *2*(11), 862–870. https://doi.org/10.5966/sctm.2013-0080

Yáñez, M., Gil-Longo, J., & Campos-Toimil, M. (2012). Calcium binding proteins. *Advances in Experimental Medicine and Biology*, *740*, 461–482. https://doi.org/10.1007/978-94-007-2888-2_19

Zhang, L., Yu, L., & Yu, C.-A. (1998). Generation of Superoxide Anion by Succinate-Cytochromec Reductase from Bovine Heart Mitochondria *. *Journal of Biological Chemistry*, *273*(51), 33972–33976. https://doi.org/10.1074/jbc.273.51.33972

Zorova, L. D., Popkov, V. A., Plotnikov, E. Y., Silachev, D. N., Pevzner, I. B., Jankauskas, S. S., Babenko, V. A., Zorov, S. D., Balakireva, A. V., Juhaszova, M., Sollott, S. J., & Zorov, D. B. (2018). Mitochondrial membrane potential. *Analytical Biochemistry*, *552*, 50–59. https://doi.org/10.1016/j.ab.2017.07.009

Appendix

List of abbreviations

5-HIAA	5-hydroxyindoleacetic acid
AD	antidepressants
ADP	adenosine diphosphate
ALDH1L1	aldehyde dehydrogenase 1 family member L1
AMP	adenosine monophosphate
AMPA	α-amino-3-hydroxy-5-methyl-4-isoxazolepropionic acid
ANT	adenine nucleotide translocase
AP	action potential
ATP	adenosine triphosphate
BCA	bichinoic acid
BDNF	brain-derived neurotrophic factor
cAMP	cyclic AMP
CoA	coenzyme A
Cx 43	Connexin 43
Cyt	cytochrome
DNA	desoxiribonucleic acid
DSM V	*Diagnostic and Statistical Manual of Mental Disorders V*
EAAT1	excitatory amino acid transporter 1
ECAR	extracellular consumption rate
ECT	electroconvulsive therapy
ELISA	enzyme-linked immunosorbent assay
EM	electron microscopy
ER	endoplasmic reticulum
ERK	extracellular signal-regulated kinases
ETC	electron transport chain
FACS	Flurorescent Activated Cell Sorting
$FAD^+/FADH_2$	flavin adenine dinucleotide
FCCP	carbonyl cyanide-*4*-(trifluoromethoxy)phenylhydrazone
FCS	fetal calf serum
FMN	flavin mononucleotide
$GABA_A$	gamma-aminobutric-acid type A
GAPDH	glyceraldehyde 3-phosphate dehydrogenase
GFAP	Glial Fibrillary Acidic Protein
GPx	glutathione peroxidase
GSH	glutathione
H_2O_2	hydrogen peroxide
HAM-D	Hamilton Depression Rating Scale
HPA axis	hypothalamus-Pituitary-Adrenal axis
IMM	inner mitochondrial membrane
IMS	intermembrane space
iPSC	induced pluripotent stem cell
LDH	lactate dehydrogenase
MAPK	mitogen-activated protein kinase
MCU	mitochondrial Ca^{2+} uniporter
MD	mitochondrial disease
MDD	Major Depressive Disorder
MELAS	Mitochondrial Encephalopathy, Lactic Acidosis, and Stroke-like episodes
MERRF	Myoclonus Epilepsy associated with Ragged-Red Fibres
MMP/Δψm	mitochondrial membrane potential
mPTP	mitochondrial permeability transition pore
mtDNA	mitochondrial DNA
NAD^+/NADH	nicotinamide adenine dinucleotide
NCLX	$Na^+/Ca^{2+}/Li^+$ exchanger
NMDA	*N*-Methyl-D-aspartic acid
NPC	neural progenitor cell
O_2^-	superoxide
OCR	oxygen consumption rate
OMM	outer mitochondrial membrane
OXPHOS	oxidative phosphorylation
PBS	phosphate buffered saline
P_i	phosphate
PMCA	Plasma Membrane Ca^{2+} ATPase
Q	ubiquinone/ubiquinol
PFA	paraformaldehyde
PSC	post-synaptic current
PSD95	post-synaptic density 95
RET	reverse electron transport
RLU	relative light unit
RMP	resting membrane potential
RNA	ribonucleic acid
ROS	reactive oxygen species
SEM	standard error of the mean
SNRI	serotonin-norepinephrine reuptake inhibitor
SSRI	selective serotonin reuptake inhibitor
TCA	tricarboxylic acid cycle
TRD	treatment-resistant depression
TSPO	translocator protein 18 kDa
UCP	uncoupling protein
VDAC	voltage-dependent anion channel
VGLUT1	vesicular glutamate transporters 1

List of units

%	percentage
A	Ampere
°C	degree Celcius
g	gram
h	hour
min	minute
s	second
L	liter
m	meter
M	molar concentration in mol L^{-1}
mol	mole
rpm	rounds per minute
t	timer
T	temperature
V	volt

List of dimensions

k	kilo (10^{3})
m	milli (10^{-3})
µ	micro (10^{-6})
n	nano (10^{-9})
p	pico (10^{-12})

List of figures

List of tables

Acknowledgements

First, I would like to express my deepest gratitude to my supervisor, Prof. Dr. Christian Wetzel, without whom none of this would have been possible. Dear Christian, thank you for your trust and your encouragements, thank you for your communicative enthusiasm and passion. Without those, this project and this experience would not have been the same.

I would like to extend my sincere thanks to Prof. Dr. Iris-Tatjana Kolassa for reviewing this dissertation and Prof. Dr. Stephan Schneuwly for accepting to serve as my third examiner. I would also like to thank Prof. Dr. Oliver Bosch for chairing my examination and PD Dr. Markus Reichold for being part of my examination committee, as well as Prof. Dr. Rainer Rupprecht as head of the Department of Psychiatry and Psychotherapy.

Thanks should also go to the GRK2174 program for providing the framework for this research and offering both a stimulating research environment and inspiring scientific interactions. This was only possible thanks to the Profs and colleagues of the GRK program and therefore, I would like to express my gratitude.

I am also grateful to my colleagues in the lab for creating a friendly and cheerful atmosphere. I am thankful that I have been welcomed by such nice people when dealing with the challenges of moving to a new country where I don't yet speak the language, during a pandemic.

Vielen Dank Tati für deine wertvollen technischen Ratschläge und deine vielfältige Unterstützung im Labor und dafür, dass du mich mit Geduld und Wohlwollen herausgefordert hast, mein Deutsch zu verbessern.

Thank you Vladi for sharing your technical and scientific expertise with me, and for your easy-going nature that inspired me to take certain things in a lighter way.

Thank you Doris, for your support and constant willingness to help, both with lab-related and administrative/ living-in-Germany-related issues, and that, always with a kind smile.

Steffi…I don't know how I would have made it without you. From the very beginning, you have taught me so much, and your determination inspired me. Thank you for sharing with me your impressive research design and problem-solving skills, and your extensive scientific knowledge. Thank you for your encouragements, and for your professional, but also emotional support through these challenging and exciting years of PhD. I am deeply grateful for the friendship we developed over these years together in the lab and I am convinced it's only the beginning.

I would like to acknowledge the students who added their own building blocks to the edifice of my project. Specifically, I thank Sonja for her massive contribution and her independence.

I am very thankful to my family and friends for their unconditional support and trust, for believing in me, for giving me the confidence to achieve my goal and for their help along the way.

MERCI!